IJHSR International Journal of High School Research

March 2021 | Volume 3 | Issue 1
ijhighschoolresearch.org
ISSN (Print version) 2642-1046
ISSN (Online version) 2642-1054

GENIUS OLYMPIAD

"Let's build a better future together"

www.geniusolympiad.org

International Environment Project Fair For Grades 9-12

Rochester, New York

RIT
Rochester Institute of Technology

@GeniusOlympiad

terra science and education

Table of Contents

March 2021| Volume 3| Issue1

Editorial Board

International Journal of High School Research

Tasty or Toxic: Evaluating the Effects of Common Food Additives on *Daphnia Magna*

Aditya Mahna, Ayush Mahna

Troy High School, 2200 Dorothy Ln, Fullerton, CA 92831, USA; adimahna@gmail.com

ABSTRACT: The adverse effects of three of the most used food additives, MSG, food color, and sodium nitrite, were investigated in this research. The hypothesis was that these food additives would have harmful effects on *Daphnia magna*. Treatment groups called control, MSG, sodium nitrite, and food color each were tested in four different concentrations. Five *Daphnia magna* that were less than 24-hours-old were tested per group and were observed after thirty minutes and after overnight incubation with each of the additives. Heart rate and mobility were measured to determine the acute toxicity of the test compounds. In MSG, the heart rate decreased significantly in all concentrations after overnight incubation. All *Daphnia* numbers were deceased within thirty minutes in sodium nitrite in both 1% and 2% concentrations, showing that sodium nitrite is toxic. However, cardiac effects did not cause this because heart rate in lower concentrations of 0.1% and 0.01% did not change significantly from control. With food dye, the heart rate decreased significantly in concentrations as low as 0.1% after overnight incubation. Finally, we can conclude that these food additives have a toxic effect on *Daphnia magna* and the severity of these effects is based on the time of exposure and quantity of food additives consumed.

KEYWORDS: Toxicology; Food Additives; *Daphnia magna*; Monosodium Glutamate; Food Color; Sodium Nitrite.

Introduction

Foods have evolved and changed tremendously in the past decade. Food additives are now applied to many different food types. Food additives are substances used to preserve the food or enhance its flavor or appearance. Recent studies have shown that these substances may have negative effects on the human body.[1,2] To test this, we decided to do experiments with the three most common food additives: MSG, food color, and sodium nitrite. MSG, or monosodium glutamate, is the sodium salt of glutamic acid, one of the most abundant naturally occurring, non-essential amino acids. It is used to intensify and enhance the flavor of food.[3] Studies have shown that it can cause headaches, asthma, and even brain damage.[4-6] Food coloring is made in a lab with chemicals derived from petroleum, a crude oil product, which is also used in gasoline, diesel fuel, asphalt, and tar.[7] Food color is used to improve the appearance of foods and is often used in advertisements and fast-food restaurants. The excessive use of food color has been shown to reduce the attention span and cause ADHD and other behavioral problems in children.[8,9] Sodium nitrite is often found in processed meats as a preservative to prevent bacteria growth.[10] Studies have shown that over-consumption of sodium nitrite can cause kidney damage and low blood-pressure.[11,12] We tested each food additive on *Daphnia magna*. *D. magna* is a tiny, semi-transparent freshwater crustacean with long antennae and prominent eyes. *D. magna* was used because they are a perfect model system, easy to handle, and are an ideal system for studying multiple stressors. They are good test subjects because of their transparent bodies, early reproduction rates, short lifespans, and gender change response system. We hypothesized that these food additives would have harmful effects on the *D. magna*.

Results and Discussion

To observe the short-term effects of food additives, *D. magna* were incubated with each of the test compounds for 30 minutes at four different concentrations: 2%, 1%, 0.1%, and 0.01%. These concentrations represent the range of relevant concentrations of food additives that can be found in the human body system. Five *D. magna* were included in each group. After 30 minutes the heart rates were measured. The average heart rate for the control group was 193 beats per minutes (bpm). No significant effect was observed in any groups for any concentration tested after 30 minutes of incubation. However, all of *D. magna* died within 30 minutes of incubation in 2% and 1% sodium nitrite and all *D. magna* died in the 2% food color group (Table 1 and Figure 1). At least one *D. magna* died in each of the concentrations tested in the food additive groups. No *D. magna* died in the control group (Table 3 and Figure 2). The deceased *D. magna* were not included in heart rate analysis.

To observe the effects of the food additives after longer incubation, *D. magna* were left overnight (12 hours) with food additives. The heart rates were measured the following day. After overnight incubation, the average heart rate for the control group was 173 bpm. The MSG and sodium nitrite groups displayed a dose-dependent increase in death of *D. magna*, indicating increased toxicity of these food additives with increased dosage (Table 3 and Figure 2). There was a significant reduction in heart rate in *D. magna* in the presence of MSG and food dye (Table 2 and Figure 1). Interestingly, 0.1% and 0.01% sodium nitrite did not display a significant

DOI: 10.36838/v3i1.1

change in heart rate compared to the control. However, all *D. magna* in 2% and 1% sodium nitrite died within 30 minutes. This indicates that sodium nitrite is highly toxic at higher concentrations but not due to cardiac toxicity.

Table 1: Heart rate in *D. magna* after 30-minute incubation with various concentrations of food additives. The black filled cells indicate the *D. magna* that died in the presence of food additives.

	Heart Rate (30 min)								
		D. magna individuals							
	Concentration	D1	D2	D3	D4	D5	Average	STDEV	P Value (Student's t-Test)
Control	N/A	200	196	192	194	184	193.2	5.9	N/A
MSG	2%	184	196		200	164	186	16.2	0.32
	1%	200	192	204		200	199	5.0	0.30
	0.1%	204	188	208		208	202	9.5	0.29
	0.01%	168	168	172	168		169	2.0	0.00
Sodium Nitrite	2%							N/A	N/A
	1%							N/A	N/A
	0.1%	188	196		168	184	184	11.8	0.22
	0.01%	184	188		180	188	185	3.8	0.16
Food Dye	2%							N/A	N/A
	1%	196		200	176	192	191	10.5	0.82
	0.1%	196	180	172	196		186	12.0	0.16
	0.01%	200		184	212	224	205	17.1	0.33

Table 2: *Daphnia magna* heart rate after 12-hour incubation with various concentration of food additives. The black filled cells indicate the *D. magna* died in the presence of food additives.

	Heart Rate (Overnight)								
Name	Concentration	D1	D2	D3	D4	D5	Average	Standard Dev	P Value (Student's t-Test)
Control	N/A	168	184	176	188	152	174	14.3	N/A
MSG	2%		128	136			132	5.7	N/A
	1%	120	128			116	121	6.1	0.015
	0.1%	116	128			124	123	6.1	0.035
	0.01%	136	132	128		156	138	12.4	0.087
Sodium Nitrite	2%						N/A	N/A	N/A
	1%						N/A	N/A	N/A
	0.1%	176			160		168	11.3	0.677
	0.01%	160	156			152	156	4.0	0.286
Food Dye	2%						N/A	N/A	N/A
	1%	92	112	96	76	112	98	15.1	0.003
	0.1%	116	140	144	96		124	22.4	0.024
	0.01%	180	164	156	120	144	153	22.5	0.189

Table 2: *Daphnia magna* heart rate after 12-hour incubation with various concentration of food additives. The black filled cells indicate the *D. magna* died in the presence of food additives.

Name	Concentration	# of Mobile *D. magna*	
		30 min	Overnight
Control	N/A	5	5
MSG	2%	4	2
	1%	4	3
	0.1%	5	3
	0.01%	5	4
Sodium Nitrite	2%	0	0
	1%	0	0
	0.1%	5	2
	0.01%	5	3
Food Dye	2%	0	0
	1%	3	3
	0.1%	5	4
	0.01%	5	5

Discussion

These results show that food additives have harmful effects on the health of *Daphnia magna*. Food dye had significant cardiovascular effects corresponding to its concentration. MSG slowed the heart rate of *D. magna* while sodium nitrite did not display any significant cardiovascular effects. However, sodium nitrite was shown to be extremely harmful in high concentrations as none of the *D. magna* were alive in trations above 0.1% after 30 minutes of incubation. MSG and food dye impacted mobility of *Daphnia magna* in a dose dependent manner. The dose dependent effects were highly evident after overnight incubation. This also shows that the

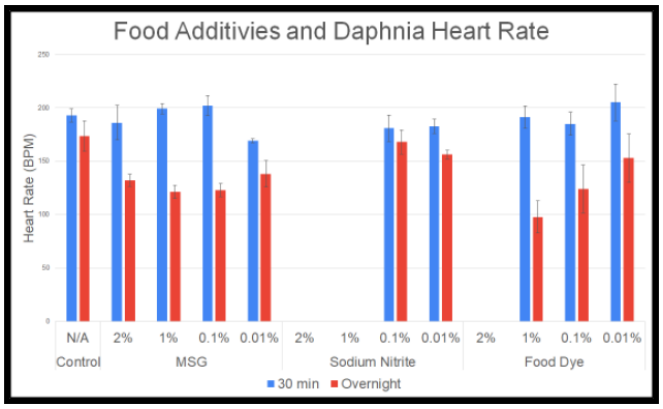

Figure 1: The effects of various food additives on *Daphnia magna* heart rate.

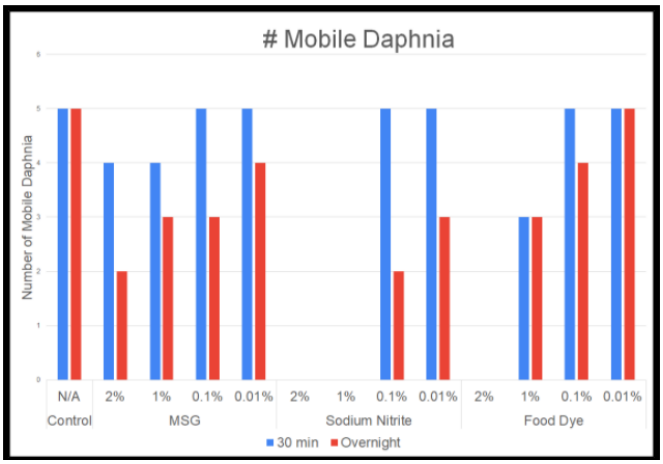

Figure 2: The effect of various food additives on the mobility of *Daphnia magna*.

overnight incubation had a much larger influence on *D. magna* than the 30-minute incubation. Overall, these results indicate that food additives have toxic effects on *Daphnia magna* and these effects are dependent on the concentration and time of exposure.

Conclusion

Based on these results obtained in this study, we can conclude that these food additives have a toxic effect on *Daphnia magna*, and the severity of these effects are based on the time of exposure to these additives and the concentrations at which the additives are used. Using these results, further studies should be performed on humans using the hypothesis derived from this study. Although humans should portray the effects found in this study, they may not because of the variations between the physical and genetic makeup of the two species.

Methods

To determine the health effects of food additives, the *Daphnia magna* were tested in four groups (control, MSG, sodium nitrite, and Quinoline yellow food color). Each food

additive was tested in four different concentrations (0.01%, 0.1%, 1%, and 2%). *D. magna* heart rate and mobility were measured as an indicator of toxicity. Five one-day-old *D. magna* were tested per group. The control group was left in spring water without any additives. The measurements for heart rate and mobility were performed after 30 minutes and overnight incubation with each food additive. The heart rate was measured by looking at *D. magna* through the microscope and counting how many beats occurred in 15 seconds. The results were multiplied by 4 to get the beats per minute (bpm). Lastly, to determine the results of mobility, the test container with *D. magna* was shaken and then observed to see if any *D. magna* moved within fifteen seconds. The results were entered into Excel and graphs were created. The results were analyzed by calculating the average heart bpm and standard deviation. The number of mobile *D. magna* was recorded by counting. The Excel data analysis tool ANOVA was used to determine if there was a significant effect due to any food additive. Once ANOVA determined that there was a significant effect due to food additive, a two-tailed, paired student t-test was performed to determine the significance of effects at each concentration of food additive in comparison to the control group. A p-value less than 0.05 was considered significant.

Acknowledgement

We thank Dr. Suman Verma for guiding and advising us throughout this project and Carolina Biological for providing us with the *Daphnia magna* as an ideal model system. Special thanks to Professor Bruce Blumberg from University of California, Irvine for advising and guiding us along this project and for giving us the opportunity to conduct our experiment in his lab. This research won first prize in the Orange County Science & Engineering Fair in the Toxicology Division and continued on to the California State Science Fair.

References

1. EFSA ANS Panel; Mortensen, A.; Aguilar, F.; Crebelli, R.; Di Domenico, A; Dusmund, B.; Frutos, M. J.; Galtier, P.; Gott, D.; Gundert-Remy, U.; et al. Re-evaulation of sodium nitrate (E 251) and potassium nitrate (E 252) as food additives. EFSA J. 2017, 15(6), 4787. DOI: 10.2903/j.efsa.2017.4787.
2. Lee, D.; Swan, C. K.; Suskind, D.; Wahbeh, G.; Vanamala, J.; Baldassano, R. N.; Leonard, M. B.; Lampe, J. W. Children with Crohn's Disease Frequently Consume Select Food Additives. Dig. Dis. Sci. 2018, 63(10), 2722-2728. DOI: 10.1007/s10620-018-5145-x.
3. Onuma, T.; Maruyama, H.; Sakai, N. Enhancement of Saltiness Perception by Monosodium Glutamate Taste and Soy Sauce Odor: A Near-Infrared Spectroscopy Study. Chem. Senses 2018, 43(3), 151-167. DOI: 10.1093/chemse/bjx084.
4. Shimada, A.; Cairns, B. E.; Vad, N.; Ulriksen, K.; Pedersen, A. M. L.; Svensson, P.; Baad-Hansen, L. Headache and mechanical sensitization of human pericranial muscles after repeated intake of monosodium glutamate (MSG). J. Headache Pain 2013, 14(1), 2. DOI:10.1186/1129-2377-14-2
5. Sharma, A.; Prasongwattana, V.; Cha'on, U.; Selmi, C.; Hipkaeo, W.; Boonnate, P.; Pethlert, S.; Titipungul, T.; Intarawichian, P.; Waraasawapati, S.; et al. Monosodium Glutamate (MSG) Consumption is Associated with Urolithiasis and Urinary Tract Obstruction in Rats. PloS One 2013, 8(9), e75546. DOI: 10.1371/journal.pone.0075546.
6. Zanfirescu, A.; Ungurianu, A.; Tsatsakis, A. M.; Nitulescu, G. M.; Kouretas, D.; Veskoukis, A.; Tsoukalas, D.; Engin, A. B.; Aschner, M.; Margină, D. A Review of the Alleged Health Hazards of Monosodium Glutamate. Compr. Rev. Food Sci. Food Saf. 2019, 18(4), 1111-1134. DOI: 10.1111/1541-4337.12448.
7. Bell, B. Food Dyes: Harmless or Harmful? https://www.healthline.com/nutrition/food-dyes#:~:text=What%20Are%20Food%20Dyes%3F,dyes%20are%20made%20from%20petroleum. (Jan. 7, 2017)
8. Cheeseman, M. A. Artificial Food Color Additives and Child Behavior. Environ. Health Perspect. 2012, 120(1), a15-a16. DOI: 10.1289/ehp.1104409.
9. Arnold, L E.; Lofthouse, N.; Hurt, E. Artificial food colors and attention-deficit/hyperactivity symptoms: conclusions to dye for. Neurotherapeutics 2012, 9(3), 599-609. DOI: 10.1007/s13311-012-0133-x.
10. EFSA ANS Panel; Mortensen, A.; Aguilar, F.; Crebelli, R.; Di Domenico, A; Dusmund, B.; Frutos, M. J.; Galtier, P.; Gott, D.; Gundert-Remy, U.; et al. Re-evaluation of potassium nitrite (E 249) and sodium nitrite (E 250) as food additives. EFSA J. 2017, 15(6), 4786. DOI: 10.2903/j.efsa.2017.4786.
11. Feelisch, M.; Akaike, T.; Griffiths, K.; Ida, T.; Prysyazhna, O.; Goodwin, J. J.; Gollop, N. D.; Fernandez, B. O.; Minnion, M.; Cortese-Krott, M.; et al. Long-lasting blood pressure lowering effects of nitrite are NO-independent and mediated by hydrogen peroxide, persulfides, and oxidation of protein kinase G1α redox signalling. Cardiovasc. Res. 2020, 116(1), 51-62. DOI: 10.1093/cvr/cvz202
12. Rosenbaek, J. B.; Pedersen, E. B.; Bech, J. N. The effect of sodium nitrite infusion on renal function, brachial and central blood pressure during enzyme inhibition by allopurinol, enalapril or acetazolamide in healthy subjects: a randomized, double-blinded, placebo-controlled, crossover study. BMC Nephrol. 2018, 19(1), 244. DOI: 10.1186/s12882-018-1035-x.

Author

Aditya Mahna is a student attending Troy High School who loves doing research and exploring new topics. He hopes to major in biology in college and continue investigating the effects of food and dietary substances on human health.

Ayush Mahna is a young scientist who enjoys the field of biology and exploring the effects of common diets on human health. He wishes to major in computer science in college to unravel biological mysteries through data analysis.

DOI: 10.36838/v3i1.1

Using Neuropeptide Y as a Marker to Track GABAergic Neurons in Rat Brains Prenatally Primed with Betamethasone

Akshara Koottala

New Rochelle High School, 265 Clove Rd, New Rochelle, NY, 10801, USA; aksharakoottala@gmail.com

ABSTRACT: Epilepsy is a common neurological disease with a strong genetic component. Epilepsy can be caused by the lack of GABAergic neurons which release γ-Aminobutyric acid (GABA), an inhibitory neurotransmitter responsible for regulating excitability in the central nervous system. It is not clear if the lack of these neurons in the cortex and striatum (two brain regions associated with several epilepsy syndromes) can be caused by prenatal exposure to a synthetic steroid, betamethasone. Therefore, we prenatally administered betamethasone to observe its effects on GABA production in rat brains. We used neuropeptide Y (NPY) as a marker for GABA to measure a change in GABA expression in the cortex and striatum of male and female rats. Results revealed that prenatal betamethasone exposure led to a significant decrease of NPY in the cortex compared to the saline-primed control. Further analysis of the cortex indicated a statistically significant sex differences, demonstrating lower GABA counts in female offspring. The striatum, however, did not show a significant difference. Ultimately, this decrease in NPY positive GABAergic neurons may make the offspring more susceptible to having seizures and developing epilepsy. The results of this study establish a link between genetics and the development of epilepsy in offspring.

KEYWORDS: Biology; Neuroscience; Epilepsy; Transgenerational Epigenetic Inheritance; Cortex; Striatum; GABAergic Neurons; Neuropeptide Y.

Introduction

Epilepsy is the fourth most common neurological disease today and it affects millions of people from all over the world and from every age demographic.[1] It is a chronic condition characterized by recurrent, unprovoked seizures which are defined as frequent changes in the electrical activity of the brain that occur without stimulus.[2] More than 25 epilepsy syndromes have been delineated that range in severity and seizure types, making it a spectrum of disorders.[1] Despite it being such a predominant disease, the etiology of epilepsy still remains a predominant issue in the medical field. Numerous studies have all concluded that the causes of epilepsy each reflect an underlying brain dysfunction.[3] In order to diagnose the cause of each specific form of epilepsy, recent studies have focused on neuronal activity in the brain controlled by the balance of neurotransmitters in the brain. These neurotransmitters, or chemical compounds responsible for communication between the neurons, ensure that cell excitability is regulated in order to prevent seizures. A decrease in expression of these neurotransmitters can cause an increase in spasms.[4] According to previous studies, stress is one of the main causes for a decrease in expression of neurotransmitters because it directly alters the epigenome, where production of neurotransmitters is regulated by gene expression. Similar to the human condition, stress in rats also can lead directly to alterations that affect neurotransmitter production. Researchers exploring the alterations made to the epigenome have found recent evidence that suggests there may be genetic predisposition to developing the disease.[5]

Betamethasone as a Model Stressor:

As mentioned before, a deficiency in neurotransmitters caused by stress may significantly contribute to occurrence of seizures, which are the hallmarks of epilepsy. Considering 75% of epilepsy begins during childhood, the developing brain is the most susceptible to epilepsy and the main reason could be the deficiency of neurotransmitters in the direct offspring of stressed mothers.[3] One method of causing stress and anxiety in these mothers is by directly injecting drugs called corticosteroids. Corticosteroids are steroid hormones synthetically made to be given by injection to start anti-inflammatory processes. One of the drugs that have yet to be thoroughly researched with regards to epilepsy is betamethasone, a synthetic corticosteroid. Severe stress or significant exposure to betamethasone during pregnancy can predispose the offspring to development of infantile spasms (also known as West Syndrome or epileptic spasms).[6] This is a form of epilepsy that predominantly occurs between 3 and 12 months. It is a catastrophic pediatric epilepsy with motor spasms, persistent seizures, mental retardation, and in some cases, autism.[7] Velisek *et al* 2007 developed a rat model of cryptogenic infantile spasms by using prenatal exposure to betamethasone combined with a postnatal trigger of spasms with N-methyl-D-aspartic acid (NMDA).[8] The general conclusion reached was that prenatal priming with betamethasone can lead to a deficiency in neurotransmitters, specifically GABAergic neurons. The lack of GABA neurons increased susceptibility of spasms and made the offspring more vulnerable to developing seizures and eventually epilepsy.

The Relationship between Neuropeptide Y and GABAergic Neurons:

GABAergic neurons release γ-Aminobutyric acid (GABA) which is the main inhibitory neurotransmitter in the cerebral cortex.[9] GABAergic inhibition allows for synchronization

DOI: 10.36838/v3i1.2

of activity in cortical networks, including gating of activity, controlling movements and dictating the manner in which activity flows.[10] It is a fundamental part of the brain because a blockade of GABA inhibition can lead to an increase in cell excitability and result in absence seizures with spike-and-wave discharges, eventually leading to epilepsy.[11] These GABA neurons carry out their functions together with neuropeptides like neuropeptide Y(NPY), which are small protein-like molecules (peptides) that are used by neurons to communicate with one another. NPY is the most abundant neuropeptide in the brain and serves as a marker for GABAergic neurons in the brain. It plays a major role in brain activity because it signals molecules that engage in many physiological functions.[12] NPY is crucial in the brain because a loss of these peptides signifies a decrease in GABA neurons which may disrupt the ability of the brain to filter incoming seizure activity. This eventually leads to neuronal injury and intractable seizures which can cause epilepsy.[13]

The two sections that have a dense NPY population and are associated with the development of epilepsy are the striatum and cortex. The striatum, a part of the basal ganglia, plays a significant role in facilitating voluntary movement, and consequently, is a major source of excitatory inputs and GABA neuron production. Similarly, the cerebral cortex is critical because the neuron activity in this region controls emotions, problem solving, critical thinking, the ability to plan, and the recognition of parts of speech.[14] The main focus of many epileptic studies is the neuronal activity in the cortex region, specifically neocortex, because its low activity is indicative of increased susceptibility to seizures, especially in newborn infants.[15] These two regions are extremely important because a recent study using a mouse model of childhood epilepsy showed that epilepsy can be triggered by impaired communication between the cortex and striatum.[11]

Goal:

There is a gap in research regarding whether the prenatal administration of the stressor drug, betamethasone, will positively or negatively affect the production of GABAergic neurons in the cortex and striatum regions. The purpose of this study was to determine the effect of prenatal treatment with betamethasone on GABAergic neuron expression in offspring by counting the NPY positive cells (marker for GABA) in the striatum and cortex. We hypothesized that prenatal exposure to betamethasone will decrease the GABAergic neuron count in the cortex and striatum.

Results and Discussion

GABAergic Count Based on Treatment:

All statistics in the study were done using two-way ANOVA with factors of sex (levels males and females) and prenatal treatment (levels saline and betamethasone). Images obtained from immunohistochemistry staining clearly show a decrease in the population of NPY in rat brains with prenatal treatment of betamethasone. The mean count of NPY-expressing cells within the cortex sections from the stressed rats treated with betamethasone was 26.676 NPY cells/mil pix (cells in the cortex standardized per 1 million pixels) whereas the average

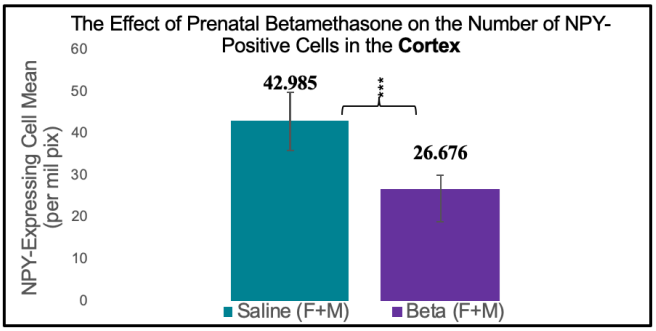

Figure 1: There is a significant decrease in the NPY Positive cells in the male and female group treated prenatally with betamethasone (shown in purple) compared to the control female brain treated prenatally with saline (shown in green) (***p<0001). This corresponds to the decrease in GABA neuron production in the offspring of stressed mothers treated with betamethasone.

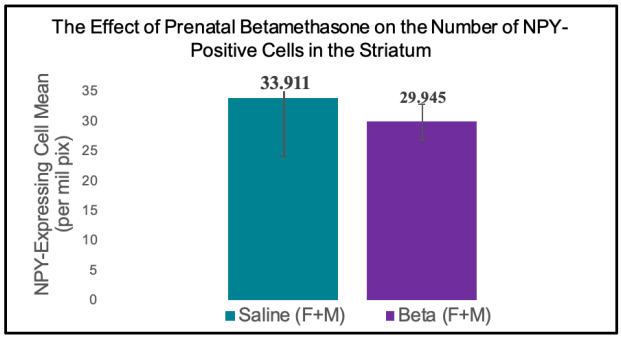

Figure 2: There is no significant decrease in the NPY-Positive cells in the male and female group treated prenatally with betamethasone (shown in purple) compared to the control female and male brain treated prenatally with saline (shown in green) (p=4295).

count in the saline/control model tissues, which did not receive the seizure-inducing treatment, was 42.985 NPY cells/mil pix (Figure 1). There was a statistically significant difference between the two treatment groups seen in the NPY count of the cortex region of the brain, as evidenced by the two-way ANOVA (p<.0001).

However, further statistical analysis revealed insignificant results in the striatum of the brain, where the mean count of NPY expressing cells in the experimental betamethasone group was 29.945 NPY cells mil/pix while the mean in the saline control was 33.911 NPY cells mil/pix (Figure 2). The two-way ANOVA test revealed there was no statistically significant difference between the two treatment groups seen in the NPY count of the striatum region of the brain (p=.4295).

Overall, the resultant deficiency of NPY in only one region, the cortex, of the experimental rat brain confirms the significant decrease in the expression of GABA neurons in the offspring of stressed mother rats (p<0.05) whereas the striatum did not show a significant decrease.

GABAergic Count Based on Sex.

Furthermore, an interaction two-way ANOVA analysis suggests a trend level difference between the presence of NPY-expressing cells between sexes in the cortex region of the brain, but not the striatum. Presence of NPY-expressing cells was significantly different among the two sexes in the cortex. Male brains had a greater amount of NPY markers in the cortex, with a mean count of 47.5 ctx/mil pix, than the cortex

DOI: 10.36838/v3i1.2

of the female group, with a mean cell count of 38.37 NPY cells/mil pix (Figure 3). Females had a statistically significant decrease in NPY expression because they are more sensitive and more vulnerable to reacting with the stressor (p=0.0235). Clearly, there is a significant decrease in NPY expression in females, indicating that they have a greater decrease in GABA production than males, and are consequently more likely to develop epilepsy. It is important to note that the treatment was not the cause for this decrease in NPY expression in females,

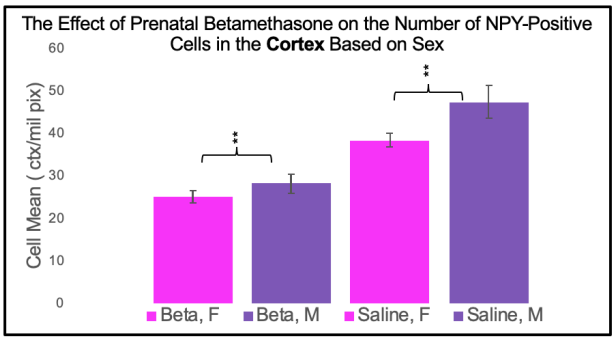

Figure 3: There is a significant decrease in the NPY-Positive cells in the cortex section of the female group (shown in pink) compared by the male group (shown in purple) in both treatment groups (**p=.0253).

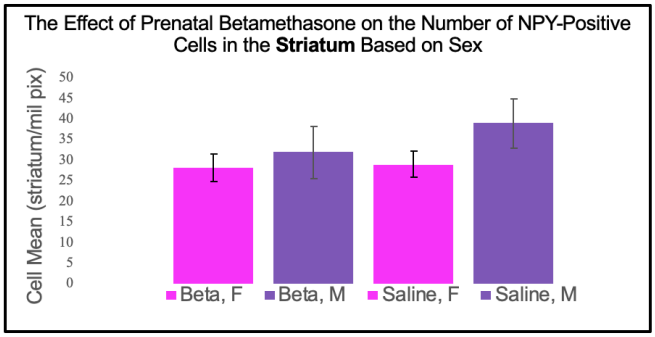

Figure 4: There is no significant difference in the NPY-Positive cells in the striatum section of either sex (p=.1782).

considering that the significant decrease is seen even in the control group treated with saline. The females had a decrease in NPY expression in the cortex region of the brain, regardless of the treatment.

However, the same statistical result was not seen in the striatum region of the brain (p=.1782). The striatum region did not show a difference in NPY expression based on sex nor based on treatment (Figure 4).

This study demonstrates that prenatal exposure to betamethasone is associated with postnatal decreased expression of NPY in only the neocortex and not the dorsolateral striatum. In addition, we found that the cortex region has a decreased expression of NPY in females, regardless of the treatment group. In other words, only the cortex region showed that there was a significant difference in treatment group of the rats (with a decrease seen in the stressed offspring prenatally treated with betamethasone) and a significant difference based on sex (with an overall deficiency of NPY expression in females only). The striatum, however, showed no significant difference in treatment groups or either sex.

A decrease in NPY in the cortex may be detrimental to the activity of the rat brain considering a decrease in NPY also indicates a decrease in GABAergic neurons. As mentioned before, a deficiency in GABA immediately results in the increase in excitability in all mammals. One possible explanation for this decrease in expression in the offspring is that the betamethasone directly regulates the fetal NPY expression and the severe stress directly caused a decrease GABA expression.

Transgenerational Epigenetic Inheritance.

Another interesting possible explanation that connects to previous studies regarding the same topic focuses on the epigenome, where GABA production is regulated. The epigenome is the cellular material that surrounds the genome that contain epigenetic "marks" which signal to genes when to turn on or off.[16] Environmental factors like diet, prenatal nutrition, and stress can all influence these epigenetic marks and make an imprint which passes to the next generation. This concept of transgenerational epigenetic inheritance can explain how stressed mothers can negatively influence the mental and physical development of the child. Thus, proving that the stress on the mother can change the epigenetic makeup of the brain, and these changes can have a negative effect on the direct offspring and future generations. Velisek *et al* 2006 conducted a study that used an animal model under stressful conditions to see how transgenerational inheritance can explain epilepsy being passed from mother to offspring.[17] Similar to the results of this study, Velisek's results showed the betamethasone stressor altered epigenomic function via post-translational modifications in the epigenome. This can mean adding or removing chemical tags that influence expression of GABA.[18] The betamethasone decreased the number of GABAergic neurons in the brain, without obvious physical effects on the mother. However, the consequence of the stressor was experienced by the offspring of the mother rat. The stress was transferred onto her offspring and decreased the number of GABAergic neurons in the younger generation's brain. Some changes may be even transmitted to the second generation of offspring, which can be addressed in the future. This decrease of GABAergic neurons seen in both studies can be detrimental to the offspring because they can no longer finely regulate cell excitability, and may become more susceptible to having seizures and more likely to develop epilepsy. Essentially, the prenatal stressor betamethasone may have damaged the epigenome in both the mother and offspring.

The results of this study represent a significant advance over previous studies which focused on the role of prenatal exposure to betamethasone and NPY expression in anxiety.[7] This study fills a gap in previous research by specifically looking at the effect of prenatal betamethasone on the production of GABAergic neurons in the neocortex and the striatum that would be consistent with susceptibility of the offspring to spasms. Statistical analysis between the two treatment groups (rats prenatally exposed to saline being the control, while rats prenatally exposed to betamethasone as the experimental) show the betamethasone caused a decrease in NPY, indicating a decrease in GABAergic neurons.

This study concluded that the cortex only showed a significant difference in GABA production based on treatment group and sex, whereas the striatum region showed none. This result has been supported by previous studies that also link epilepsy with the cortex region of the brain. In fact, this can be explained by the fact that focal epileptic seizures are linked to abnormalities in three main brain regions: ipsilateral piriform cortex, temporal neocortex, and ventromedial prefrontal cortex.[19] All three of these regions are part of the cortex region of the brain. This may be due to their enhanced sensitivity to prenatal betamethasone exposure. The sensitivity can be determined by differential genetic composition that regulate the concentration of glucocorticoid receptors. Glucocorticoids act via a number of direct and indirect routes that influence the developing epigenome. A change in concentration of these receptors can make offspring more vulnerable to changes caused by a stressor.[20] Significant decrease in this neuronal population may contribute to enhanced propensity to development of spasms in the model of infantile spasms.

Interestingly, the study also found that sex plays a major role in the diagnosis of epilepsy. It found that females have a greater deficiency in GABA production, as evidenced by the significant lack of NPY-positive cells in females when compared to males. This can possibly be explained by the fact that females are more vulnerable to accepting the change the stressor induces. The alteration acquired from the mother is stronger in the daughter's cells and consequently, has the strength to decrease GABA expression in female cells. Thus, these results can support the conclusion reached in a previous study done by Christensen *et. al* 2005[21] that found more women than men were diagnosed with idiopathic generalized epilepsy in two epilepsy populations.

These results can prove to be useful when applied to human treatment of health issues. Previous studies have shown that repeated antenatal administration of betamethasone is frequently used as a life-saving treatment in obstetrics. In fact, the trend in clinical practice has become to repeat the administration of synthetic corticosteroids, like betamethasone, in pregnant women at risk for premature delivery. However, no study has looked into the beneficial or detrimental effects of single antenatal corticosteroid administration. This study can serve as a starting point for future research considering how prenatal betamethasone can act as a stressor and lead to an increased likelihood of developing certain types of epilepsy. To put it simply, this research offers a possible explanation for the cause of epilepsy in patients. Other areas of future research can possibly look into how transgenerational inheritance of this stress can affect generations beyond the direct offspring, perhaps focusing on the grandchildren of mother rats. As mentioned before, it is definitely a possibility that sex can be a significant factor that can affect the GABAergic production in stressed rats.

Future Research .

Although the results of this study show significant progress from previous studies, there are ways to continue this study that can provide further evidence to confirm the link between epilepsy and genetics. In this experiment, the cortex and striatum were the only regions considered for GABA expression count, which may obscure the effects of betamethasone on other regions of the brain. Therefore, an experiment might be designed to examine the effect of betamethasone on GABA count in the hypothalamus region of the brain. Exploring hypothalamus region allows us to explain why it is a region that can cause many types of seizures in people with epilepsy and can progress the current study. In addition, the current study analyzes the brains of stressed rat mothers' direct offspring, but it should be investigated whether the decrease in GABA count is also seen in the grandchildren of the stressed mothers. This can help confirm that epilepsy is a hereditary disorder because of alterations made to the mother's epigenome due to stress.

■ Conclusion

Prenatal exposure to betamethasone directly leads to decreased expression of NPY in the cortex of female and male brains. Since NPY serves as the marker for GABAergic neurons, a decrease in NPY indicates a decrease in the GABAergic neuron population in rats that were offspring of stressed mother rats. Ultimately, this indicates that the deficiency in GABAergic neurons may be the reason for impaired regulation of cell excitability, which increases the susceptibility to seizures. Prenatal betamethasone acted as a stressor and led to a decrease in GABA neurons in only the cortex region (not the striatum), so the hypothesis is refuted. This study expands on previous research, which primarily focused on repeated administration of betamethasone that actually proved to be beneficial to the mother rat. This study shows that single administration of betamethasone will induce great stress on the mother rat and will cause a decrease the production of GABA which is then passed onto the offspring. Chachua *et al* 2011[4] established a rat model in her research that supports the conclusions of this study considering she was able to conclude that prenatal stress leads to an increase in spasms, which is explained by the decrease in GABA seen in this study. This research also proposes an explanation as to why the risk of epilepsy among people who have parents or siblings with the disorder is about 4% to 8%, whereas the risk in the general population is 1% to 2%.[22] The possible explanation is transgenerational epigenetic inheritance considering this study showed that stressed mothers give birth to epileptic offspring due to the modifications made in the epigenome that ultimately cause a decrease in GABA expression.

■ Methods

Overview .

In order to see if one dosage of betamethasone would negatively affect the offspring, NPY was used as a marker to indicate either a decrease or increase in GABA neuron production. Since NPY is the marker for GABA, an increase of NPY signifies an increase in GABA neurons and a decrease in NPY signifies a decrease in GABA.

Preparing the Brains .

The brains used in this experiment were prepared by the mentor (Figure 5A). For the experimental group, the mentor injected the mother rat with prenatal betamethasone (2x 0.4 mg/kg in 1 ml/kg of saline on gestational day 15; 08:00 and

DOI: 10.36838/v3i1.2

18:00), while the control group was injected with the saline. The experimental brains will be referred to as prebeta brains (short for prenatal betamethasone). The control brains will be referred to as presaline brains. The litter pups were sacrificed using euthanasia, and the brains were dissected and collected by the mentor. These brains were dissected from the rat bodies and preserved in a matrix solution in July 2019 and were kept in a -80°C freezer for further use. Brains from both sexes of the two groups were gathered: one male prebeta, one male presaline, one female prebeta and one female presaline. These brains were perfused in a matrix solution and kept in a -80°C freezer for future usage by the student when cutting.

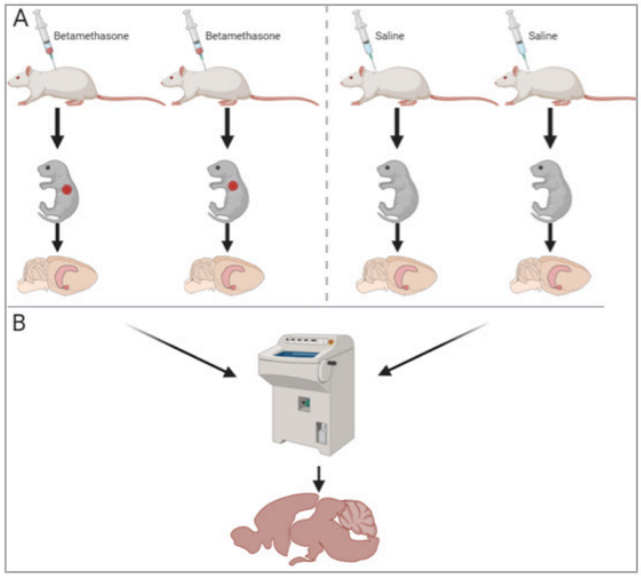

Figure 5: (A) Mentor created experimental and control group by injecting betamethasone and saline perspective and dissected brain out of newborn. (B) Student cut brains using cryostat to produce sagittal cuts of tissue.

Cutting the Brains .

First, the tissue from the four rat brains (two experimental, two control) had to be collected in order to stain for neuropeptide Y. The tissue was acquired by using a cryostat, a machine capable of cutting very fine slices of frozen tissue (Figure 5B). Four brains were cut in total: male prebeta, male presaline, female prebeta and female presaline. The purpose was to have parallel data, making analysis easier and more consistent to compare. The brain was set up by gluing it down onto a steel holder using a matrix solution, which ensured the brain would be held in place. While waiting for that to freeze, the blade (which was in the freezer) was set up and positioned at an angle to get a smooth cut. The cryostat was set to cut slices of 40 micrometers, using the sagittal cut (cutting parallel with the plane of brain symmetry). Each slice of tissue was carefully picked up with a paintbrush and transferred into well plates filled with phosphate-buffered saline (PBS) to preserve and clean the tissue. The tissue collected in well plates was later used for immunohistochemistry. However, every fifth slice was transferred onto a gelatin microscope using the PBS solution to make it stick to the slide. These slides were used later for cresyl violet, a general staining technique for histological overview of the structures.

Cresyl Violet .

Some of the brain tissue can be folded and damaged. In order to have a reference and identify specific sections of the brain when scanning and analyzing the experimental tissue, the tissue that was collected onto gelatin microscope slides was used for cresyl violet. This is a process in which the tissue is generally stained purple to identify specific parts and structures of the brain when scanning and analyzing the experimental tissue. The slides with the fresh tissue were left overnight to dry. In order to clean slides, the tissues first had to be put into xylene for five minutes, followed by additional xylene for another five minutes. Then slides were transferred into 100% alcohol for three minutes, then 95% alcohol for three minutes and then 75% alcohol for three minutes. The purpose of this procedure is not only to clean and sterilize the tissue but dehydration, lipid removal and rehydration, which are all necessary for proper staining. The slides were then placed in cresyl violet for three minutes, allowing the tissue to be stained a purple color and the alcohol process was repeated to rinse the tissue.

Immunohistochemistry .

The process of immunohistochemistry (IHC) was used to stain the tissue for a specific antigen, using a corresponding antibody as a marker (Figure 6).[23] The tissues that were collected in the well plates were washed with PBS three separate times, with ten minutes on the Rotoshaker (multi-action platform which gently shakes the tissues in the PBS) in between each wash. These washes ensured the tissues were cleaned and rehydrated with buffer solution. After washing and cleaning tissues, the blocking buffer was prepared using normal goat serum, BSA (bovine serum albumin), PBS and triton, which made the membranes in the tissue permeable for the antibody to enter. After letting it sit for 90 minutes, the blocking buffer made sure to prevent non-specific binding and ensured only the attachment on the NPY antigen. Once it was removed from the tissue, the primary antibody, anti-NPY (the primary antibody at a 1:1000 concentration) was left incubating the tissue for 3 nights in order to tag the NPY antigen.

After the three nights, day 2 of the IHC process began by removing the primary antibody and washing the tissue three separate times in PBS for ten minutes each. The secondary antibody was diluted in biotinylated anti-rabbit serum, BSA and PBS. with a concentration of 1:200. As the tissue incubated in this solution for 60 minutes, it tagged onto the primary antibody and aided in marking the NPY antigen. Following the incubation with the secondary antibody, the avidin-biotin (AB) solution was prepared with 1:1:2 concentration and PBS. After another 3 washes with PBS, the tissues were incubated in the AB solution for 60 minutes in order to bind to the biotin on the secondary antibody. Lastly, the tissues were washed three times again with PBS and were stained with diaminobenzidine (DAB), a general brown stain that binds to the avidin and made the primary antigen (NPY) molecules visible so that one can count each NPY-positive cell.

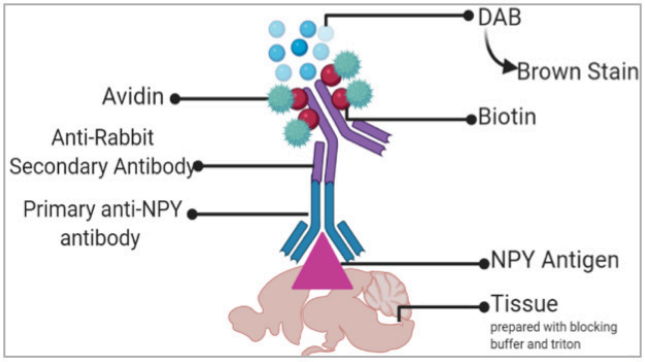

Figure 6: Process of immunohistochemistry includes layers of components interacting to stain a single antigen.

Mounting and Cover Slipping .

In order to view the stained tissues, they were transferred from the well plates onto 2% gelatin microscope slides using PBS and camel-hair paint brushes. Each group produced 4 slides of tissue (with roughly 5 slices per slide). In total, there were 82 slides. The tissues on these slides were preserved by using a cover slip made of glass that sealed off the tissue and ensured no bacteria/debris contaminated it. This process, referred to as cover slipping, involved using xylene (to clean the slides) and Permount (acting as a glue to stick coverslip onto the slide) in order to seal the slide and prevent any debris as well as air from entering.

Scanning Slides .

Before viewing the slides under the fluorescent light microscope, the slides must be cleaned using a blade to scrape excess dirt and washed with Permount and ethyl alcohol to clean. The slides were viewed at 10x magnification, specifically looking at the cortex and striatum regions of the brain to view the GABA neurons indicated by dark spots in the tissue. High quality snapshots were taken of the tissue using Olympus CellSens Dimension software on computer. Using a process called stitching, multiple magnified shots of the tissue were matched together to create a bigger 4x1 or 3x1 picture of the entire (cortex and striatum) region of the brain.

Data Analysis .

The images gathered from microscope scanning were analyzed using Fiji software. This program counted the GABA neurons in the cortex and striatum region of the brain. This process was carried out by creating a digital window for a specific section of each tissue with specific dimensions. Everything surrounding the window was then erased, leaving behind only the area inside the window to count NPY positive cells. The area measurement for the window was in pixels and the same measurement was used to make the same digital window for every tissue, which made sure that the data was equally distributed. These boxes highlighted the most concentrated of NPY positive cells which allows each individual dark spot to be counted. Each dark spot signified the presence of an NPY positive cell that was tagging onto a GABA neuron (Figure 7). All statistics in order to find the mean expression of NPY-positive cells across all four brains were transferred onto a Google Excel spreadsheet, which, included the brain group, section of the brain, the area of the section, and the count of neuron. Statistical analysis was done by the mentor who ran the two-way ANOVA tests that provided a p-value. The p-value was used to determine whether there was a statistically significant difference between the different brain tissues. A p-value less than or equal to .05 confirmed the data showed a statistically significant difference.

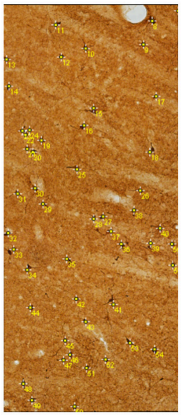

Figure 7: NPY positive cell count (56) of Male Striatum treated with betamethasone.

Acknowledgement

I am truly grateful for the aid from my mentor, Dr. Libor Velisek at New York Medical College who made the success of this project possible. I was lucky enough to have this opportunity granted by Dr. Velisek and his tremendous guidance made the completion of this project possible. In addition, I would like to thank my science research teacher, Jeff Wuebber, for his dedication and guidance with this report.

References

1. England M.J.; Liverman C.T.; Schultz A.M.; Strawbridge L.M. Epilepsy across the spectrum: Promoting health and understanding. Epilepsy & Behavior 2012, 25, 266–276.
2. Epilepsy Foundation Home Page. https://www.epilepsy.com/learn/about-epilepsy-basics/what-epilepsy (accessed August 14, 2019).
3. Stafstrom, C. E.; Carmant, L. Seizures and Epilepsy: An Overview for Neuroscientists. Cold Spring Harbor Perspect. Med. 2015, 5(6), a022426.
4. Chachua, T.; Yum, M.-S.; Velíšková, J.; Velíšek, L. Validation of the rat model of cryptogenic infantile spasms. Epilepsia 2011, 52(9), 1666–1677.
5. NYU Langone Medical Center / New York University School of Medicine. Largest study of epilepsy patients ever conducted reveals new and surprising genetic risk factors, 2013. ScienceDaily. www.sciencedaily.com/releases/2013/08/130812103004.html (accessed June 30, 2020).
6. Yum, M.S.; Chachua, T.; Velíšková, J.; Velíšek, L. Prenatal stress promotes development of spasms in infant rats. Epilepsia 2011, 53(3), e46-e49.
7. Price, M. G.; Yoo, J. W.; Burgess, D. L.; Deng, F.; Hrachovy, R. A.; Frost, J. D.; Jr Noebels, J. L. A triplet repeat expansion genetic mouse model of infantile spasms syndrome, Arx(GCG)10+7, with interneuronopathy, spasms in infancy, persistent seizures, and adult cognitive and

DOI: 10.36838/v3i1.2

behavioral impairment. J. Neurosci. 2009, 29(27), 8752–8763.
8. Velísek, L.; Jehle, K.; Asche, S.; Velísková, J.; Model of infantile spasms induced by N-methyl-D-aspartic acid in prenatally impaired brain. Ann. Neurol. 2007, 61(2), 109-119.
9. Khazipov, R.; GABAergic Synchronization in Epilepsy. Cold Spring Harbor Perspect. Med. 2016, 6(2), a022764.
10. Trevelyan, A.J.; Muldoon, S.F.; Merricks, E.M.; Racca, C.; Staley, K.J.; The role of inhibition in epileptic networks. J. Clin. Neurophysiol. 2015, 32(3), 227-234.
11. Miyamoto, H.; Tatsukawa, T.; Shimohata, A.; Yamagata, T.; Suzuki, T.; Amano, K.; Mazaki, E.; Raveau, M.; Ogiwara, I.; Oba-Asaka, A.; Hensch, T. K.; Itohara, S.; Sakimura, K.; Kobayashi, K.; Kobayashi, K.; Yamakawa, K. Impaired cortico-striatal excitatory transmission triggers epilepsy. Nature communications 2019, 10(1), 1917.
12. Velíšek, L.; Shang, E.; Velíšková, J.; Chachua, T.; Macchiarulo, S.; Maglakelidze, G.; Wolgemuth, D. J.; Greenberg, D. A. GABAergic neuron deficit as an idiopathic generalized epilepsy mechanism: the role of BRD2 haploinsufficiency in juvenile myoclonic epilepsy. PloS one 2011, 6(8), e23656.
13. Velísková, J.; Velísek, L. Beta-estradiol increases dentate gyrus inhibition in female rats via augmentation of hilar neuropeptide Y. J. Neurosci. 2007, 27(22), 6054–6063.
14. The Revisionist. (2018, November 19). The Role of the Prefrontal Cortex in our Cognitive Function. The Revisionist. https://therevisionist.org/reviews/role-of-prefrontal-cortex-in-cognitive-function/ (accessed December, 2019).
15. Clynen, E.; Swijsen, A.; Raijmakers, M.; Hoogland, G.; & Rigo, J. M. Neuropeptides as targets for the development of anticonvulsant drugs. Mol. Neurobiol. 2014, 50(2), 626–646. https://doi.org/10.1007/s12035-014-8669-x.
16. Cloud, J. Why Your DNA Isn't Your Destiny. Time Inc, 2010. http://content.time.com/time/magazine/article/0,9171,1952313,00.html (accessed 10 Jul. 2020).
17. Velíšek, L. Prenatal Exposure to Betamethasone Decreases Anxiety in Developing Rats: Hippocampal Neuropeptide Y as a Target Molecule. Neuropsychopharmacology 2006, 31(10), 2140–2149.
18. Kobow, K.; Reid, C.A.; Vliet, E.A.; Becker, A.J.; Carvill, G.L.; Goldman, A.M.; Hirose, S.; Lopes-Cendes, I.; Khiari, H.M.; Poduri, A.; Johnson, M.R.; Henshall, D.C.; Epigenetics explained: a topic "primer" for the epilepsy community by the ILAE Genetics/Epigenetics Task Force, 2020. Wiley Online Website. https://onlinelibrary.wiley.com/doi/full/
19. Pedersen, M.; Curwood, E. K.; Vaughan, D. N.; Omidvarnia, A. H.; Jackson, G. D. Abnormal Brain Areas Common to the Focal Epilepsies: Multivariate Pattern Analysis of fMRI. Brain Connectivity 2016, 6(3), 208–215.
20. Moisiadis, V.; Matthews, S. Glucocorticoids and fetal programming part 2: mechanisms. Nat. Rev. Endocrinol. 2014, 10, 403–411.
21. Christensen, J.; Kjeldsen, M.J.; Andersen, H.; Friis, M.L.; Sidenius, P. Gender differences in epilepsy. Epilepsia 2005, 46(6), 956-960.
22. Institute of Medicine (US) Committee on the Public Health Dimensions of the Epilepsies, England, M.J.; Liverman, C.T.; Schultz, A.M.; Strawbridge, L.M. Epilepsy Across the Spectrum: Promoting Health and Understanding. Washington (DC), National Academies Press (US) 2012. https://doi.org/10.17226/13379 (accessed on August 14, 2020)
23. Taylor, C. R.; Shi, S.; Barr, N. J. Techniques of Immunohistochemistry. Diagnostic Immunohistochemistry 2011,1-41..

Author

Akshara Koottala, the author of this paper and conductor of this research, is a rising senior at New Rochelle High School. She is interested in neuroscience and is passionate to establish a possible link between genetics and epilepsy. She plans to major in biology at the university she will attend.

The Electrochemical Reduction of CO_2 into Ethanol Utilizing Novel Doped Cu/SiO_2 Nanoparticles and Electrolytes

Ashish Pothireddy, Clarence Ramirez, Sulav Regmi

Governor's School at Innovation Park, 9485 Innovation Dr, Manassas, Virginia, 20110, USA; clarencegr21@gmail.com

ABSTRACT: With the growing negative anthropogenic impact of the 21st century, it has become imperative to devise alternative means of fuel synthesis. One promising method is the electrochemical reduction of carbon dioxide to ethanol using copper nanoparticles, as it offers a direct conversion of a greenhouse gas to a fossil fuel. However, this process is limited by steep overpotentials, low Faradaic efficiency, and corresponding low selectivity for ethanol. This study aimed to provide a comprehensive overview of factors involved in the reduction reaction. The first phase of this study developed a novel method to produce doped copper nanoparticles, at a size of 2-5 nanometers (based on photon correlation spectroscopy results). The second phase determined that sodium chloride was the most efficient electrolyte at a concentration of 0.4 M. The third phase of this study determined that carbon and lead was the best cathode-anode combination based on consistent high current response at the necessary overpotential of 1 V. The fourth phase of this study utilized Self-Consistent Field calculations, a quantum computational method of approximating the Fermi energy and total energy of a system, to determine the silica supported copper nanoparticle graphene electrode would enable selective reduction to ethanol. This study's novel nanoparticle synthesis methodology is widely applicable to many fields and yields effective particle sizes. This synthesis methodology coupled with analysis of significant factors make the electrochemical reduction of carbon dioxide a more feasible means of fuel synthesis.

KEYWORDS: Electrochemistry; Reduction; Catalyst; Copper; Nanoparticles.

Introduction

Mass carbon emissions in the past century have paved the way for the environmental crisis humanity is currently facing. The rate at which carbon is being emitted has been increasing rapidly on an annual basis, resulting in environmental issues such as rising sea levels, increased global temperature fluctuations, air quality degradation, and ocean acidification. The most prominent facilitator of carbon emissions has been the use of fossil fuels as a primary source of energy. According to the Environmental Protection Agency, it accounted for 65% of the total global greenhouse gas emissions in 2014, with the percentage having grown since then.[1] Regarding fuel, the end goal is to decrease the net emissions of carbon generated from fuel consumption. One promising method is to synthesize ethanol, a conventional fuel for motor vehicles, from captured carbon dioxide. As opposed to retrieving fossil fuels from the earth and burning it to expel additional carbon dioxide into the atmosphere, this synthesized fuel would be comprised of carbon dioxide that was previously present in the atmosphere, so when burned, it would emit no additional carbon dioxide (making the fuel inherently carbon neutral). Fortunately, scientists have stumbled across an innovative method of synthesis that may prove applicable. While being a process still in its infancy, this method of fuel synthesis might be the key to an effective production of a carbon neutral fuel. A team of scientists at the Department of Energy's Oak Ridge National Laboratory took "carbon dioxide, a waste product of combustion," and essentially pushed the "combustion reaction backwards with very high selectivity to form a useful fuel."[2] The process entails a sample of carbon dioxide dissolved in water to be exposed to a nitrogen-doped copper nanoparticle catalyst with an electrode input of electrons to induce an electrochemical reaction that directly converts the carbon dioxide into ethanol.[3] When delving deeper into their methodology, some inconclusive factors appear to foster room for improvement. They explicitly state that the "overpotential (which might be lowered with the proper electrolyte, and by separating the hydrogen production to another catalyst) probably precludes economic viability for this catalyst."[3] This begs the question, what optimizes the utilization of copper nanoparticle catalysts in the conversion of carbon dioxide into ethanol through electrochemical reduction on the basis of distinct dopants and electrolytes?

Developments in the electrochemical reduction of carbon dioxide (CO_2) to hydrocarbon products have given rise to its application towards the innovation of modern fuel synthesis, especially for the purpose of environmental conservation. Today's research is quite broad and neglects to tackle various components that could serve pivotal in improving the efficiency of this process. Non-catalytic variables such as the role of doping and the role of differing electrolytes are gaps in research. Investigating the synergistic properties of these variables could bring to light optimizations that have yet to be discovered. This literature review outlines the current state of research in this field and the key aspects that remain the foundation of this investigation.

Ethanol Production from CO_2:

In investigating the procedures for the electrochemical reduction of CO_2 and the potential for ethanol production, it is imperative to study preceding studies and breakdown the various elements that can be applied and tested.

DOI: 10.36838/v3i1.3

The Department of Physics within the Technical University of Denmark published in *Energy* and *Environmental Science* the article "How Copper Catalyzes the Electroreduction of Carbon Dioxide into Hydrocarbon Fuels." Their research focused on the integration of density functional theory calculations to delve into the specifics behind how copper is uniquely able to convert CO_2 into hydrocarbons and the implications of it towards [photo-]electrochemical means of fuel synthesis. Their major gap in research is the high overpotential required for the conversion process that is otherwise efficient in quantity and selectivity through the utilization of copper catalysts. The effectiveness of copper in the reduction of CO_2 using a copper electrode was determined by applying voltage to dissolved CO_2 in water and quantifying the various hydrocarbons products. Their study documented "product distribution and total current produced as a function of applied potential (versus reversible hydrogen electrode, RHE) in the electrochemical reduction of CO_2 at a copper electrode in 0.1 M KHCO3 (pH 6.8) at 18.5 °C."[4] Since copper catalysts commonly have high selectivity for methanol production from a CO_2, CO, and H_2 mixture, the researchers' discovery that methanol was not the dominant hydrocarbon product demonstrated a discrepancy between conventional electrochemical thought and the implementation of copper catalysts. The significance of a copper catalyst electrode, specifically in the electrochemical reduction of CO_2, is further supported by the Department of Applied Chemistry at Chiba University in their article "Selective Formation of C2 Compounds from Electrochemical Reduction of CO_2 at a Series of Copper Single Crystal Electrodes." Their methods described a spherical copper crystal being attached to a copper stick (made from 99.999999% copper) using the Bridgeman method, which employs a graphite crucible after the position of the crystal was deemed sufficient with the use of the X-ray Laue back reflection method.[5] The results of the study include that the formation rates of the gas products remaining "virtually constant."[5] The researchers also state that a higher selectivity in the reduction reaction is desirable for practical applications of the concept, such as future reduction into ethanol.

Copper Silicon Dioxide Nanoparticles:

The catalyst utilized in the electrochemical reduction of CO_2 into ethanol provides the novelty of such a unique fuel synthesis. Based on research conducted by the Oak Ridge National Laboratory, experimentation of metal-based catalyst in the context of electrochemical reduction has indicated copper as the most electrochemically promising catalyst, having been able to generate over 30 different hydrocarbons.[3] Copper has a unique set of characteristics that allows it to serve as an effective catalyst: abundance, conductivity, and corrosion resistance. However, the limitation of copper nanoparticles as a catalyst is that they produce an overwhelming range of resultant hydrocarbons when ethanol alone is the desired product. According to the *Journal of the American Chemical Society*, the moderate binding energy of copper and carbon monoxide, a "major intermediate during the [reduction] reaction," prevents both high selectivity and faradaic efficiency for desired resultant products.[6] Corresponding high overpotentials and low selectivity restrict wide application of this reduction resultant products.[6] Corresponding high overpotentials and low selectivity restrict wide application of this reduction reaction into fuel conversion. There are developments in the works that seek to limit these obstacles of overpotential while also attempting to increase the selectivity of C_2 and C_3 compounds. The Key Laboratory for Green Chemical Technology of the Ministry of Education in China sought to solve these issues by supporting the copper nanoparticles with silica. Their findings indicated that silica support did achieve the "coexistence of CuO and Cu^+" and generated such catalytic activity to favor ethanol as the output.[7] Though in its stages of infancy, the correlation between a greater selectivity for ethanol and silica supported copper nanoparticles provide insight into lowering overpotential and increasing selectivity. Furthermore, an article in Physical Chemistry Chemical Physics titled "Electrochemical CO_2 Reduction on Cu_2O-Derived Copper Nanoparticles: Controlling the Catalytic Selectivity of Hydrocarbons" sought to achieve higher levels of selectivity for ethanol. The researchers noted that a stable and robust cathode material that could selectively convert CO_2 and H_2O to useful products at low overpotentials does not yet exist (current methods of electrochemical reduction have high overpotentials and involve rapid degradation of the catalytic activity). The researchers sought to quantify the performance of "electrochemically produced Cu_2O coated copper substrates towards CO_2 reduction" in terms of "selectivity, activity, and long-term stability."[8] Thermally produced thick oxide films were reported to decrease the overpotential of reduction without losing activity after an extended period of electrolysis.[8]

Sol-Gel Synthesis Procedures:

Synthesis procedures for copper nanoparticles vary based on chemical needs, but one procedure stands out due to its efficiency and cost-effectiveness: the sol-gel synthesis method. A study published in the International Journal of Research in Engineering and Innovation mixed glacial acetic acid with hydrated copper chloride, and then added highly concentrated sodium hydroxide to form a precipitate. The study noted that they were able to produce copper oxide nanoparticles at 16 nm, with reaction time and the concentration of the base playing a major role in the size of the nanoparticles.[9] While this method does in fact generate fine nanoparticles that are easily applicable to the electrochemical reduction of carbon dioxide, this method lacks the critical silica support necessary for high selectivity for ethanol. A study published in *Chem. Mater.* chose to mix sodium hydroxide (4 mol/L) with copper nitrate (0.5 mol/L) and then add aqueous silica solution to the precipitate to produce a gel. The gel was then aged, filtered, and washed to isolate the catalyst. The addition of silica gel was to provide critical stability for the microparticles.[10] A study published in Pharmaceuticals similarly documented the benefits of the sol-gel technique. The study noted that the sol-gel technique ensured "rigorous control of the nanoparticle size," while optimizing the dimensions of the resultant nanoparticles.[11] Altogether, the sol-gel synthesis procedure is both cost-effective and efficient in that it produces uniform nanoparticles with consistent morphology.

DOI: 10.36838/v3i1.3

Role of Doping in Catalyst Production:

The process of doping entails applying various atoms that function as impurities into the composition of a catalyst substance. Doping a substance can have varying effects, but predominantly results in the formation of a lattice shape structure of a substance used in a reaction. This can cause the substance to become significantly more conductive, where even some doped catalysts have the potential to increase conductivity by a factor of 10^6.[12] With the foundation of nitrogen-doping (n-doping), new molecules within the catalyst will possess 5 outer elections. Its applicability is apparent in the fact that extra electrons remain unbound by the crystalline structure of the catalyst, transferring freely over the conduction band of the molecule, reducing the band gap that is required to overcome. Though this characteristic implies efficiencies in the electrochemical reduction process, researchers from the University of Qingdao have noted molecules that "occupy at the edge or defect sites" of n-doped catalyst as having reduced the electro-catalytic effect at the center of the reaction.[13] There is much potential in doping the catalyst to increase efficiency and productivity in the electrochemical reduction of CO_2 into ethanol, meriting alternative dopants to be further investigated.

Role of Electrolytes in Electrochemical Reduction:

Electrolytes are key components to the process of electrochemical reactions. The article "Electrolyte Effects on the Electrochemical Reduction of CO_2" reviewed the influence of electrolytes on the electrochemical reduction of CO_2 and sought to uncover insights on ways to lower overpotential and boost selectivity. Accordingly, the researchers of the study mention that the "addition of salts to form the aqueous electrolyte can induce a salting out effect, further lowering CO_2 solubility in the Electrolyte," which induces mass transfer limitations in instances of an operation at higher current densities.[14] In cases where gas is diffused in the set-up, a faster diffusion of CO_2 is achieved in the presence of electrolytes near areas of an electrocatalyst surface, sustaining higher current densities. Additionally, they discuss that pH dictated by electrolytes is a critical parameter in controlling the electrocatalytic selectivity due to the formation of OH. It was noted that "local" pH also plays an important role in the electrochemical reduction of CO_2 to hydrocarbons on copper electrodes. While the formation of methane was found to be pH sensitive, the formation of ethylene was found to be pH insensitive, suggesting separate pathways for the production of these hydrocarbons."[14] This provides information on how selectivity can be achieved through the differentiation of pH based on electrolytes. Furthermore, in "High-Selectivity Electrochemical Conversion of CO_2 to Ethanol using a Copper Nanoparticle/N-Doped Graphene Electrode" from the journal Chemistry Select, the electrochemical scientists comment on electrolytes within their experimentation on CO_2 reduction and ethanol production through the use of copper nanoparticles and a nitrogen-doped graphene electrode. They reflect on their findings and state overpotential "might be lowered with the proper electrolyte, and by separating the hydrogen production to another catalyst."[3] This provides an inherent gap in research that can be pivotal in generating a feasible and effective means of ethanol production from the reduction of CO_2.

Software Analysis of the Electrochemical Reduction of CO_2:

For analysis into thermodynamic qualities and ground states of electrochemical systems, there exists two forms of software-based research: density functional theory (DFT) and the chemical process simulators. DFT offers a set of functionals that utilize quantum computing to generate approximations of many-body systems. Singh *et al.*, researchers at the National Laboratory in Berkley, produced a DFT model to answer several key questions for the electrochemical reduction of carbon dioxide using silver particles. The researchers modeled their system by constructing a 3 x 3 x 4 atom cell which represented their electrode surface. Singh *et al.* performed first free energy calculations with 72 explicit water molecules and then replaced 36 of them with an implicit electrolyte. The researchers "treated [the solvent] as a continuum dielectric" and analyzed it with a "linearized Poisson-Boltzmann model." They finally calculated the electrode potential with the resultant Fermi energy. The analysis of the free energy profiles of the CO_2RR (CO_2 Reduction Reaction) and HER (Hydrogen Evolution Reaction) noted that the first electrons transferred to H_2O split the molecule into H and OH^-. The second electron acted similarly but joined the two H atoms to produce H_2. The reaction mechanisms indicated that CO_2 is reduced to COOH which is then reduced to CO using H and H_2O.[15] In Huang J. *et al.*, researchers at the Laboratory of Nanochemistry for Energy in Switzerland, utilized Quantum Espresso (QE) and Environ (a module extending the functionalities of QE) to study the degradation of the copper nanoparticles under operation conditions.[16] Huang J. *et al.* first modeled their base nanoparticle and then modified certain parameters to determine variances in the potentials provided.[16] The researchers utilized this methodology to analyze the overpotentials and formation energies of the reduction reaction. The researchers continued their quantum calculations by determining interface energies through first developing copper supercells. They then tested interface energies over a range of potential differences. Their results indicated that the adsorption of either H atoms or CO molecules on the crystal surface would degrade them at a sufficiently negative potential. Their study further showed the smaller nanoparticles indicated a higher selectivity in the CO_2RR.[16] In Kirk *et al.*, researchers at Stanford University, conducted a similar investigation into the electrochemical reduction of carbon monoxide for single metal atoms embedded in graphene.[17] Their modeling consisted of the development of a supercell with a 4 x 4 lateral size. The unit cell was first allowed to relax to decrease the force acting on each individual atom. The researchers further noted the irregularities of the graphene nanostructures at various levels of nitrogen doping; these irregularities were ignored to generate simplified models.[17]

Results and Discussion

Copper Nanoparticle Synthesis:

The primary goal was to determine the most effective means of obtaining nanoparticle catalysts (smallest aggregates of catalyst). Table 1 provides the results of the nanoparticle synthesis

DOI: 10.36838/v3i1.3

method seen in the study conducted by Gong *et al.* proving to be ineffectual.[7] The addition of silica into the catalyst solution suggested initially unexpected results. Photon correlation spectroscopy indicated that the particle sizes of the catalyst were entirely outside of the nanoscale, generating particles in micrometers. Regardless of silica concentration or copper nitrate and sodium hydroxide ratios, the results for the most part were lackluster, leaving clumpy catalysts that would leave suspension overtime. The addition of nitric acid and sulfuric acid produced a significant change in the particles themselves, while boric acid offered little improvement. The particles synthesized without these acids were clearly visible and would not remain in suspension due to their size (Table 1). The copper particles synthesized with dopants were not visible and did remain in suspension, indicating a much smaller size (Table 1). Unexpectedly, photon correlation spectroscopy indicated no difference in doped samples containing silica and doped samples without silica. The high polydispersity index resulting from these subsets of samples indicates nanoparticle aggregation is likely occurring, producing particles in the microscale (Table 1). This supports the idea that silica support alone does not lower the interfacial tension of the particles to a high enough degree. Based on the high polydispersity index, nanoparticles were most likely initially produced, in the range of 2-5 nanometers, but aggregated after being produced. Given that the size of the silica nanoparticles is about 40 nm, this method of synthesis yields copper supported silica nanoparticles rather than silica supported copper nanoparticles, as originally intended. The copper nanoparticles initially being so much smaller than the silica nanoparticles may play a role in silica's inability to properly promote the stability of the copper particles. Research was halted prior to attempting a means of stabilization of the nanoparticles; however, a novel approach to not only catalyze nanoparticle synthesis, but nanoparticle synthesis in general was formed within this phase of experimentation.

Electrolyte Conductivity Investigation:

Of the collected voltage outputs from sodium chloride, a concentration of 0.4 M was the most conductive while a concentration of 0.5 M performed the least for this particular electrolyte, producing on average a voltage of 0.84 V and 0.79 V respectively (Table 2). Among the sodium chloride voltage averages for the various concentrations, there was a standard deviation of 0.043. As for the electrolyte potassium bicarbonate, 0.2 M generated the greatest voltage with 0.824 V while 0.4 M generated the least with 0.809 V (see Table 2). There was a standard deviation of 0.010 for the average voltages across the varying concentrations of potassium bicarbonate. Lastly, for calcium chloride, the most conductive concentration was 0.1 M with 0.79 V and the least conductive concentration was 0.5 M with 0.740 V (see Table 2). Calcium chloride's standard deviation regarding its average voltage per concentration was 0.021. Accordingly, sodium chloride was the electrolyte that generated the greatest voltage for the electrolytic cell on average. It was followed by potassium bicarbonate and then calcium chloride that performed the weakest in terms of conductivity. There appears to be no specific trend for the concentration of electrolyte and generated voltage, and based on the low standard deviations, the differences are not significant; however, there is a clear differentiation among voltage output and the type or electrolyte. Across all three electrolytes, the highest generated voltages occur at different concentrations. Regardless, based up the collected data, the applicable electrolyte can be implemented into an electrochemical reduction process based upon desired conductivity now that voltage outputs have been determined.

Table 1: The size, ability to plate an electrode, suspension, and visibility of copper nanoparticles following varied inductions of silica and doping acids. Unless otherwise specified, the synthesis procedure will use 4 M sodium hydroxide, 0.5 M copper nitrate, and no silica.

Variation of nanoparticle	Results of photon correlation spectroscopy (μm)	Ability to plate an electrode	Suspension in distilled water	Visible particles
Cu particles with 10 mL of silica after precipitation	~ 30	No	No	Yes
Cu particles with 7.5 mL of silica after precipitation	~ 30	No	No	Yes
Cu particles with 5 mL of silica after precipitation	~ 30	No	No	Yes
Cu particles with 2 mL of silica after precipitation	~ 30	No	No	Yes
Cu particles with 1 mL of silica after precipitation	~ 30	No	No	Yes
Cu particles from 0.5 M copper nitrate	> 30	No	No	Yes
Cu particles from 0.3 M $Cu(NO_3)_2$	> 30	No	No	Yes
Cu particles from 0.1 M $Cu(NO_3)_2$	> 30	No	No	Yes
Cu particles oxidized with 12 M H_2SO_4	NA	Yes	Yes	No
Cu particles oxidized with 12 M HNO_3	NA	Yes	Yes	No
Cu particles oxidized with 6 M HNO_3	~ 25	Yes	Yes	No
Cu particles oxidized with 6 M H_2SO_4	~ 25	Yes	Yes	No
Cu particles oxidized with 0.5 M H_3BO_3	~ 25	NA	Temporary suspension	Yes
Cu particles oxidized with 6 M HNO_3 with 2 mL of silica	~ 25	Yes	Yes	No

Concentration (M)	Avg NaCl (V)	Avg $KHCO_3$ (V)	Avg $CaCl_2$ (V)
0.1 M	0.840 V	0.803 V	0.799 V
0.2 M	0.810 V	0.824 V	0.769 V
0.3 M	0.823 V	0.823 V	0.749 V
0.4 M	0.846 V	0.809 V	0.748 V
0.5 M	0.795 V	0.831 V	0.740 V

Table 2: The average electrolytes' (sodium chloride, potassium bicarbonate, and calcium chloride) impact on generated voltage at differing concentrations from 0.1 M - 0.5 M.

		CO Present in the System	CO_2 Present in the System
Graphene Electrode	Change in Fermi Energy	0.16 eV	-0.28 eV
	Change in Total Energy of the System	-43 Ry	-74 Ry
Graphene Electrode Plated with Copper Nanoparticles	Change in Fermi Energy	0.15 eV	0.19 eV
	Change in Total Energy of the System	-41 Ry	-72 Ry
Graphene Electrode Plated with Silica Supported Copper Nanoparticles	Change in Fermi Energy	0.08 eV	0.18 eV
	Change in Total Energy of the System	-42 Ry	-74 Ry

Cathode-Anode Electrochemical Analysis:

Normal Pulse Voltammetry allows for identification of potentials at Faradaic reactions through application of increasing amplitudes of potential differences in steps or "pulses." For selective reduction to ethanol, the ideal cathode anode combination would exhibit the highest Faradaic response at -1 V, the overpotential of the reduction to ethanol. The carbon-aluminum and carbon-lead combinations (see Figures 1 and 4 respectively) were the only two that exhibited the ideal sigmoid shapes around -1 V. The carbon and lead combination visibly displayed the greatest consistency with a current increase of 2000 μA, while carbon and aluminum displayed the second greatest consistency with a current increase of 22000 μA. The carbon and iron (Figure 2) combination's sigmoid shape was not present for the first trial, preventing accurate analysis. The potentials corresponding to the spikes in its data were -1.9 V and -2.7 V, far removed from -1 V. The potentials corresponding to the trials for carbon and zinc (See Figure 3) were even more sporadic. Carbon and iron had a current increase of 30500 μA, and carbon and zinc had a current increase of 6100 μA. Differential Pulse Voltammetry allows for the identification of potential differences of faradaic current activity. The average potential difference for the carbon and aluminum, carbon and iron, carbon and zinc spikes (see Figures 5, 6, and 7 respectively) correspond to -1.5 V, -2.4 V, and -0.27 V. Furthermore, the carbon and aluminum and carbon and iron each had one trial omitted due to irregular results, while carbon and zinc had two trials omitted. Carbon and lead (Figure 8), however, had an average potential difference of -1.2 V with three consistent trials, two of which were centered around -1 V. Thus, the data display overwhelming support for a carbon cathode and lead anode combination, due to higher consistency around -1 V. The fluctuations in data across trials for the other combinations may have resulted from minor changes in the orientation of the electrodes; however, the carbon and lead combination did not exhibit these fluctuations. Additional data is necessary to draw a clear conclusion regarding the most efficient combination.

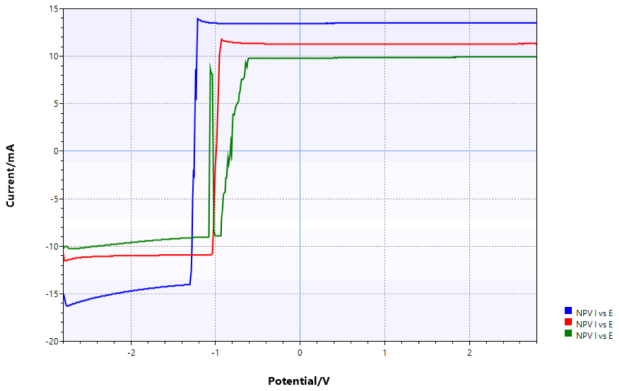

Figure 1: The normal pulse voltammograms for the three separate trials of the carbon and aluminum combination. The blue, red, and green curve correspond to the first, second, and third trial, respectively. The carbon and aluminum combination exhibit faradaic reactions around -1 V.

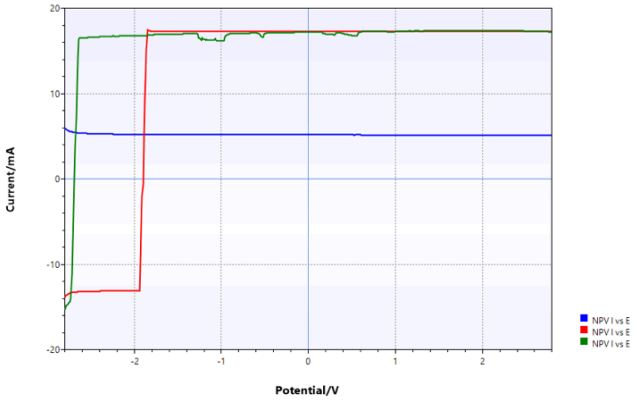

Figure 2: The curves depicting the normal pulse voltammograms for the three separate trials of the carbon and iron combination. The blue, red, and green curves correspond to the first, second, and third trial, respectively. For the blue curve, no significant data was derived due to its irregularity and is not considered in the data analysis. The carbon and iron combination displayed inconsistent faradaic reactions across different potentials.

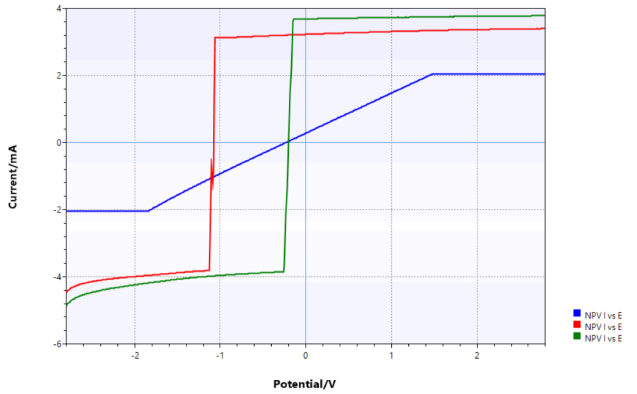

Figure 3: The normal pulse voltammograms for the three separate trials of the carbon and zinc combination. The blue, red, and green curve correspond to the first, second, and third trial, respectively. Carbon and zinc displayed inconsistent faradaic reactions at varying potentials.

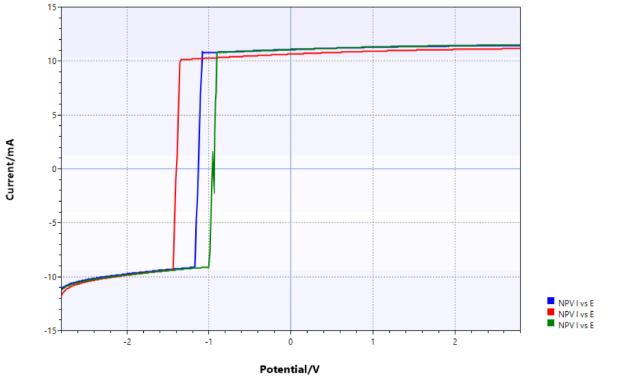

Figure 4: The normal pulse voltammograms for the three separate trials of the carbon and lead combination. The blue, red, and green curve correspond to the first, second, and third trial, respectively. Carbon and lead displayed consistent faradaic reactions around -1 V.

DOI: 10.36838/v3i1.3

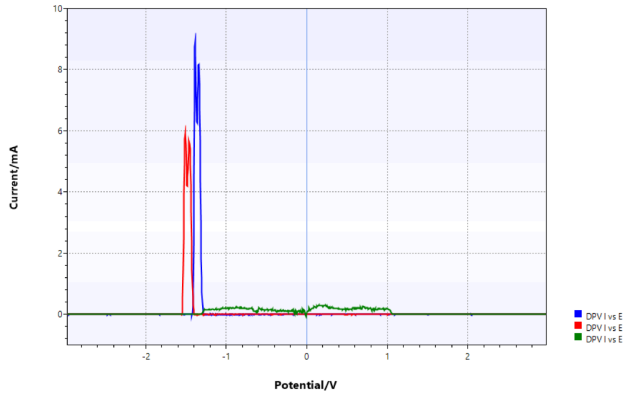

Figure 5: The various differential pulse voltammograms for the carbon and aluminum combination. The blue, red, and green curves correspond to the first, second, and third trial in the data table. The third trial was omitted from the data analysis due to its irregularity. Carbon and aluminum displayed erratic current spikes beyond -1 V.

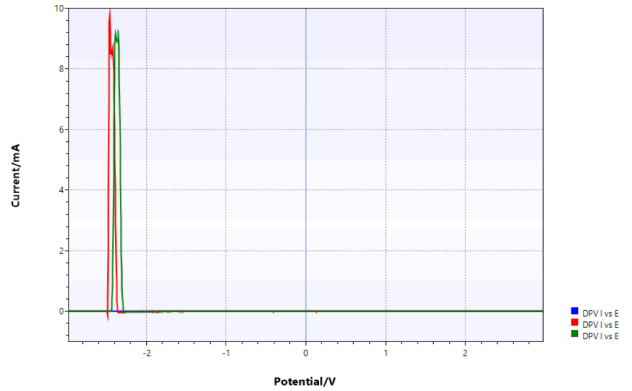

Figure 6: The various differential pulse voltammograms for the carbon and iron combination. The blue, red, and green curves correspond to the first, second, and third trial in the data table. The first trial was omitted from the table as it did not exhibit a significant spike. Carbon and iron displayed current response around -2.4 V.

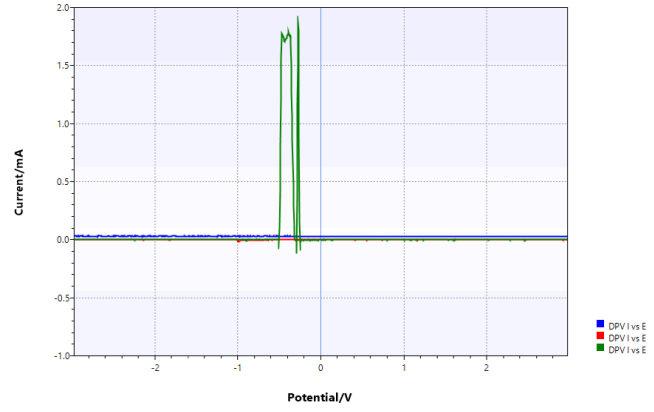

Figure 7: The various differential pulse voltammograms for the carbon and zinc combination. The blue, red, and green curves correspond to the first, second, and third trial in the data table. The first and second trials were omitted from data analysis due to their irregularity. Carbon and zinc displayed minimal current response across three trials.

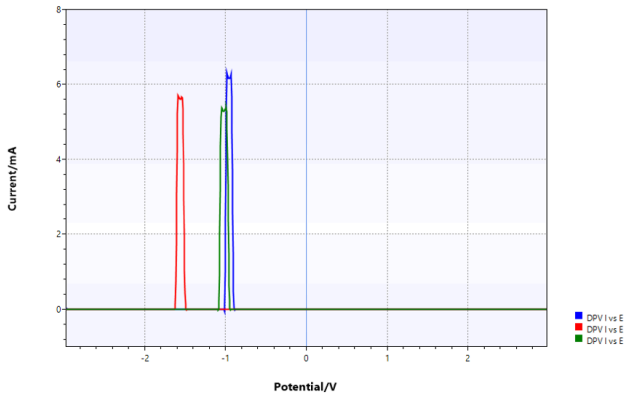

Figure 8: The various differential pulse voltammograms for the carbon and lead combination. The blue, red, and green curves correspond to the first, second, and third trial in the data table. While not the highest, carbon and lead's current response was around -1 V.

Catalyst Structure and Catalyst-Cathode-CO_2 Interaction Computational Analysis:

Self-consistent field calculations (SCF) generate approximate Hamiltonians and solve the Schrödinger equation to obtain a more precise set of orbitals. Hamiltonian refers to an operator that contains the sum of all the kinetic and potential energies in an observed system. These calculations continue to run with the new data points until the difference between two calculations is lower than the threshold value established. The Fermi energy refers to energy of the highest occupied state of the system. This means that even if the system were cooled to near absolute zero, the electrons in the system would have a kinetic energy close to the Fermi energy. Existing literature indicates the formation of carbon monoxide is an important intermediate in selective reduction to ethanol; thus, the ideal electrode variant would require minimal energy for the adsorption of carbon monoxide and much more energy for the adsorption of carbon dioxide. The graphene electrode's data provides that lower energy is necessary to be in thermodynamic equilibrium with carbon dioxide, resulting in decreased adsorption of carbon monoxide (Table 3). This indicates the graphene electrode would not enable selective reduction to ethanol. The lower energy required to be in thermodynamic equilibrium with carbon dioxide would likely result in higher adsorption of carbon dioxide than adsorption of carbon monoxide. The graphene electrode plated with copper nanoparticles required 41 Rydbergs for the adsorption of carbon monoxide and 72 Rydbergs for the adsorption of carbon dioxide. The graphene electrode plated with copper and silica nanoparticles required 42 Rydbergs for the adsorption of carbon monoxide and 74 Rydbergs for the adsorption of carbon dioxide. The increase in Fermi energy with carbon monoxide for the electrode with copper and silica nanoparticles was 0.08 eV, while the increase in carbon monoxide for the electrode with copper nanoparticles was 0.15 eV. Thus, despite the electrode with silica and copper nanoparticles requiring minimally more energy for the adsorption of carbon monoxide, the lower increase in Fermi energy suggests an ability to enable selective reduction to hydrocarbons.

Table 3: Values for the change in fermi energy and total energy of the system with the inclusion of carbon dioxide and carbon monoxide in the specified system. The graphene electrode plated with silica supported copper nanoparticles will enable selective reduction to ethanol as it requires lower energy for the adsorption of carbon monoxide.

		Fermi Energy	Total Energy of System	Harris-Foulkes Estimate
Graphene Electrode	No Additional Compounds	5.7375 eV	-1458.61 Ry	-1458.61 Ry
	Carbon Dioxide in System	5.4606 eV	-1532.76 Ry	-1532.76 Ry
	Carbon Monoxide in System	5.9146 ev	-1501.09 Ry	-1501.09 Ry
Graphene Electrode Plated with Copper Nanoparticles	No Additional Compounds	11.6081 eV	-9076.97 Ry	-9076.97 Ry
	Carbon Dioxide in System	11.7937 eV	-9149.22 Ry	-9149.22 Ry
	Carbon Monoxide in System	11.7553 eV	-9117.99 Ry	-9117.99 Ry
Graphene Electrode Plated with Silica Supported Copper Nanoparticles	No Additional Compounds	11.7711 eV	-7142.28 Ry	-7142.28 Ry
	Carbon Dioxide in System	11.9534 eV	-7216.36 Ry	-7216.36 Ry
	Carbon Monoxide in System	11.8538 eV	-7184.60 Ry	-7184.60 Ry

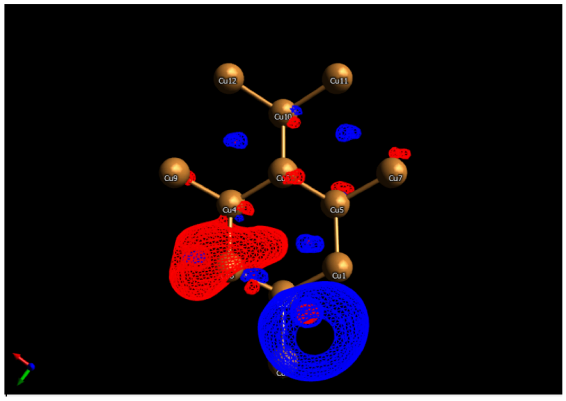

Figure 9: A visualization of the LUMO of copper mimicking the shape of the graphene molecule. In this instance, geometric optimization was implemented to derive a molecular structure with high stability, with the structure's lowest unoccupied orbital depicted above.

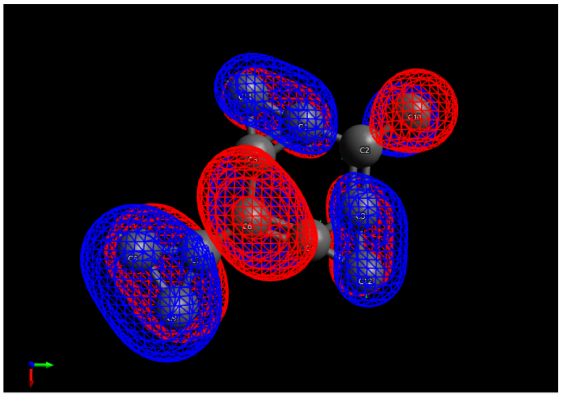

Figure 10: A visualization of the LUMO of the graphene molecule. Geometric optimization was utilized to discover the molecular structure in which energy is the lowest; therefore, yielding the highest stability.

Conclusion

Although the focus of this investigation was solely on concrete electrochemical aspects, the integration and culmination of findings from each phase has significant implications in innovating fuel synthesis for generations to come. The aspects of electrochemical reduction were isolated and tested to determine the optimal variance, and when put together for potential wide scale application, it can become greatly beneficial to remediating human environmental impact. It is known that most of the environmental deterioration of the Earth is caused by human fuel consumption. Mass carbon emissions are polluting the atmosphere and leading to a rise in global temperatures. If the current infrastructure moved away from fossil fuels and towards carbon dioxide reduced ethanol, especially with the implementation of captured carbon dioxide and renewable energy, the net output of carbon dioxide would reduce substantially, and the adverse effects of carbon emissions along with it.

From a purely economic standpoint, the utilization of synthesized ethanol from the reduction of ethanol has significant implications in the future of national expenditures, as well as the energy industry as a whole. The current most abundant source of energy are fossil fuels such as coal, petroleum, and natural gas. These products are becoming increasingly scarce with each coming year. As a result, it is becoming more of a financial burden. Eventually, human consumption of these fossil fuels will inevitably outpace Earth's supply, forcing humans to become entirely fossil fuel independent. Until then, their costs will continue to become a deeper economic pit. One of the greatest benefits is that synthesizing ethanol from carbon dioxide is a renewable process in which the ethanol output will not run out. Furthermore, ethanol is compatible with the vehicle infrastructure of today. As opposed to hydrogen fuel and other biofuels, entirely new engines do not have to be developed for the fuel to be implemented. This means that the hundreds of millions of cars do not need to be modified, saving even more money. Ethanol from carbon dioxide is essentially carbon neutral as well, therefore the costs of environmental remediation that fossil fuels are associated with do not apply here. In looking towards a more economically beneficial fuel alternative, let alone environmentally friendly, ethanol from reduced carbon dioxide is optimal.

Suggestions:

The means of precipitation-gel catalyst synthesis, while cost-effective, does not amount to the mass production of the electrochemical reaction that other methods can. One example that could be further investigated is chemical vapor deposition in which precursor chemical reactions are able to coat substrates with immense precision. Additionally, the implementation of molecular beam epitaxy has the ability to grow catalyst crystals at the atomic level. A last suggestion for the future of this investigation is to delve into utilizing Environ in Quantum Espresso. This would enable linearized Poisson-Boltzmann models with the addition of an electrolyte, taking in an additional factor for computation.

DOI: 10.36838/v3i1.3

Methods

Copper Nanoparticle Synthesis:

Three groups of copper silicon dioxide nanoparticles were synthesized (unaltered, nitrogen-doped, and sulfur-doped). To generate the initial copper silicon dioxide nanoparticles, 2.6 mL of 4 M sodium hydroxide was added to a 50 mL beaker. 10.2 mL of fully saturated copper nitrate was then introduced into the solution where it was placed on a magnetic stirrer. A stirrer was placed in the beaker and the solution was let to stir for 10 minutes, after which 5 mL of colloidal silica was immediately added. This was repeated with 1/3 of the samples being nitrogen-doped by pouring 5 mL of 6 M nitric acid and another 1/3 of the samples being sulfur-doped by pouring 5 mL of 6 M sulfuric acid to the catalyst solutions. Subsequent trials modified the amount of doping acid and the amount of silica. All samples were then placed under photon correlation spectroscopy, a technique that utilizes light diffraction patterns from collisions with nanoparticle samples, to determine the particle sizes of each catalyst.

Electrolyte Conductivity Investigation:

Three electrolytes (sodium chloride, potassium bicarbonate, and calcium chloride) were tested on the basis of conductivity. Beginning at 0.5 M, 300 mL of each electrolyte was poured into a 500 mL beaker. A copper cathode and a zinc anode were inserted, secured by a sheet of parafilm. A voltmeter was then attached accordingly and utilized to measure the voltage output in the initial 5 seconds. The electrolyte solutions were then diluted and tested for potential difference at 0.4 M, 0.3 M, 0.2 M, and 0.1 M. Measurements were recorded over 3 trials per electrolyte per concentration.

Cathode-Anode Electrochemical Analysis:

A single compartment electrochemical cell was created using 2 electrodes and a beaker (capped off with parafilm). The cell was filled with 355 mL of carbonated water to act as carbon dioxide dissolved in water. A carbon electrode was utilized as the constant cathode for the entire experimentation while the anodes tested varied from aluminum, iron, lead, and zinc. To test each anode combination an EmStat3 Potentiostat applied to the cathodic and anodic compartments of the electrochemical cell was then connected to a recording device and PSTrace Software was opened. The techniques conducted were Normal and Differential Pulse Voltammetry with the following specifications: -2.98 V (E begin), 2.98 V (E end), 0.005 V (E step), 0.025 V (E pulse), 0.07 s (t pulse), and 0.025 V/s (scan rate). Measurements for each technique were collected in real time. This process was repeated for 3 trials for each anode variation set up (contents cleaned upon reuse).

Catalyst Structure and Catalyst-Cathode-CO2

Interaction Computational Analysis:

For the generation of the Quantum Espresso model, a graphene electrode had to be created. In the Burai interface, the graphene electrode was produced by importing the molecule from Materials Project. A supercell was then produced to accurately depict an electrode. The dimensions of 3 x 3 x 2 were used to create the electrode surface. Atoms that made up the outside of the supercell along with relevant interior atoms were changed to copper to simulate the plating. The top layer of the supercell had no copper atoms as copper nanoparticle plating will not cover the upper portion of the electrode. To generate the variation necessary for carbon monoxide, a carbon atom and an oxygen atom were manually inserted into the supercell. To generate the variation for carbon dioxide, a carbon atom and two oxygen atoms were manually inserted into the supercell. Depending on the interface used, the calculation was completed by setting the Burai mode to SCF and autogenerating the necessary values. The threshold energy necessary for convergence, however, was lowered by an order of magnitude of two in order to be able to achieve convergence in a reasonable amount of time. The calculation was run through command prompt by first pasting the path of the plane-wave self-consistent field executable into the command window. The path of the -input file was then pasted into the command window, surrounded by a less than symbol on the left side and a greater than symbol on the right side. The path of the blank output file was then pasted into the command window to complete the command. Additionally, to perform Orca software specific calculations, Avogadro first needed to be opened. A graphene molecule was created rather than importing from Materials Project. A geometry optimization was conducted to optimize bond angles and the positioning of the atoms. An input file was created through extensions. The auto-generated basis sets (a set of DFT functions) were used, but the type of calculation was changed to geometric optimization rather than single point energy. This process was repeated but rather than producing the shape of a graphene molecule with carbon atoms, the same shape was produced with copper atoms.

Acknowledgement

The researchers would like to thank Dr. Patanarut, with George Mason University, for supervising the completion of their project, facilitating the entirety of their experiments, and guiding them through plausible independent and dependent variables. Dr. Patanarut's insight into the development of nanoparticles proved integral to establishing the foundation of this project. The researchers would like to further extend their thanks to Dr. Psaker, with George Mason University, for obtaining equipment critical to the data collection of this project, a Potentiostat. The purchase of this equipment through the physics department provided the research team with the ability to obtain quantitative measurements of the electrochemical reduction that were utilized to determine the most efficient form of the catalyst.

References

1. Global Greenhouse Gas Emissions Data. (2019, September 13). United States Environmental Protection Agency. https://www.epa.gov/ghgemissions/global-greenhouse-gas-emissions-data.
2. Nano-spike catalysts convert carbon dioxide directly into ethanol. (2016, October 12). Oak Ridge National Laboratory. https://www.ornl.gov/news/nano-spike-catalysts-convert-carbon- dioxide-directly-ethanol.
3. Song, Y., Peng, R., Hensley, D., Bonnesen, P., Liang, L.,

Wu, Z., Meyer, H., Chi, M., Ma, C., Sumpter, B., & Rondinone, A. (2016). High-Selectivity Electrochemical Conversion of CO2 to Ethanol using a Copper Nanoparticle/N-Doped Graphene Electrode. Chemistry Select, 1(19), 6055- 6061. https://doi.org/10.1002/slct.201601169.

4. Peterson, A., Abild-Pederson, F., Studt, F., Rossmeisl, J., & Nørskov J. (2010, July 12). How copper catalyzes the electroreduction of carbon dioxide into hydrocarbon fuels. Energy & Environmental Science, 3, 1311-1315. doi: https://doi.org/10.1039/C0EE00071J.
5. Hori, Y., Takahashi, I., Koga, O., & Hoshi, N. Selective Formation of C2 Compounds from Electrochemical Reduction of CO2 at a Series of Copper Single Crystal Electrodes. (n.d.). The Journal of Physical Chemistry, 106(1), 15-17. doi: https://doi.org/10.1021/jp013478d.
6. Kim, J., Choi, W., Park, J., Kim, C., Kim, M., & Song, H. (2019). Branched Copper Oxide Nanoparticles Induce Highly Selective Ethylene Production by Electrochemical Carbon Dioxide Reduction. Journal of the American Chemical Society, 141(17), 6986-6994. doi: https://doi.org/10.1021/jacs.9b00911.
7. Gong, J., Yue, H., Zhao, Y., Zhao, S., Zhao, L., Lv, J., Wang, S., & Ma, Z. (2012). Synthesis of Ethanol via Syngas on Cu/SiO2 Catalysts with Balanced Cu0–Cu+ Sites. Journal of the American Chemical Society, 134(34), 13922-13925. doi: https://doi.org/10.1021/ja3034153.
8. Kas, R., Kortlever, R., Milbrat, A., Koper, M., Mul, G., & Baltrusaitis, J. (2014, April 29). Electrochemical CO2 reduction on Cu2O-derived copper nanoparticles: Controlling the catalytic selectivity of hydrocarbons. Physical Chemistry Chemical Physics, 16, 12194-12201. doi: https://doi.org/10.1039/C4CP01520G.
9. Thanoon, H., Hubeatir, K., & Al-Amiery, A. (2017). Synthesis of Copper Oxide Nanoparticles via Sol-Gel Method. International Journal of Research in Engineering and Innovation, 1(4), 43-45. https://www.academia.edu/35363925/Synthesis_of_copper_oxide_nanoparticles_via_sol-gel_method.
10. Huang, Z., Cui, F., Kang, H., Chen, J., Zhang, X., & Xia, C. (2008, March 4). Highly Dispersed Silica-Supported Copper Nanoparticles Prepared by Precipitation-Gel Method: A Simple but Efficient and Stable Catalyst for Glycerol Hydrogenolysis, Chemistry of Materials, 20, 5090-5099. https://doi.org/10.1021/cm8006233.
11. Grigore, M., Biscu, E., Holban, A., Gestal, M., & Grumezcu, A. (2016, August 17). Methods of Synthesis, Properties, and Biomedical Applications of CuO Nanoparticles. Pharmaceuticals, 9(4), 75. https://dx.doi.org/10.3390%2Fph9040075.
12. Guo, C., Li, Y., Xu, Y., Xiang, Q., Sun, L., Zhang, W., Li, W., Si, Y., & Luo, Z. (2019, January 15). A Highly Nanoporous Nitrogen-Doped Carbon Microfiber Derived from Bioresource as a New Kind of ORR Electrocatalyst. Nanoscale Research Letters, 14(22). doi: 10.1186/s11671-019-2854-9.
13. Lv, Q., Si, W., He, J., Sun, L., Zhang, C., Wang, N., Yang, Z., Li, X., Wang, X., Deng, W., Long, Y., Huang, C., & Li, Y. (2018, August 23). Selectively nitrogen-doped carbon materials as superior metal- free catalysts for oxygen reduction. Nature Communications, 9(3376). doi: https://doi.org/10.1038/s41467-018-05878-y.
14. Pupo, M. M., & Kortlever, R. (2019). Electrolyte Effects on the Electrochemical Reduction of CO 2. ChemPhys Chem, 20(22), 2926–2935. doi: 10.1002/cphc.201900680.
15. Singh, M. R., Goodpaster, J. D., Weber, A. Z., Head-Gordon, M., & Bell, A. T. (2017). Mechanistic insights into electrochemical reduction of CO2 over Ag using density functional theory and transport models. Proceedings of the National Academy of Sciences, 114(42). doi: 10.1073/pnas.1713164114.
16. Huang, J., Hörmann, N., Oveisi, E., Loiudice, A., Gregorio, G. L. D., Andreussi, O., Marzari, N., & Buonsanti, R. (2018). Potential-induced nanoclustering of metallic catalysts during electrochemical CO2 reduction. Nature Communications, 9(1). doi: 10.1038/s41467-018-05544-3.
17. Kirk, C., Chen, L. D., Siahrostami, S., Karamad, M., Bajdich, M., Voss, J., Nørskov, J., & Chan, K. (2017). Theoretical Investigations of the Electrochemical Reduction of CO on Single Metal Atoms Embedded in Graphene. ACS Central Science, 3(12), 1286–1293. doi: 10.1021/acscentsci.7b00442.

Author

An avid researcher, Ashish Pothireddy aspires to solve the world's pressing issues with innovative solutions that merge his interest in engineering and business. Studying computer/data science, materials science, and business innovation, Ashish hopes to use his scientific and research talents to tackle global issues like climate change.

Clarence Ramirez is a student researcher aiming to develop innovative solutions to some of the world's greatest issues. Currently in the Biotechnology Program at OPHS, while taking introductory Biology courses at GMU, Clarence is pursuing a Medical Degree in hopes to one day become one of the nation's leading surgeons.

Sulav Regmi is a student attending the Governor's School program at George Mason University, studying and researching his interests in Biology and Chemistry. Whilst completing and participating in a multitude of scientific projects and competitions, Sulav continues to pursue a career as a world-renowned Cardiovascular Surgeon.

DOI: 10.36838/v3i1.3

Ultrasonic Planimals! The Bioacoustics of Fusing Cyphastrea Coral

Camila Rimoldi Ibanez

Sebring High School, 3514 Kenilworth Blvd., Sebring, Florida, 33870, USA; camilarimoldi03@gmail.com

ABSTRACT: Communication is vital for all organisms to grow and exchange information. The coral species Cyphastrea was tested for its hypothesized communication via ultrasonic sounds when undergoing fusion at different times of the day (morning, afternoon, nighttime). Both live and dead corals were tested with a digital oscilloscope in which the trigger level was raised above the highest peak of electrical noise to differentiate the ultrasounds emitted by the corals and the electrical noise. Because precautions towards unwanted electrical voltages were taken and the dead coral displayed no spikes in the 30 trials, it ensures that the spikes observed for the live coral were produced and emitted by the corals. Notably, 52 % of all spikes occurred during the nighttime intervals in comparison to 28 % during afternoon and 20 % during morning intervals. Ostensibly, there may be a connection between the different growth rates of the individual corals and the number of spikes recorded for each. Still, this proposes that live coral can emit ultrasounds and more actively do so during the nighttime than any other time of the day. This could help to understand the importance of corals and make a new foundation to restore corals worldwide.

KEYWORDS: Earth and Environmental Science; Climate Science; Marine Biology; Corals; Ultrasounds.

Introduction

Corals are one of the most prevalent saltwater lifeforms that contribute to the health of the planet. Although corals have been part of Earth's ecosystems for the past millions of years, much is still to be discovered about the coral species. There is still much to be done to help with the bleaching epidemics that are affecting corals all over the world.

Corals provide much to society by generating jobs and over billions of dollars from fish and tourism, and to the ocean by supporting 25 % of sea life (home to over 1 million marine species). It is extraordinary to think corals can do all this and cover less than 1 % of the ocean floor.[1] The researcher investigated the ultrasonic sound emissions from fusing coral fragments. A hypothesis is being put forth to further try to understand the complex multicellular system that make up corals.

The hypothesis is that corals emit bio-acoustical ultrasonic sounds when undergoing fusion at different times of the day, predicting more activity at night than the other times of the day. There are numerous studies that led the way for this hypothesis mostly based off from a scientific breakthrough that acknowledges plants can communicate with each other in different ways including ultrasonic sounds, chemical compounds through the roots, and chemical gases through the leaves.[2] Most specifically is a study that shows plants emit ultrasonic sounds with a frequency range of 20-100 kHz and an amplitude range of 0-60 dB.[3] There are studies that lead researchers to consider the fact that corals may be able to make ultrasonic sounds. Similar studies that have shown that corals communicate with fish via chemical signals and that coral larvae have sensory modalities that allow them to follow the sound of the coral reef.[4,5] Regarding the part of the hypothesis about corals emitting more ultrasounds at nighttime, research shows that corals sexually reproduce once a year precisely two hours after the moonrise, during nighttime.[6] For corals to carry out an important developmental event such as sexual reproduction at night, one might expect them to be more active at nighttime as well.

With the current bleaching, pollution, climate change, and other adversities that coral reefs face, 50 % of the world's coral have been lost during the last 30 years.[7] If the hypothesis presented by the researcher is demonstrated, it may help with the restoration of the fast-dying corals because if the ultrasonic sounds are harnessed and enhanced, it might facilitate developing of techniques to help the corals reproduce and grow more effectively.

Methods

In order to test the hypothesis that the coral specie Cyphastrea have the ability to generate sound to potentially communicate with other members of its specie via ultrasonic communication at different times of the day (morning, afternoon, and nighttime), three coral fragments were tested as an experimental group. Each of the total six experimental groups were tested with a RIGOL DS1052E Oscilloscope and a Hydrophone (with Frequency Range of 20-100 khz). Each coral group was given two twelve-minute trials at each of the three specific times of the day: nighttime (7-11 pm), afternoon (2-6 pm), and morning (7-11 am), throughout the month of November. These results were compared to that of dead coral, which were tested with the same equipment and testing procedures· At the same time growth was measured and tracked, weekly, for each individual coral fragment. Although moon phases have been observed to affect corals, and specifically coral reproduction, moon phases were not taken into consideration in this investigation as the

DOI: 10.36838/v3i1.4

purpose of this research was to identify if corals can generate ultrasonic sounds.

Precautions:

There were a few basic precautions taken for variables such as the time of the day, the duration of the trials, the saltwater element levels that were directed towards both experimental groups. The saltwater element levels, and their consistent value range are, a temperature of around 25.6 °C; salinity between 1.024 – 1.026 ppm; nitrate less than 30 ppm; nitrite level of 0; pH levels of 7.8- 8.1; an ammonia level of 0; alkalinity of 8-10 dkh; a calcium level between 380 – 450 ppm; magnesium levels between 1300-1450 ppm; light levels of 7 hours of blue light and 3 hours of white light. Due to the lack of research regarding the exact frequency or range of ultrasonic sounds corals produce, specific precautions were taken to differentiate background electrical noise from possible coral ultrasonic spikes. The precautions ensured that the researcher knew exactly what was producing the ultrasonic spikes as they were applied to both dead control coral and live coral experimental groups. The first of the precautions taken was to turn all the power of surrounding devices off, so that there were no unexpected electrical charges affecting the measurements. Secondly, after the average noise level created by electrical connections between the Oscilloscope and the Hydrophone were determined, the trigger level on the Oscilloscope was raised to double the average noise level. Thus, the Oscilloscope would display a signal only when it passed the trigger level and hence, surpass all electrical noise.

Besides setting up the RIGOL DS1052E Oscilloscope to display a signal only when it passed the trigger level, other specifications were set up on this device. First, Channel 1 of the two on the Oscilloscope was turned on so that the only signal displayed was the one received through the hydrophone. Then, setting Channel 1 Coupling to AC. This way it corresponds to the hydrophone input. Secondly, the Fast Fourier Transform (FFT) system was turned on throughout the experimentation. The FFT system is a combination of sine waves that represent the frequency and amplitude of the signal. By having this feature on throughout the trials, the Oscilloscope will give indications of the different characteristics of the ultrasonic spikes. To analyze these characteristics properly set the frequency as the subcategory of time. Lastly, the Trigger Level were set to Normal to enable the researcher to increase the Trigger Level to that of twice of the electrical noise.

Positive Control Group:

With these experiments it was clear that the hydrophone worked as expected and that it could capture the expected range of ultrasonic sounds. The Ultrasonic Cleaning Machine that was used as the source of ultrasounds for these experiments emitted ultrasounds at a frequency of around 40 kHz. The oscilloscope displayed frequencies at or very near to 40 kHz, only ranging from 34 kHz (the lowest recorded frequency) to 49 kHz (the highest recorded frequency). The consistency of the rectangular wave that the oscilloscope produced based of the signal received through the hydrophone acts as the final check for everything working properly.

Results and Discussion

As can be seen in Figure 1, the average noise level does not surpass the ~15 mV trigger level, this is concluded since throughout the trial there were no ultrasonic electrical noise spikes that passed this trigger level. As a result, when testing the live and dead coral the trigger level was set to ~35-40 mV which is more than double of the trigger level that the background noise level did not pass. This guaranteed that any ultrasonic spikes observed would be coming from the testing group and not from background noise. Therefore, since the only variable between control group and testing group was whether the corals were alive or dead, any spikes would represent ultrasonic sounds emitted by either group. Because in this investigation the dead control group corals did not have any spikes throughout the 6 hours of the 30 trials conducted, it strengthens the conclusion that the spikes observed during the measurement of the experimental groups were emitted by the live corals.

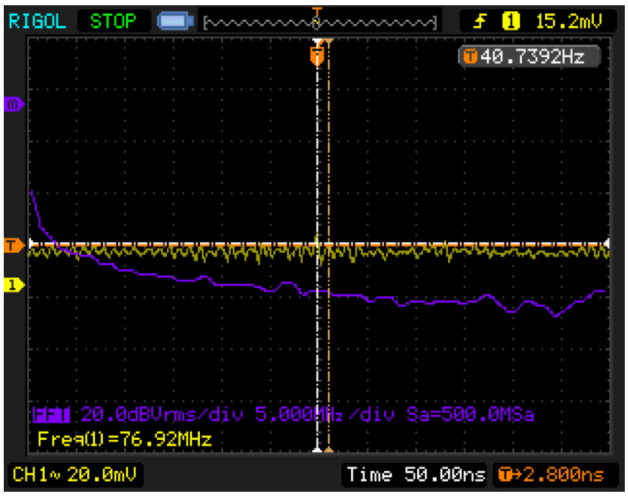

Figure 1: Control Coral #5, Afternoon Trial 3.

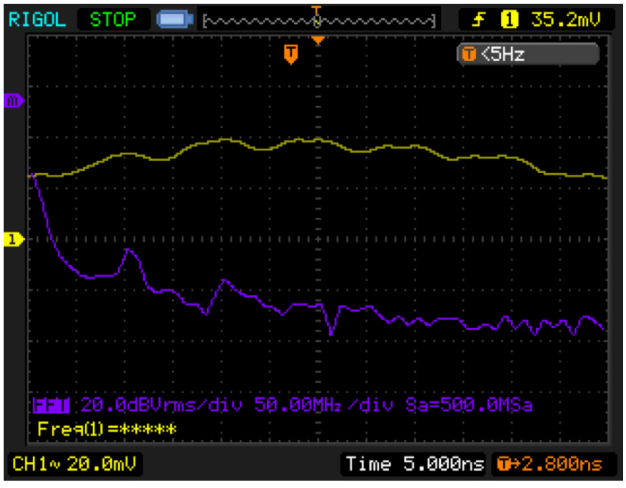

Figure 1: Control Coral #5, Afternoon Trial 3.

Ultrasonic Spikes:

The most important aspect tested in this investigation was whether corals had the ability to emit ultrasonic waves and potentially communicate with each other. This appears to be true

DOI: 10.36838/v3i1.4

as there was a total of 25 ultrasonic spikes recorded from the Live Coral Testing Groups while no spikes were recorded for the dead corals. After recording the spikes, they were analyzed with the time of day they were measured as well as the growth rates of the individual corals (see example in Figure 2).

There was a strong connection between the different times of the day and the number of spikes. When considering all spikes, there were a total of 13 spikes during the nighttime intervals (7-11 pm), 7 spikes during the afternoon intervals (2-6 pm), and 5 spikes during the morning intervals (7-11 am). All of these spikes had an average intensity of 47.81 MHz. On average, the live corals emitted 62 % more ultrasounds during the nighttime intervals than during the morning. Likewise, the live corals emitted 46 % more ultrasounds during the nighttime intervals than during the afternoon. The corals were significantly more active during the nighttime recordings than other times of the day. The afternoon recordings proved to be the time of the day, second to nighttime, in which corals emitted most ultrasounds. The live corals emitted 30 % more ultrasounds during the afternoon intervals than morning. On average, 52 % of all spikes occurred during the nighttime intervals, 28 % during the afternoon, and 20 % during morning (Figure 3). The standard deviation for the different number of spikes at the three testing intervals is 4.16 and considering the mean of the same values is 8.33, double the standard deviation, there is significant difference between the time of day and number of associated ultrasonic spikes.

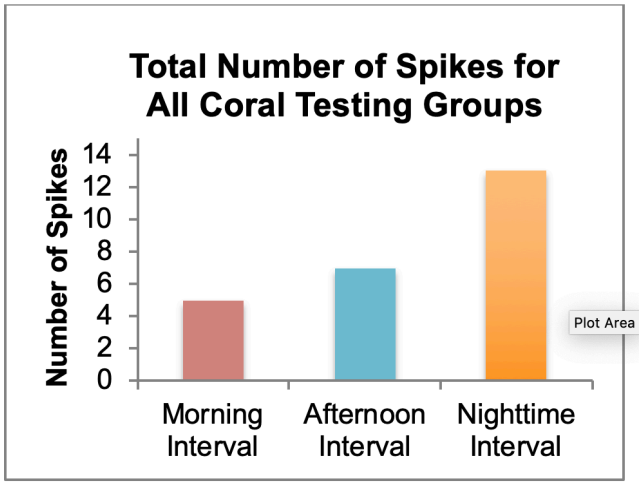

Figure 3: Total number of spikes for all coral testing groups. Nighttime spikes are more prevalent.

When independently analyzing each experimental group and their corresponding spikes, similar results are observed (Figure 4). In 2 out of 6 experimental groups, the nighttime intervals had more spikes than morning and afternoon. Although also in 2 out of the 6 experimental groups, all three intervals had the same number of spikes: 1 per interval, 3 spikes total. The afternoon interval was the interval with most spikes for 1 of the 6 testing groups, this was not seen for any of the morning intervals. Therefore, the nighttime intervals had the most spikes when independently observing the experimental groups as well as were the most prominent in overall number of spikes as 52 % of all spikes occurred during the nighttime intervals.

Table 1: The ultrasonic spikes observed during the three testing daytime intervals in correspondence to the experimental group from which they were observed from.

	Morning Interval	Afternoon Interval	Nighttime Interval	Total
Testing Group #1	None	1	1	2
Testing Group #2	1	4	1	6
Testing Group #3	None	None	6	6
Testing Group #4	1	1	1	3
Testing Group #5	1	1	1	3
Testing Group #6	2	None	3	5
Total	5	7	13	

Secondly, corals' spikes were compared to the growth rates. There seems to be a smaller connection between spikes and the growth rates of the corals as there was with the times of days. All corals showed signs of growth at some point in the 7-week period experimentation. However, 3 of the 18 live corals did start to shrink because they started to die. The rate of growth is seen in the line graphs, the percentages represent an average of the growth in length and height of the corals. These percentages are related to the original size of the coral. All growth rates start at 100 %, as this represents that the corals started with 100 % of their original surface area. For example, experimental group #2, Coral D is seen to have 12.5 % growth increase by Week 7. To calculate this percentage the difference between the percentage point for Week 7 (~112.5 %) and the initial 100 % point is calculated, resulting in 12.5 %, and since it is positive it means the coral grew. Coral M in experimental group #4 on the other hand, is seen to have lost surface area as the difference between the percentage point for Week 7 (~45 %) and the initial 100 %-point results in a -55 % change.

The measurements did not show similar growth trends for all three corals in each testing tile. This is seen in experimental group #2 (Figure 4). By Week 7, Coral D had grown a 12.5 %, Coral E a 15 %, and Coral F a 34.19 % - more than half of the other corals on the same tile. This relation between the different corals of the same tiles were evident in the two tiles that had dying corals. While some of the testing group corals in a tile showed significant growth rates the third coral was decreasing its size. For instance, in Testing Group #4 (Figure 5), Coral M showed a 45.10 % decrease of the original size- this means that the coral lost about 55 % of its original size. The other corals on this tile only showed growth such as Coral N with a 4.17 % growth and Coral O with 15.34 % growth. Both tiles with dying corals also had corals that only showed signs of growth, this reinforces how the tiles were not consistent with growth trends. Live Coral Testing Groups #2 and #3 both had a total of 3 spikes each and yet Testing Group #2 had Coral M, was one of the dying corals, that lost 55 % of its original size (Figure 4) and Testing Group #3 had Coral K, the coral with most growth. The same observation was observed for experimental group #5. This tile had two of the three dying corals of this investigation and yet had the second greatest number of spikes. Experimental group #5 had a total of five spikes, however, it had Coral P which lost 48 % of its original size and Coral Q which lost 67 % of its original size (Figure 6).

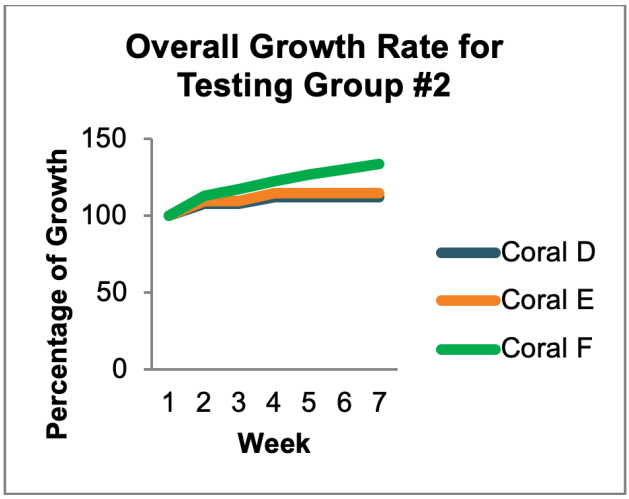

Figure 4: Percent of Coral Growth over Time for Testing Group #2. All corals grew slightly or stayed the same.

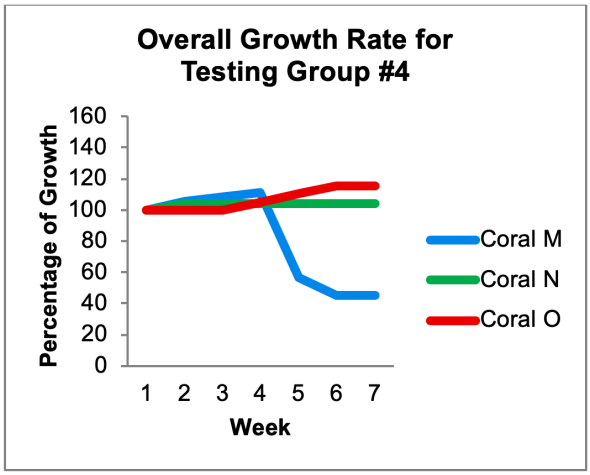

Figure 5: Percent of Coral Growth over Time for Testing Group #4. Coral M decreased in size.

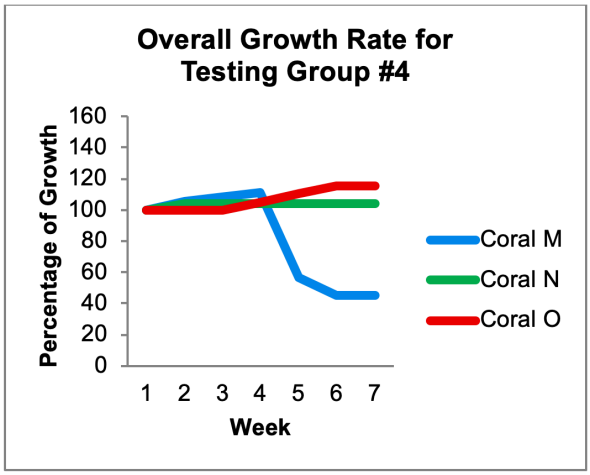

Figure 6: Percent of Coral Growth over Time for Testing Group #5. Second Most Spikes present.

Conclusion

After conducting a total of 66 trials, the hypothesis has been partially shown to be correct. The coral fragments emitted 52 % of all the ultrasonic spikes during the nighttime intervals. The first important aspect to acknowledge is that corals can emit ultrasonic sounds. There has been new research about plants communicating with ultrasounds but none for corals, and so recognizing the corals' potential to do this might give corals the ability to make sounds. Whether the sound generation is related to the coral polyp or the zooxanthellae algae that lives within the coral cannot be determined from this investigation but is a future research endeavor in better understanding coral ultrasonic sounds. Due to the fact that special precautions were taken to distinguish noise from possible ultrasonic spikes and the 5 individual dead corals tested did not display any ultrasonic spikes throughout any of the 30 trials while the live coral testing groups did display multiple ultrasonic spikes, it is concluded from this investigation that the coral specie Cyphastrea has the ability to generate ultrasonic sounds, and potentially enable some kind of communication among other corals of its species. A second aspect that is important to acknowledge is that communication is the exchange of information between living organisms, irrespective to their level of biological organization.[8] Although the ultrasounds that were observed by the corals of this investigation were affected by the different times of the day, the purpose of the ultrasounds portrayed is not known.

However, with this newly discovered potential for information exchange in corals much is to be discovered, such as what the corals are communicating and how they are doing so. Something similar occurred with the micro-fusion method. Researcher Dr. Vaughan and his team in the MOTE International Center for Coral Reef Research and Restoration discovered that when corals are cut into smaller pieces their growth rates increase significantly, hence the start of the micro-fusion method which is now the foundation of numerous restoration projects. This could equally happen with the study of communication among corals and, ultimately, develop techniques to encourage communication among corals to promote health and growth of coral reefs around the world. Likewise, as the emission of ultrasounds is further studied it may lead to other discoveries.

Acknowledgement

I would like to thank Mrs. Andrea Ibanez de Rimoldi for her assistance in getting the supplies for this experimentation and for her help editing the written sections.

References

1. About Coral Reefs. https://www.icriforum.org/about-coral-reefs/ (accessed Nov 2019).
2. Cossins, D. Plant Talk. http://www.the-scientist.com/features/plant-talk-38209 (accessed Nov 2019).
3. Veits, M.; Khait, I.; Obolski, U.; Zinger, E.; Boonman, A.; Goldshtein, A.; Saban, K.; Ben-Dor, U.; Estlein, P.; Kabat, A.; Peretz, D.; Ratzersdorfer, I.; Krylov, S.; Chamovitz, D.; Sapir, Y.; Yovel, Y.; Hadany, L. Flowers respond to pollinator sound within minutes by increasing nectar sugar concentration. http://www.biorxiv.org/content/10.1101/507319v1.full (accessed Oct 2019).

DOI: 10.36838/v3i1.4

4. Amid, C.; Olstedt, M.; Gunnarsson, J. S.; Le Lan, H.; Tran Thi Minh, H.; Van den Brink, P. J.; Hellström, M.; Tedengren, M. Additive effects of the herbicide glyphosate and elevated temperature on the branched coral Acropora formosa in Nha Trang, Vietnam. http://www.ncbi.nlm.nih.gov/pmc/articles/PMC5978828/ (accessed Sep 2019)
5. Puyana, M. www.eolss.net/Sample-Chapters/C06/E6-52-04-04.pdf (accessed Nov 2019).
6. Dr. David Vaughan, senior scientist and head of Coral Restoration program in the Florida Keys
7. Loria, K. The world's oceans are in even worse shape than we thought. http://www.businessinsider.com/new-studies-show-oceans-losing-oxygen-rapid-coral-bleaching-2018-1 (accessed Oct 2019).
8. Gagliano, M. Green symphonies: a call for studies on acoustic communication in plants. https://doi.org/10.1093/beheco/ars206 (accessed Sep 2019).

Authors

Camila Rimoldi Ibanez, a senior high school student from Sebring, Florida, and admires Florida's oceanic ecosystems. Moving from Argentina, she took advantage of the opportunity to study in Florida by learning about her new home, leading to her interest in ocean life and corals. She is currently working on her high school diploma and A.A. degree, she aspires to attain a PhD in Marine Biology.

A Novel Arsenic Filtration System for Low-Income Families in Rural Bangladesh

Ishraq A. Haque

Academic Magnet High School, 5109 Enterprise St, North Charleston, SC, 29405, USA; ishraqhaque101@gmail.com

ABSTRACT: Over 200 million people globally are affected by arsenic-contaminated water. Moreover, groundwater from tube wells is often contaminated with arsenic which, if ingested, can result in diarrhea, blood vessel diseases, and cancers. Arsenic filtration processes, like the SONO filter, 3-Kolshi filter, and ion exchange methods are promising developments that significantly reduce arsenic levels. However, cost, maintenance, and availability of these methods prevent many low-income families from using them. The aim of this project is to engineer a novel filtration system that significantly reduces arsenic and is maintainable and affordable for poverty-stricken populations. In this project, laterite soil was substituted for iron as the method of arsenic filtration to reduce costs. Through analysis, the constructed One Step Red Soil Filtration (OSRSF) was found superior to the 3-Kolshi filter, making it an economically beneficial option for poor people to have safe drinking water.

KEYWORDS: Chemistry; Arsenic; SONO filter; Composite Iron Matrix (CIM); Tube Well Water; 3-Kolshi; One Step Red Soil Filtration (OSRSF); Laterite Soil; Bangladesh.

Introduction

Arsenic is an element from within the Earth's crust and can contaminate water. In its inorganic form it is extremely toxic.[1-3] Arsenic-contaminated water is an exceedingly prevalent occurrence in rural areas. In these areas, families use tube wells to pump out groundwater, which is often contaminated.[1,2] Because of this, over 200 million people drink high levels of arsenic-contaminated water.[4] High concentrations of arsenic can lead to arsenic poisoning, a health issue in countries like Chile, India, and Bangladesh.[1] Arsenic poisoning causes complications such as diarrhea, affected hair and nails, darkened skin tone, and skin and bladder cancer.[1,5-8] The World Health Organization (WHO) and the Human Rights Watch have named Bangladesh a country largely affected by arsenic-contaminated water, so this study was held in Bangladesh to find a new approach to reducing arsenic levels in the water for poor people. In Bangladesh, over 20 million people drink arsenic-contaminated water and over 43,000 people die from arsenic related illnesses annually.[6,8]

Research into reducing arsenic levels in groundwater has been conducted in several countries. Filtration is the most viable solution to removing arsenic from water.[9] In 2006, Bangladeshi chemist and professor Abul Hussam invented the SONO Arsenic Filter to filter tube well water. The filter is made of 3 stacked buckets filled with coarse river sand, a 4-5 cm thick layer of a specifically designed composite iron matrix (CIM), charcoal, and wet brick chips. By pouring water through the buckets, large particles are filtered through the sand, arsenic is removed through chemical reactions in the CIM, and the charcoal and wet brick chips remove organics. The creation of the SONO filter has led to a significant decrease in arsenic levels in drinking water and has been implemented in many villages.[10,11]

While the SONO filter has had unprecedented success, it does have several drawbacks. A questionnaire administered in rural Bangladeshi villages revealed problems such as breakage, maintenance issues, high cost, weak sludge-disposal guidance, and slow flow rate of filtered water.[12] Alternative household tube wells have since been developed, but these also have issues with slow water release as well as complicated set-up and maintenance.[13,14] Additionally, many Bangladeshi villagers have a daily income of less than five USD, so the 60-70 USD replacement filter cartridges is unaffordable.

The CIM, where the arsenic is removed, is considered very beneficial for the SONO filter. It works using the following chemical reactions:[10]

Equation 1: $FeOH+H_2AsO_4^- \rightarrow FeHAsO_4^- + H_2O$ ($K=10^{24}$)

Equation 2: $FeOH+HAsO_4^{2-} \rightarrow FeHAsO_4^{2-} + H_2O$ ($K=10^{29}$)

Based on existing literature, the author hypothesized that applying laterite soil, commonly known as red soil, is lieu of an iron matrix will remove arsenic.[14] To test this hypothesis, a one-step arsenic filter was developed that was economic and efficient in lowering arsenic levels in water to a safe range. While CIM is the most efficient way to remove arsenic, poverty-stricken families cannot afford to maintain the SONO filters. The author invented a novel approach, called One Step Red Soil Filtration (OSRSF). Water sampling, testing, and data collection came from a small village in Assasuni Upazila of the Satkhira District in Bangladesh (Figure 1). This study presented a filter consisting of laterite soil and sand, cloth, charcoal, and brick chips (Figure 2).

This study aims to reduce arsenic in water to a tolerable level for poor people unlike other filters that significantly reduce arsenic levels to WHO standards.[1,8]

DOI: 10.36838/v3i1.5

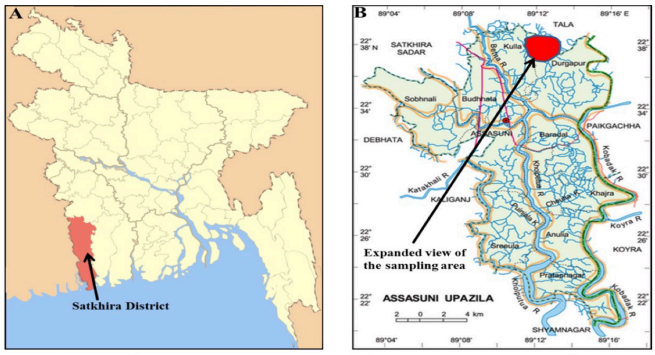

Figure 1: A map of arsenic-conteminated area in Satkhira District, Bangladesh from where water samples were taken. (A) Bangladesh map with Stahkira district highlighted. (B) Expanded view of Assasuni Upazila highlighting the study area. Map A was adapted from Wikipedia and Map B was adapted from WordPress.com.

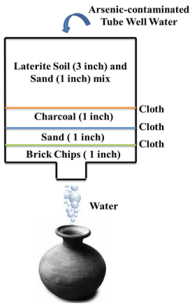

Figure 2: Development of a novel filtration system to reduce arsenic in tube well water.

Methods

Before implementing the novel OSRSF, collecting water samples from a low-income region was essential. Data collection occurred in a small village in Bangladesh where samples from thirty tube wells were collected. The arsenic concentrations were measured in each sample using the Hach EZ Arsenic High Range Test Kit. The kit included test strips, a reaction bottle and cap, two reagents, and a comparison chart (Figure 4). A test strip containing mercuric bromine was inserted into the special cap that locks onto the strip. A reaction bottle was filled with 50mL sample water. The two reagents, labeled "Reagent 1" and "Reagent 2" by Hach, were added to trigger sulfamic acid crystals to acidify the sample. The cap was attached to the bottle and swirled for one minute and then left for 40 minutes to react, the liquid being swirled twice.[16,17] During this time, the air reacted with the sample solution and imprinted the product on the test strip.[17] After the reaction time was over, the test strip was removed and compared to the chart to determine the arsenic concentration in parts per billion (ppb) in the sample. This process was repeated for each sample.

The OSRSF was held in a tin, octagonal prism with a height and diameter of 7" and the whole system was enclosed in a tin, octagonal prism with a height of 25" and a diameter of 10". A plastic stand held the filtration system in the larger tin container. The OSRSF included a 4" layer of the 3:1 laterite soil to sand ratio, a 1" layer of charcoal, a 1" layer of sand, and a 1" layer of brick chips. All the layers were separated by sari cloth (Figure 2, Figure 5).

Three liters of each sample, 100 ppb, 250 ppb, and 500 ppb, were collected and filtered through the OSRSF. Filtration took approximately 45 minutes for each sample. The filtered water was then collected in a kolshi, is the traditional vessel used in Bangladesh to collect and carry water (Figure 5). The author tested the OSRSF and the 3-kolshi system with the most prevalent concentrations: 100 ppb, 250 ppb, and 500 ppb. The 3-kolshi system was considered the control.

Statistical Analysis:

Statistical analyses were performed by the author's t-test. Any p-value less than or equal to 0.05 is considered statistically significant.

Results

Testing arsenic levels:

Tube well water samples were taken to find the range of arsenic concentrations in the Satkhira village region. With the villagers' consent, 30 tube wells were selected and marked for this project (Figure 3). Water samples were then collected and tested using the Hach EZ Arsenic High Range Test Kit.

Figure 3: Arsenic concentrations tested from 30 tube wells in a rural village in Bangladesh.

Information about the samples, including the well's owner, the depth, the arsenic concentrations, and a comment on the concentrations, were recorded (Table 1). The study's participants are not well educated, so providing information about the arsenic levels as well as the local guidelines for arsenic-contaminated water is helpful to them. The maximum arsenic concentration measured was 500 ppb. Twelve samples had a 250 ppb concentration, and fifteen had a concentration of 100 ppb (Table 1). The tube well depths were measured to test a correlation between arsenic levels and well depth, which was not found.

Testing OSRSF :

Arsenic levels were measured using Hach EZ Arsenic High Range Test Kit (Fig. 4). By using OSRSF (Figure 5), arsenic concentrations of tube well water could be reduced to a at least 50 ppb, the safe level according to Bangladeshi regulations.[1] WHO sets a much lower threshold, 10 ppb, for drinkable water, but the Bangladeshi government set their own standard for rural populations because they drink tube well water that contains extremely high levels of arsenic.

The OSRSF was first tested with sample of 250 ppb concentration. In one filtration, the concentration dropped to 50 ppb

(Figure 6). A 100 ppb concentration sample was reduced to 25 ppb with one filtration of the OSRSF (Figure 7). A third trial was done a 500-ppb sample, the maximum arsenic level measured. The sample required two filtrations to reach the acceptable limit. The first run through lowered the concentration to 100 ppb, and the second filtration lowered it again to 25 ppb (Figure 8).

Table 1: Tube well depth and arsenic concentration in tube well water.

Tube Well	Owner	Depth (feet)	Arsenic Conc. (ppb)	Comment
01	Abul Khaer	220	250	High
02	Mohidul Mallik	200	250	High
03	Alimuddin Sardar	160	100	Moderately high
04	Ebadul Sardar	200	500	Very high
05	Asadul Islam	220	250	High
06	Shahidul Islam	200	500	Very high
07	Nazrul Islam	200	250	High
08	Majed Dhali	200	100	Moderately high
09	Alamgir Hossain	200	500	Very high
10	Abubakar Siddique	200	250	High
11	Shahidul Islam	200	100	Moderately high
12	Mizanur Dhali	240	250	High
13	Mizanur Rahman	200	100	Moderately high
14	Shahaban Sardar	200	100	Moderately high
15	Hachim Sardar	180	100	Moderately high
16	Nurul Sardar	180	100	Moderately high
17	Faruq Hossain	200	100	Moderately high
18	Monarul Islam	200	100	Moderately high
19	Sayed Mali	200	250	High
20	Aktarul Islam	180	100	Moderately high
21	Abdul Qafi	200	100	Moderately high
22	Zahiruddin Dhali	220	250	High
23	Abdul Quddus	150	100	Moderately high
24	Mfizul Islam	150	250	High
25	Radwan Mehedi	200	100	Moderately high
26	Mukter Hossain	200	100	Moderately high
27	Emdadul Hossain	200	250	High
28	Abdul Hai	220	100	Moderately high
29	Khalil Sardar	200	250	High
30	Amjed Sardar	200	250	High

Figure 4: Materials for testing arsenic concentrations in tube well water.

Figure 5: Picture of the newly developed OSRSF.

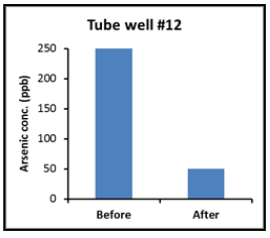

Figure 6: Bar graphs depicts before and after filtering with OSRSF on a 250 ppb sample from tube well #12. For 250 ppb sample, OSRSF was effective in bringing arsenic level down to 50 ppb.

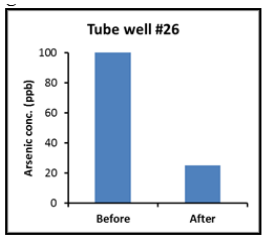

Figure 7: Bar graph depicts before and after filtering with OSRSF on a 100 ppb sample from tube well #26. For 100 ppb sample, OSRSF was effective in bringing arsenic level down to 25 ppb.

Comparison of OSRSF with existing filtration system:

The OSRSF system was compared to a locally made 3-kolshi system. The 3-kolshi filter also required two run throughs to get a 500 ppb concentration down to an acceptable level (Figure 8). Three liters of water were poured into each system and about 2.8 liters came out for both. For the 500-ppb concentration, the filtered water from the 3-kolshi system had 200 ppb after the first filtration whereas the water filtered using the OSRSF had a concentration of 100 ppb (Fig. 8). The difference between the results is noticeable from just the first filtration. During the second filtration the OSRSF brought the concentration from 100 ppb to 25 ppb, and the 3-kolshi brought the concentration from 200 ppb to 50 ppb, which is still an acceptable arsenic level for Bangladesh. The OSRSF and the 3-kolshi both yielded identical results for the 100 ppb and 250 ppb samples.

Statistical analyses and calculations were performed on the 250 ppb concentration samples (Figure 9). The average concentration after filtering through the 3-kolshi system was 43.75 ppb while the average concentration after OSRSF was 41.66 ppb. The 3-kolshi system's standard deviation was 11.31 and 12.31 for the OSRSF. The t-test was used to calculate the statistical significance. The p-value was 0.36, so there was no

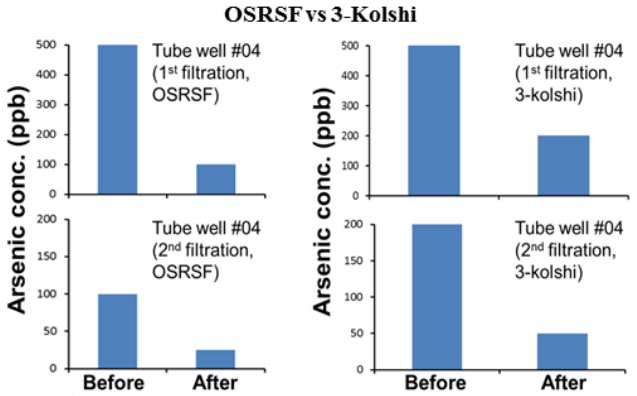

Figure 8: Bar graphs depict before and after filtering with OSRSF (left) a 3-kolshi (right) on a 500 ppb sample from tube well #04. Results suggest that the second filtration by OSRSF was very effective in making the water sample drinlable in terms of Bangladeshi rules and regulations.

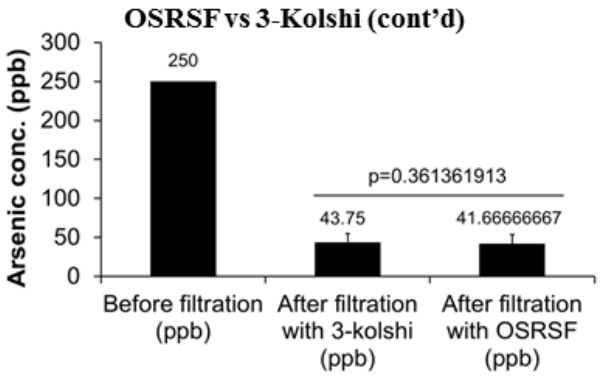

Figure 9: Bar graphs depicts arsenic levels before and after filtering with 3-kolshi and OSRSF. Statistical analysis suggests that water samples obtained from OSRF were comparable to 3-kolshi and can be economically beneficial for low income rural populations.

DOI: 10.36838/v3i1.5

statistical significance. However, the data suggests the OSRSF and the 3-kolshi systems are equally as effective.

Discussion

It was observed that the OSRSF system filtered arsenic better than the locally used 3-kolshi system. There is no statistical significance in using either the 3-kolshi system or the OSRSF (Figure 9). However, the OSRSF is realistically superior. It is the much cheaper option, and many villagers reported the OSRSF to be easier in use and maintenance via a questionnaire. Based on this data, the laterite soil may be able to better handle high levels of arsenic in comparison to iron chips found in the 3-kolshi even with the drawbacks of the soil.

The project is strengthened due to the OSRSF's low cost. It is cheaper than either the SONO filter or the 3-kolshi system. The total construction of the OSRSF was approximately 3 USD while the 3-kolshi production cost was reported by Satkhira villagers as 10 USD. The laterite soil needed to maintain the OSRSF is available in Satkhira for free. The tin containers are approximately 2 USD, and the charcoal and brick chips are less than 1 USD. Additionally, OSRSF owners may use a private collection of any of the needed materials. It is recommended the filter soil be replaced weekly to restore the amount of iron in the filter.

Compared to similar systems like the SONO filter and the 3-kolshi system, the OSRSF is cheaper, easier to maintain, and can be easily reproduced without a custom iron matrix. The 3-kolshi is effective, but the OSRSF is superior in usage, affordability, and efficiency. The OSRSF may not filter arsenic as well as the SONO filter, which can reduce levels to less than 10 ppb1, and was also not tested in this study. This study is novel in its application of a one-step filtration system for the poor that exploits the natural iron content in the local soil.

There are some limitations to the OSRSF. It takes approximately 45 minutes to filter water and only small amounts of water can be filtered at a time. While the OSRSF is not currently large-scale, one could recreate a proportionally scaled OSRSF to filter more water. Another concern is the possibility of pathogens in the filtered water due to the laterite soil. If such a problem occurs, boiling the filtered water can kill harmful pathogens.

Conclusions

This novel filtration system is economical for poverty-stricken populations to afford and maintain safe drinking water. The quality of life is improved for rural, low-income populations through this filtration system. Based on the results of this study, several conclusions were made on the OSRSF's effectiveness:

1) The OSRSF reduces arsenic levels of up to 500 ppb down to the Bangladeshi safe standard of 50 ppb. The 500-ppb sample had to be filtered twice to reach the safe level using the OSRSF, but it occurred in the 3-kolshi system as well.

2) The OSRSF is economically advantageous for poverty-stricken people, costing about 3 USD.

3) Laterite soil seems to be an acceptable replacement to the SONO filter's CIM and the 3-kolshi system's iron chips for low-income populations in Satkhira because laterite soil is readily available in that area.

4) Limitations of the OSRSF include no large-scale usage, slow water flow, and possible pathogenic contamination.

The future of the study may include finding an alternative to laterite soil for areas with a little to no laterite soil so the residents can still have an affordable arsenic water filter. Participants of the study have continued using the OSRSFs implemented in their village, and so examination of their hair and nails as well as skin status could be useful. Testing these may indicate a health improvement in the population, and it would also allow comparison between the health of OSRSF users versus users of other filters and/or those who do not use filters.

In summary, this project devised an alternative arsenic filtration system for poverty-stricken people and reduced the arsenic levels in contaminated water to a tolerable level. With the OSRSF system, the poor can drink safe water that will improve their quality of life, and the implementation of the OSRSF in other villages can improve rural quality of life around the world.

Acknowledgements

I would first like to thank my parents for their support throughout this project. I would also like to thank MR. Nazmul Haque and Mr. Redwan Mehidi who helped me interact with local villagers to collect water samples. I would also like to thank Mr. Rafiqul Haque for assisting me in gathering information about arsenic-affected populations in rural Bangladesh as well as helping me construct the OSRSF. I would finally like the participants of my study who allowed me access to their tube wells. Without these contributions, this project would not have been possible.

References

1. Arsenic.https://www.who.int/en/news-room/fact-sheets /detail/arsenic (accessed Sep 22, 2019).
2. Flanagan, S. V.; Johnston, R. B.; Zheng, Y. Arsenic in Tube Well Water in Bangladesh: Health and Economic Impacts and Implications for Arsenic Mitigation. Bulletin of the World Health Organization 2012, 90 (11), 839–846.
3. Water Treatment Solutions. https://www.lenntech.com /periodic/elements/as.htm (accessed Sep 22, 2019).
4. George, C. M.; Sima, L.; Arias, M. H. J.; Mihalic, J.; Cabrera, L. Z.; Danz, D.; Checkley, W.; Gilman, R. H. Arsenic Exposure in Drinking Water: An Unrecognized Health Threat in Peru. Bulletin of the World Health Organization 2014, 92 (8), 565–572.
5. Mandal, B. K.; Ogra, Y.; Suzuki, K. T. Speciation of Arsenic in Human Nail and Hair from Arsenic-Affected Area by HPLC-Inductively Coupled Argon Plasma Mass Spectrometry. Toxicology and Applied Pharmacology 2003, 189 (2), 73–83.
6. Uddin, R.; Huda, N. H. Arsenic Poisoning in Bangladesh. Oman Medical Journal 2011, 26 (3), 207.
7. Smith, A. H.; Lingas, E. O.; Rahman, M. Contamination of Drinking-Water by Arsenic in Bangladesh: A Public Health Emergency. Bulletin of the World Health Organization 2000, 78 (9), 1093–1103.
8. Das, N. K.; Sengupta, S. R. Arsenicosis: Diagnosis and Treatment. Indian Journal of Dermatology, Venereology and Leprology 2008, 74 (6), 571–581.

9. Hussam, A.; Munir, A. K. M. A Simple and Effective Arsenic Filter Based on Composite Iron Matrix: Development and Deployment Studies for Groundwater of Bangladesh. Journal of Environmental Science and Health, Part A: Toxic/Hazardous Substances and Environmental Engineering 2007, 42 (12), 287–303.
10. Ashraf, S. Pittsburgh Post-Gazette. PG Publishing Company August 7, 2007.
11. Shafiquzzaman, M.; Azam, M. S.; Mishima, I.; Nakajima, J. Technical and Social Evaluation of Arsenic Mitigation in Rural Bangladesh. Journal of Health, Population and Nutrition 2009, 27 (5), 674–683.
12. Munir, A. K. M.; Rasul, S. B.; Habibuddowla, M.; Alauddin, M.; Hussam, A.; Khan, A. H. Evaluation of Performance of Sono 3-Kolshi Filter for Arsenic Removal from Groundwater Using Zero Valent Iron through Laboratory and Field Studies. Proceedings International Workshop on Technology for Arsenic Removal from Drinking Water, Bangladesh University of Engineering and Technology and United Nations University, Japan 2005, 171–189.
13. Delowar, H. K. M.; Uddin, I.; El Hassan, W. H. A.; Perveen, F.; Irshad, M.; Islam, A. F. M. S.; Yoshida, I. A Comparative Study of Household Groundwater Arsenic Removal Technologies and Their Water Quality Parameters. Journal of Applied Sciences 2006, 6 (10), 2193–2200.
14. Maji, S. K.; Pal, A.; Pal, T. Arsenic Removal from Aqueous Solutions by Adsorption on Laterite Soil. Journal of Environmental Science and Health, Part A: Toxic/Hazardous Substances and Environmental Engineering 2007, 42 (4), 453–462.
15. EZ Arsenic High Range Test Kit. https://www.hach.com/ez-arsenic-high-range-test-kit/product?id=7640217305 (accessed Sep 22, 2019).
16. George, C. M.; Zheng, Y.; Graziano, J. H.; Rasul, S. B.; Hossain, Z.; Mey, J. L.; Geen, A. V. Evaluation of an Arsenic Test Kit for Rapid Well Screening in Bangladesh. Environmental Science & Technology 2012, 46 (20), 11213–11219.
17. Van Geen, A.; Cheng, Z.; Seddique, A. A.; Hoque, M. A.; Gelman, A.; Graziano, J. H.; Ahsan, H.; Parvez, F.; Ahmed, K. M. Reliability of a Commercial Kit to Test Groundwater for Arsenic in Bangladesh. Environmental Science & Technology 2005, 39 (1), 299–303.

Author

Ishraq Haque is a senior at the Academic Magnet High School in North Charleston, South Carolina. Ishraq has been fascinated by science his whole life. He is inspired by his mother, a research specialist in in neurology, and his father, a professor of microbiology and immunology, to pursue a career in science. He is part of his school's science club, works with bone scientists in a nearby medical university and completed a project with them. Outside of school, Ishraq is an avid martial artist, a pianist, a violinist, a published poet, and a volunteer for a local children's museum. Ishraq wants to become a physician scientist in the medical field and help people around the world.

DOI: 10.36838/v3i1.5

Emotion and Consumption Profiles in a COVID-19 Environment

Melissa Han

3115 Windsong Drive, Oakton, VA, 2212, USA; melissahxy02@gmail.com

ABSTRACT: Since the outbreak of COVID-19, the world has learned how to live during and respond to a pandemic. The emotional trauma and confusion people are experiencing lead to behavioral changes during this unprecedented time. This paper aims to study people's emotional and purchasing pattern changes after the COVID-19 outbreak. The survey results revealed that 83.9% of all respondents decreased their shopping at grocery store while 60.5% increased online shopping. Additionally, significant increases occurred in negative emotions such as being frightened, annoyed, and anxious. This increase, in turn, led to the changes in purchasing amounts of toilet paper, bags of rice, and face masks. The data reflected that the respondents' purchasing patterns are necessity driven.

KEYWORDS: Biology; Coronavirus; COVID-19; Emotions; Consumption patterns; China; Survey; Health; Economics.

Introduction

The 2019-identified Coronavirus COVID-19 has changed the way the world acts as infection rates and death tolls continue to rise even under recommended and mandatory regulations. As of September 7th, 2020, there have been 27,249,308 confirmed cases and 890,971 confirmed deaths worldwide.[1] Over the week beginning August 31st to September 7th, 2020, there has been an average of 40,525 reported cases per day in the United States.[2] As of September 7th, 2020, the U.S. has 6,300,075 reported cases and 189,182 confirmed deaths since the virus was first identified on January 21st, 2020.[3]

The overwhelming spread of the virus and the multiple impacts of coronavirus increase anxiety and uncertainty. Mandatory health orders, while decreasing the possibilities of infection, increase isolation, stress, and fear.[4] Additionally, since the COVID-19 virus outbreak, countries have experienced unexpected unemployment levels, which heavily affected their economies. The International Labour Organization (ILO) reports "over one in six young people surveyed have stopped working since the onset of the COVID-19 crisis." The ILO also states that working hours have declined by "10.7 percent relative to the last quarter of 2019, which is equivalent to 305 million full-time jobs." [5] Since mid-March, the United States has lost 20.6 million jobs, corresponding to an unemployment rate of 14.7%, a level not seen since the Great Depression in the 1930s.[6] This significant drop in employment rates and the huge hit on economies have significantly raised stress and anxiety levels.

The new normal of living during this pandemic – quarantine and social distancing, alertness of contact and possible infection, reduction in leisure activities, financial and economic instability – increases stress levels.[7] This escalated uncertainty and fear has led to changes in the purchasing profiles of people. For instance, certain people purchase more than they need in response to fear, and certain people restrict the consumption and purchases of goods in fear of, one day, not having enough monetary savings.

In this paper, Section II reviews various research and reports discussing and analyzing topics regarding the impact of infectious diseases and public health crisis on emotions and purchasing behaviors. Section III discusses the results gathered from a survey. The outcomes are grouped into multiple trends; some are aligned with our assumptions while some are not. Section IV analyzes the underlying reasons for why the results are the way they are. Additionally, it examines the connection between the results and economics. Section V reflects on the accomplishments and limitations of the project and survey. Lastly, Section VI concludes the paper by connecting the findings of this paper to a broader context and future references.

This paper studies the change and relationship between emotions and purchasing patterns during the uncertain time caused by COVID-19. How has COVID-19 influenced emotional patterns? How have those emotional changes affected purchasing behaviors? What type of emotion most heavily influences purchasing patterns during the uncertain times caused by COVID-19?

Literature Review:

Previous papers and articles have researched the impact of infectious diseases on human emotions; other papers have investigated the influence of emotions on purchasing patterns. These previous papers form the theoretical foundation of this paper.

Restubog, Ocampo, and Wang[8] (2020) showed the consistent relationships between an outbreak of infectious disease and chain-reactions of psychological and behavioral consequences. Within their commentary, they highlight the negative psychological effects such as greater incidents of depression and psychological distress, worry, anxiety about being infected, and subjective well-beings.

Additionally, McGinty, Presskreischer, Han, and L. Barry[9] (2020) compared their April 2020 survey results regarding symptoms of psychological distress and loneliness within U.S. adults with national data from 2018. Their resulted comparison – 13.6% of April 2020 surveyed U.S. adults reported signs of

DOI: 10.36838/v3i1.6

serious psychological distress compared to the 3.9% in 2018 – further exemplifies the psychological and emotional strain COVID-19 has caused.

McGinty, Presskreischer, Han, and L. Barry (2020) recount that along with other stressors such as fear of contracting the disease and uncertainty for the future, the necessary mitigation strategies such as those imposed for COVID-19 (e.g., social distancing, home quarantine, and travel restrictions) can negatively affect mental health.

Jin, Song, Zhao, and Yao[10] (2020) investigated the impact of COVID-19 on the purchasing behavior of Chinese citizens. They unveiled that by increasing the risk perception, fear, and boredom of citizens, COVID-19 accelerates purchases based on bandwagon effects, impulsive purchasing, and scarcity level.

One especially interesting report from Lee and Ward[11] (2020) demonstrates the increase of substance use in response to increasing distress among people. Lee and Ward (2020) report on the shift in the social relationships and increase in distress of people during the Coronavirus pandemic. To demonstrate, Lee and Ward surveyed 562 adults and found that 50% or more reported symptoms of anxiety nearly every day or several days a week since COVID-19. 28% of all respondents' report uses of alcohol or other drugs to make themselves feel better.

Based on these reports, this paper explores further the relationship between COVID-19 and emotions and purchasing patterns. Additionally, the paper analyzes the surveyed results with various demographic factors such as age and living country to explore alternative influences that might impact the emotions and behaviors of people.

Results

A total of 187 respondents completed the surveys, with 47 respondents from the English version and 140 from the Chinese version. The respondents range from ages of 12 to 64. The survey participants comprise of 40.7% male respondents and 59.3% female respondents. Additionally, the respondents indicated their educational level and their annual household income. These demographic-targeting questions aim to demonstrate the background information of respondents. Additionally, these questions were used to discover correlations between factors such as age and COVID-19-related responses from the surveyed groups.

The results collected display multiple noticeable changes in the psychological and behavioral responses of the surveyed groups. Most of these changes align with the predictions of the research, while others stray away due to both expected and unexpected factors.

The first pattern is the increase in intensity of negative emotions since the outbreak of COVID-19. Respondents were asked to rate the intensity of 8 positive and negative emotions on a scale of 0 (least intense) to 10 (most intense). The responses demonstrate that negative emotions such as being frightened, annoyed, and anxious display an increase in intensity from before the outbreak. Positive emotions such as excited, calm, and confident present a decrease in intensity. Figure 1 documents the difference between rated intensities of emotions from the respondents. The most noticeable change between ratings is the emotion "frightened." Of the 187 respondents, the average rating of the intensity of the emotion "frightened" was 2.6 before the outbreak of COVID-19. When asked to rate the same emotion, based on emotional experiences post COVID-19 outbreak, this average rating increased to 4.4.

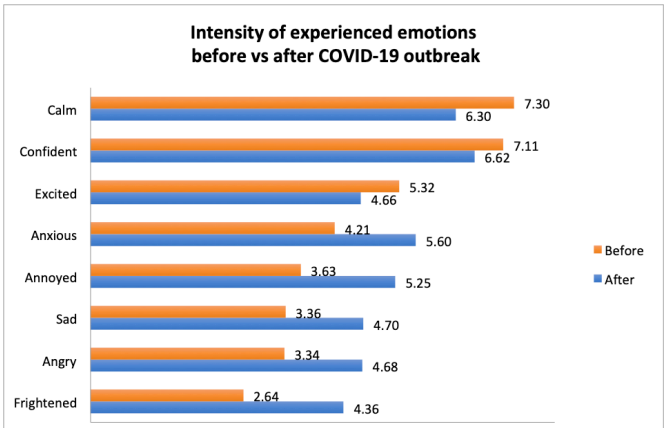

Figure 1: Intensity of experienced emotions before vs after COVID-19 outbreak. The intensity of all three positive emotions decreased while the five negative emotions increased. The three emotions with largest difference from before to after COVID-19 outbreak were *Frightened, Annoyed,* and *Anxious.*

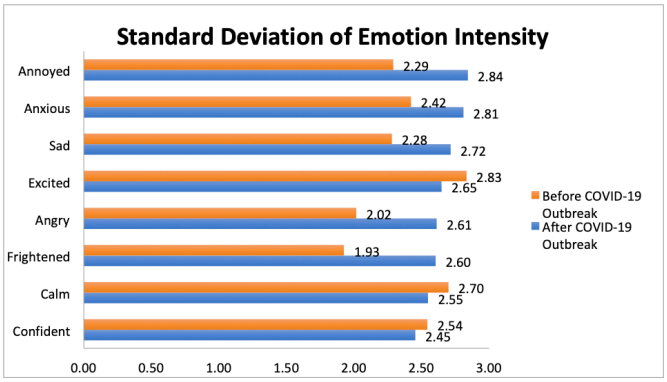

Figure 2: Standard Deviation of Intensity of experienced emotions before vs after COVID-19 outbreak. Demonstrates the standard deviation of the intensity of each emotion.

The second pattern, displayed through Figures 3, 4, and 5, demonstrated that people have decreased their overall consumption of goods and shopping at grocery stores while increasing their online grocery shopping: 44.6% of all respondents decreased their overall consumption of goods; 83.9% of all respondents shop at grocery stores less frequently; 60.5% of all respondents increasing their online grocery shopping.

The third pattern is demonstrated through comparing the shopping influences from before and after the outbreak of COVID-19. The survey asks the respondents to choose the three most important factors they base their purchases on when shopping. As expected, displayed by Figure 6, the choices such as level of necessity, affordability, and availability increased in chosen frequency for the post-COVID-19 outbreak. In contrast, choices such as personal satisfaction, brand reputation, and design uniqueness decreased in frequency. Due to the outbreak of COVID-19, the determining factors change as priorities shift from personal preferences to level of necessities and safety oriented.

DOI: 10.36838/v3i1.6

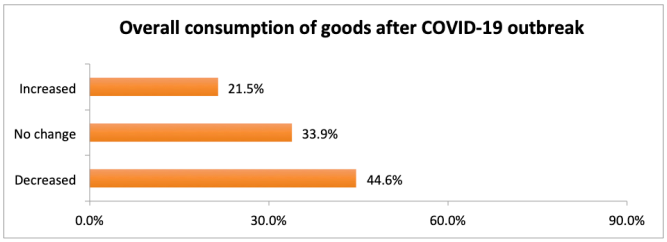

Figure 3: Change in overall consumption of goods after COVID-19 outbreak. Almost half of the respondents (44.6%) decreased overall consumption of goods, while 21.5% increased overall consumption of goods.

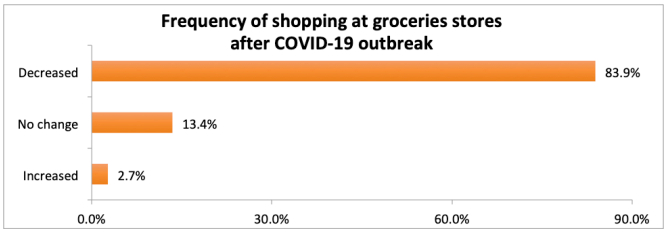

Figure 4: Frequency of shopping at groceries stores after COVID-19 outbreak. Most of the respondents (83.9%) decreased grocery store shopping.

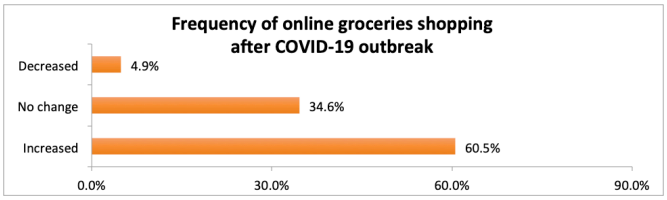

Figure 5: Frequency of online groceries shopping after COVID-19 outbreak. Over 60% of the respondents increased online grocery shopping.

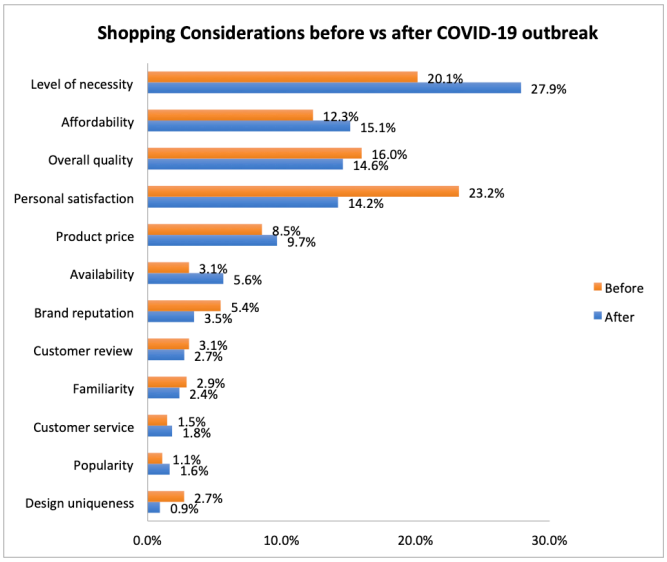

Figure 6: Shopping considerations before vs after COVID-19 outbreak. The influences of Level of Necessity, Affordability, and Availability increased for post-COVID-19 outbreak, while Personal Satisfaction, Brand Reputation, and Design Uniqueness decreased.

The fourth pattern is identified through the questions targeting changes in purchased amount of toilet paper (English version only) and bags of rice (Chinese version only). When designing the English version survey, it seemed necessary to include questions that could reflect whether the respondents increased their toilet paper stock due to COVID-19. It was publicized that in response to the outbreak of COVID-19, many Americans stocked up on- in addition to other essentials- rolls of toilet paper. Media outlets such as TIME[12], Nature[13], and NBC[14] news have reported on the massive amount of toilet paper buying. To test this behavior, the surveys provided the questions "approximately, how many rolls of toilet paper do you currently have in stock for yourself?" and "did you increase your stock of toilet paper due to COVID-19?"The results align with the toilet media-reported paper-buying phenomenon: Figure 7 demonstrates that 54.3% of all United States respondents stated they increased their stock by a certain percentage while 45.7% of all respondents stated they did not increase their stock of toilet paper.

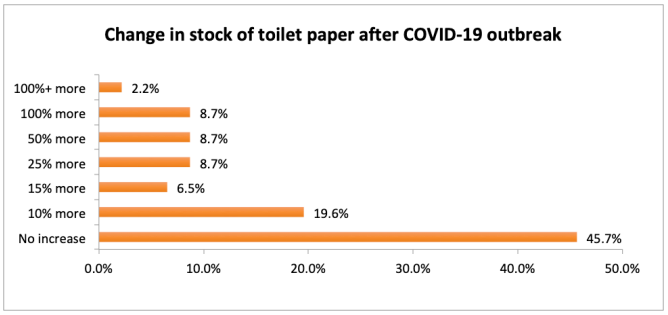

Figure 7: Change in stock of toilet paper after COVID-19 outbreak. 54.3% of the United States respondents increased their toilet paper stock while 45.6% did not.

While many Americans stocked up on toilet paper, the Chinese version of the survey targeted what was thought to be an essential to save for Chinese people – rice. Surprisingly, the results display that 65.0% of the respondents who answered the Chinese version did not increase their stock of bags of rice· Figure 8 displays the data from further analysis of this surprising phenomenon. To investigate, the results from the question "did you increase your stock of rice due to COVID-19" were analyzed based on the reported living location. It is hypothesized that maybe their current living location might impact why they did not stock up on rice. The eating habits of Chinese culture show that people who live in southern China consume more rice while those living in northern China consume more flour. Therefore, it was hypothesized that the majority of the respondents came from northern China due to result in the lack of savings in stock of rice. After further study, the data demonstrate that, despite the larger number of respondents not increasing their rice stock, there was still 8.7% more southern China respondents who reported increasing rice stock than northern China respondents (shown in Figure 7). This difference still confirms the previous assumption based on Chinese cultural eating habits but implies that there are other reasons leading to the reported outcome documented in Figure 8.

Finally, the fifth pattern is the differences and similarities between the number of masks people in China or America bought. The survey asks all participants to approximate the number of masks they have both for themselves since the outbreak of COVID-19. After summarizing the responses, a few patterns can be seen (through Figure 9).

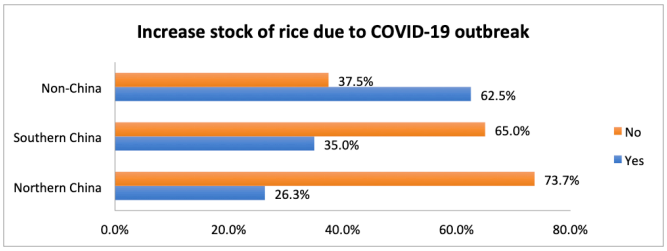

Figure 8: Increase stock of rice due to COVID-19 outbreak. 62.5% of respondents living outside China increased their stock of rice. Compared to respondents living in Northern China, an increase of 8.7% Southern Chinese respondents increased their stock of rice.

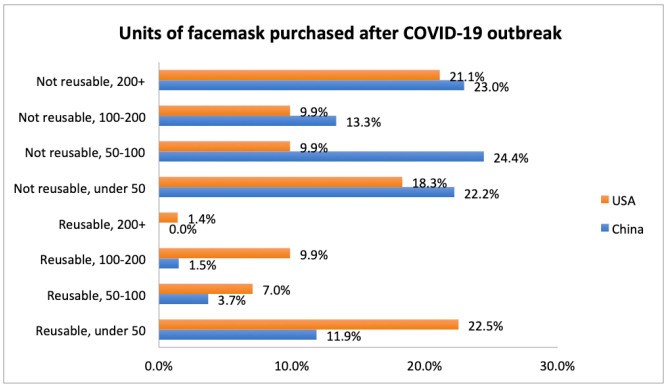

Figure 9: Units of facemask purchased after COVID-19 outbreak.

Firstly, the data suggests that people who live in China prefer purchasing non-reusable masks more than reusable masks. When given the same masks unit, more respondents stated they bought them in a non-reusable form than reusable. Secondly, respondents who live in the United States seem to purchase more reusable masks. More percentage of United States participants purchased a certain unit of reusable masks than did participants who live in China. For instance, 9.9% of United States respondents purchased 100-200 units of reusable masks when only 1.5% of Chinese respondents purchased the same type and amount. Similarly, respondents who live in China purchase more non-reusable masks of the same unit than did United States respondents.

Discussion

1.Why did the most intense emotions change the way they did? :

As shown in Figure 1, the comparison between rated intensities of emotions from before COVID-19 to after COVID-19 demonstrates an increase in negative emotions and decrease positive emotions. It is expected that people have experienced various negative emotions more frequently and intensely. According to the survey, many respondents accounted for their increased intensity of anxious, sad, frightened, annoyed, and angry on the fears of infection, societal disorder, and national economic downturn (shown in Figure 9). The increase in such negative emotions, in turn, leads to many changes in purchasing patterns.

2.What accounts for the overall change in grocery purchasing behavior? :

Based on the second identified pattern and Figures 3 through 5, there is a decrease in overall consumption of goods and shopping at supermarkets while online grocery shopping increases. People visit grocery stores less and opt for online shopping as much as they can to avoid possible contact with other people. The fear of going outside and being infected leads to lesser shopping at supermarkets. The respondents imply that, due to COVID-19, they only go grocery shopping if it is necessary. To compensate for lesser visits at the grocery stores, people would turn to online shopping. Although there were questions of whether one can be infected if receiving a package, the respondents seem less frightened to shop online compared to shopping in person.

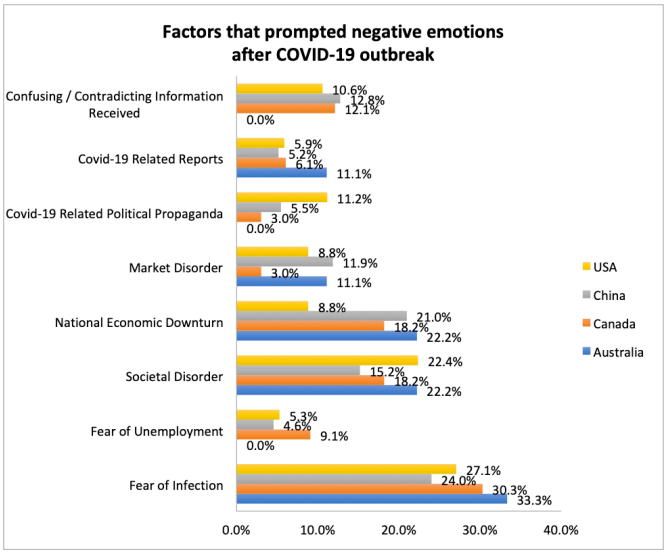

Figure 10: Factors that prompt negative emotion after COVID-19 outbreak. Fear of Infection and Societal Disorder are the top 2 factors prompting negative emotions regardless of living countries.

3.Why did more people choose "the level of necessity," "affordability," and "overall quality" as the three most important factors when shopping post COVID-19 outbreak? :

The outbreak of COVID-19 changed the demands of people. Before the pandemic, emotional needs and wants likely influenced people's purchasing intention. However, as the pandemic intensified, the needs of people shifted to necessity driven and realistic purchases.

When asked to choose the three most impactful factors when shopping after the outbreak of COVID-19, the choices that had the highest amount of increased chosen percentage, as shown in Figure 6, were "the level of necessity," "affordability," and "availability." In contrast, the choices that had the highest amount of decreased chosen percentage were "personal satisfaction," "brand reputation," and "design uniqueness." This result is quite expected – amid a global pandemic, the purpose and determining reasons of a purchase is more constricted and concise. Due to the pandemic, people make more rational choices since they are more concerned on price factors than before the outbreak. Almost all purchases are made with the effects of the pandemic in mind.

Firstly, many of the purchases made after the outbreak were for combating the disease. People are afraid of getting infected, so they purchase what is necessary for protection. This fear leads to the increase in the level of necessity, which is reflect

DOI: 10.36838/v3i1.6

ed in the response. Additionally, with one of the main fears being national economic downturn, many might save their money anticipating instable income flow and large amounts of layoffs and business closings since the outbreak. With more constraints on their money, the demand for luxuries decreases while the demand for necessities increases. Luxuries are never necessary: they are items that help improve the quality of living but are not indispensable for living. As people begin to live amid a pandemic, the need for luxuries decrease and the level of necessities increase.

"Affordability" works in the same fashion as "level of necessity." During COVID-19, many of the purchases are carefully thought out. People must take into consideration whether they can afford a purchase during times with inconsistent income flow. The fear of not having enough savings prompts people to reconsider when they face a purchase that affects their financial stability. The income level and affordability of a person is, therefore, another determining factor of whether they make a purchase or not.

Once people have concluded that they are able to afford a purchase, the issue of "availability" then arises. Many items previously not considered essential, are now prioritized. For instance, many respondents have reported an increase in their stocks of toilet paper and purchases of large amounts of masks. Due to this sudden increase in demand, the supply cannot catch up to the demand. Therefore, there are frequent shortages in these items. With this type of situation frequently occurring, people proceed to purchase based on availability. As soon as they see these necessities are available, people might purchase large amounts of it in fear of having to buy more when they have shortages.

With fear and anxiety influencing people during the purchasing process, factors such as "personal satisfaction," "brand reputation," and "design uniqueness" are not as influential as before. In the face of a pandemic, previously enjoyed purchases that satisfy these three factors are probably eliminated as people are focusing on protection, safety, and health.

4.Why did the United States respondents stock up on toilet paper? :

First, it is necessary to understand why toilet paper is a main item of saving up since the outbreak of COVID-19. Toilet paper is a necessity that every person uses daily. What makes it even more important is that there are no close substitutes for toilet paper and humans are long past the years where primitive cleaning methods are still in use. Therefore, with no substitutes for toilet paper, people, reasonably, increased their stock of toilet paper when informed they will be quarantined. Besides this reason, other psychological factors also prompted the massive amounts of saving on toilet paper.

The first psychological impact, according to TIME, is that it is not the toilet paper itself that draws customers; it is the idea that there are inadequate supplies that frightens and, therefore, attracts people. With toilet paper already being a necessity that people need to purchase, the fact that there is a lack of it increases the anxiety within people. According to the idea of scarcity, the scarcer something is, the more valuable and attrac According to the idea of scarcity, the scarcer something is, the more valuable and attractive it is.[15] Knowing that there is a lack of toilet paper scares people, especially since toilet paper is something irreplaceable.

The second psychological impact comes from the fear of missing out, or FOMO, the modern expression for herd psychology. According to Michigan Live[16] and BBC[17], the fear of missing out is the reason why toilet paper is flying off the shelves at grocery stores. When people start "panic-buying," others tend to follow because they fear they will not get any for themselves. Additionally, people might think, seeing the amounts of reports of people stacking up toilet paper, that there is a reason for people to purchase toilet paper, leading them to believe they must have it. This phenomenon is especially magnified when the item people are panic buying is considered necessary and irreplaceable.[16]

Both influences are driven by fear of not having enough of something irreplaceable, and the wide media coverage on the lack of toilet paper does not help control it. With publication about toilet paper, and regardless of whether one fears missing out or falls into the notion of scarcity, the result is the same: more and more people purchase stacks of toilet paper, leading to its lack of supply.

5.Why did respondents who live in China not save up on rice in the same way as United States respondents for toilet paper? :

When it comes to the amount of rice savings, there is a fundamental difference between rice and toilet paper: the two items the survey framed as necessities. Both these items are necessities because people must use toilet paper daily, and many people living in China consume carbohydrates like rice daily. However, the fundamental difference between the two is that toilet paper does not have substitutes, but rice does. People can consume different types of carbohydrates in replacement of rice if they do not have any. Unfortunately, this difference was not considered when creating the survey. It was presumed that rice would act in the same way as toilet paper does, when in fact it had substitutes, leading to a lesser level of necessity. Therefore, this difference is the reason for the results demonstrated in Figure 8.

The fact that fewer people are stocking up on rice in China than there are outside of China reflects a few reasons. Firstly, at the time of the survey (July 12th, 2020 to July 26th, 2020), the infection rates of COVID-19 in China have already been controlled. Even after the second wave of outbreak in Beijing that began in June 2020, infections were quickly contained. After July 5th, no new cases were detected.[18] With effective containment and lower cases, the fear and the need to stock up on essentials might have decreased, leading to the results summarized in Figure 8. Lower infection rates equate to fewer negative emotions such as fright and fear that could prompt changes in purchasing patterns.

Secondly, when looking at Americans purchasing toilet paper, media outlets have greatly impacted the actions of people saving up toilet paper. With more media reports on toilet paper running out of stock more people go buying them. With this cycle snowballing bigger and bigger, the demand for toilet paper increases while the supply is still trying to catch up.[19]

Comparatively, the media within China is controlled, especially during a pandemic, in order to minimize any possible fear and fright within the society. Any story or information that might increase anxiety and fear is controlled in order to main societal order. Therefore, there were little to none reports on whether people are purchasing more bags of rice or not. With no media reports of rice running out of stock, people might not feel the fear of possibility lacking a necessity.

6.Why do United States respondents tend to purchase reusable masks while respondents who live in China buy non-reusable ones? :

Figure 8 shows that United States respondents tend to purchase more reusable masks than the respondents who live in China. This occurrence can be explained through a few possible reasons. Firstly, it might be presumed that, compared to reusable masks, non-reusable masks and medical masks are better at combating against COVID-19. Throughout the pandemic, there have been specialists who stated that disposable masks are effective in combating the virus so long as they are worn properly.[20] Additionally, although many have chosen to use reusable masks, to many people who live in China where populations are crowded and cities are much more compact, a reusable mask might have more risks than a non-reusable mask Since people dispose of non-reusable masks as soon as they finish using it, people might believe that is safer. In China, it is possible that citizens are much more anxious and concerned as COVID-19 was first discovered there. With months of combating the disease on their own, it is possible that the citizens are much more cautious in protecting themselves against infection. In result, this fear and anxiety of possible contamination might lead to more purchases of non-reusable masks.

On the other hand, COVID-19, although having the highest reported death toll in the United States at this moment, seems to stir less fear in America. According to a July Axios-Ipsos poll, almost one in three Americans believes that the death toll of the COVID-19 is not as high as the official counts.[21] Also, according to a March NPR PBS NewsHour Marist poll, about 56% of Americans think COVID-19 is a real concern and threat, a 10% drop since February. The poll also states that a growing number of Americans think the coronavirus is being "blown out of proportions.[22] With growing suspicion and disbelief, it is possible that some of the surveyed United States participants simply thought there is no need to purchase much of non-reusable masks because they, in turn, are not that anxious and frightened of the new pandemic.

Reflection:

Overall, the survey helped provide a great basis of data that allowed for extensive analysis. The discovered relationship gave insight into the emotional and purchasing changes that occurred so far during an infectious pandemic. However, there were a few issues that could improve the analysis and conclusions if resolved. Firstly, when finding participants for the survey, the groups from each country were not controlled, leading the number of people from each country to be different. Although this still provided sufficient data, this difference could affect the conclusions if the numbers of each groups were controlled. For instance, the data currently shows that people who live in America tend to purchase reusable masks due to, possibly, environmental consciousness, affordability, and availability. However, since there were only 47 United States respondents, this conclusion could change if more participated. Additionally, there were only three participants from Australia and 11 participants from Canada. With such small numbers of participants from these two countries, it was not accurate and correct to analyze data with such a small pool of respondents. Similarly, because the surveyed group was not controlled and all of them were volunteers, the surveyed groups demonstrated an overall higher household annual income level (shown in Figure 10). It was expected that one of the highest chosen negative-emotion-prompting factors was fear of employment. However, since the surveyed group had a higher income level, this assumption was not demonstrated. Once again, this shows that the uncontrolled survey group has brought an amount of bias into the conclusion.

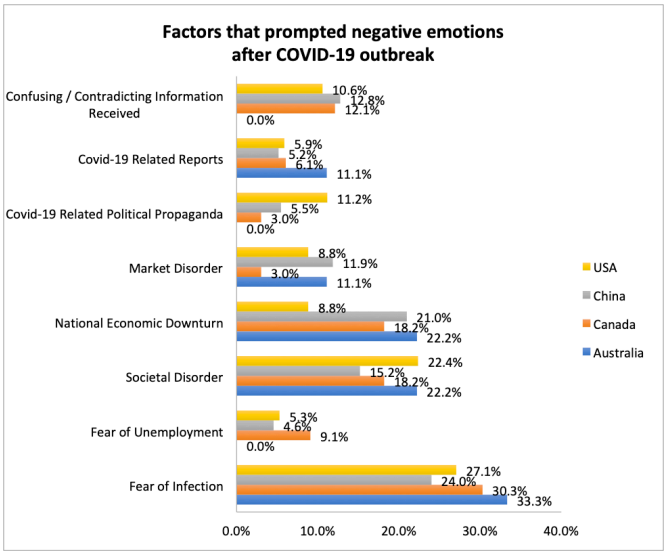

Figure 11: Respondent household annual income. 75.1% respondents' annual income is above $50K.

Another error-prompting decision was comparing toilet paper to rice as the essential good that people purchase in China. Toilet paper is irreplaceable, but rice is not. Therefore, rice might not lead to the best comparative results even though it generated a great amount of analysis.

Additionally, according to feedback, some questions had confusing wording, which could have led to inaccurate and invalid data. For instance, the question asking the participants to rate the experienced intensity of 8 emotions out of 0 to 10, some respondents stated that this question was hard to comprehend. Although the data demonstrated a clear trend, it could still have errors in it. For the future, it would improve the accuracy of the results if the survey were tested with more people who did not participate in the final process. They can provide feedback and help enhance the survey.

Conclusion

In conclusion, the survey and analysis demonstrate the different changes influenced by COVID-19. The participants demonstrated that, due to COVID-19, they experience negative emotions more frequently and intensely. Their actions also

DOI: 10.36838/v3i1.6

display a decrease in consumption of goods and grocery store shopping as they opt for more online shopping. Americans do have a tendency of saving toilet paper due to their lack of supply and fears that they will not have enough. This phenomenon is especially intensified due to media reports as they publicize its great demand but lack of supply. On the other hand, another presumed essential, rice, was not over-purchased since there were no media outlets publicizing the purchases, leading people to have no fear of running out and missing out. Lastly, the respondents demonstrate that the three most important factors determining their purchases are now more realistic and necessity-driven than personal needs and satisfaction fulfillment.

This research project provides deeper insight into how a global health crisis can change the way people feel, think, and buy. Although future research is needed to perfect and correct the problems discovered during the process of this project, it provided a base for the questions regarding the emotional and behavioral influence of a pandemic.

Methods

The data summarized in this paper were collected through an online survey designed in two languages – English and Chinese. Using bilingual versions and websites, the survey receives responses from people who currently reside in China, the United States, Canada, and Australia (62.6% live in China, 29.9% live in the United States, 5.9% reside in Canada, and 1.6% reside in Australia). The motivation to create the survey in two languages is to target a wider group of respondents living in different countries speaking different languages. Both the English and Chinese versions have the same questions, with only one exception. The English version included a question asking whether the participants increased their stock of toilet paper. In contrast, the Chinese version questioned whether the participants increased their purchases of bags of rice. These two questions target the two daily-use items that people in different countries view as necessities. The survey was started on July 12th, 2020, and concluded two weeks later, on July 26th, 2020.

Acknowledgement

I would like to thank my parents for their endless support during this process. I am also grateful for Professor Yochanan Shachmurove's guidance throughout this project. Additionally, I am thankful for the team at IJHSR and all survey respondents. Without your help, I would not have completed this research.

References

1. COVID-19 Map, 2020. Johns Hopkins Coronavirus Resource Center. https://coronavirus.jhu.edu/map.html.
2. Coronavirus in the U.S.: Latest Map and Case Count, 2020. The New York Times. https://www.nytimes.com/interactive/2020/us/coronavirus-us-cases.html.
3. New Cases of COVID-19 In World Countries, 2020. John Hopkins Coronavirus Resource Center. https://coronavirus.jhu.edu/data/new-cases.
4. Mental Health and Coping During COVID-19, 2020. Centers for Disease Control and Prevention. https://www.cdc.gov/coronavirus/2019-ncov/daily-life-coping/managing-stress-anxiety.html.
5. ILO Monitor: COVID-19 and the World of Work. 4th Edition, 2020. International Labour Organization. https://www.ilo.org/global/topics/coronavirus/impacts-and-responses/WCMS_745963/lang--en/index.htm.
6. Soucheray, Stephanie. US Job Losses Due to COVID-19 Highest since Great Depression, 2020. CIDRAP.https://www.cidrap.umn.edu/news-perspective/2020/05/us-job-losses-due-covid-19-highest-great-depression.
7. Survey Finds Large Increase in Psychological Distress Reported among US Adults during the COVID-19 Pandemic, 2020. ScienceDaily. https://www.sciencedaily.com/releases/2020/06/200603132550.htm
8. Restubog, Simon Lloyd D., Anna Carmella G. Ocampo, and Lu Wang. Taking Control amidst the Chaos: Emotion Regulation during the COVID-19 Pandemic 2020. Journal of vocational behavior, 2020. https://www.ncbi.nlm.nih.gov/pmc/articles/PMC7206430/
9. McGinty, Emma E., Rachel Presskreischer, Hahrie Han, and Colleen L. Barry. Psychological Distress and Loneliness Reported by US Adults in 2018 and April 2020, 2020. JAMA. https://jamanetwork.com/journals/jama/fullarticle/2766941.
10. Jin, Xiaotong, Wei Song, Taiyang Zhao, and Feng Yao. The Impact of Public Health Event on Irrational Consumption Behavior of Residents, 2020 维普资讯 Journal of Xi'an Jiaotong University (Social Science). http://lib.cqvip.com/Qikan/Article/Detail?id=7102492717
11. Lee, Shawna J., and Kaitlin P. Ward. STRESS AND PARENTING DURING THE CORONAVIRUS PANDEMIC, 2020. Parenting In Context Research Lab, 2020. https://www.parentingincontext.org/uploads/8/1/3/1/81318622/research_brief_stress_and_parenting_during_the_coronavirus_pandemic_final.pdf
12. Kluger, Jeffrey. Why Shoppers Are Hoarding Toilet Paper, 2020. TIME. https://time.com/5803273/hoarding-toilet-paper/.
13Why the Pandemic Unleashed a Frenzy of Toilet-Paper Buying, 2020. Nature. https://www.nature.com/articles/d41586-020-01836-1.
14. Carroll, Linda. Who Bought All the Toilet Paper? Study Suggests Who Was Most Likely to Stockpile during COVID-19, 2020.NBC. https://www.nbcnews.com/health/health-news/who-bought-all-toilet-paper-study-suggests-who-was-most-n1230586.
15. Mittone, L., & Savadori, L. The Scarcity Bias. Applied Psychology, 2009. 58(3), 453-468
16. Lofton, Justine. Why Are People Hoarding Toilet Paper during Coronavirus Pandemic? It's FOMO, 2020. MLIVE. https://www.mlive.com/coronavirus/2020/03/why-are-people-hoarding-toilet-paper-during-coronavirus-pandemic-its-fomo.html
17. Mao, Frances. Coronavirus Panic: Why Are People Stockpiling Toilet Paper?, 2020. BBC. https://www.bbc.com/news/world-australia-51731422.
18. Wu, Zunyou, Quanyi Wang, Jing Zhao, Chun Huang, Zijian Feng, Jennifer M. McGoogan, and Peng Yang. Time Course of a Second Outbreak of COVID-19 in Beijing, China, June-July 2020, 2020. JAMA. https://jamanetwork.com/journals/jama

fullarticle/2769930.
19. Scarcity, 2020. Wikipedia. https://en.wikipedia.org/wiki/Scarcity.
20. Rabin, Roni Caryn. Many in China Wear Them, but Do Masks Block Coronavirus?, 2020. The New York Times. https://www.nytimes.com/2020/01/23/health/coronavirus-surgical-masks.html.
21. Talev, Margaret. Ipsos Poll: The Coronavirus Death Toll Skeptics Are Growing, 2020. Axios. https://www.axios.com/axios-ipsos-poll-gop-skeptics-growing-deaths-e6ad6be5-c78f-43bb-9230-c39a20c8beb5.html?utm_source=twitter
22. Allyn, Bobby, and Barbara Sprunt. Poll: As Coronavirus Spreads, Fewer Americans See Pandemic As A Real Threat, 2020. NPR. https://www.npr.org/2020/03/17/816501871/poll-as-coronavirus-spreads-fewer-americans-see-pandemic-as-a-real-threat.

Author

Melissa Han is a senior at Flint Hill Upper School. She enjoys learning and studying social issues in the works of business. Melissa plans to double major in business and behavioral economics in college.

DOI: 10.36838/v3i1.6

Quantifying the LEctenna: Measuring the Invisible Made Visible

Michelle L. Yu

Thomas S. Wootton High School, 2100 Wootton Pkwy, Rockville, MD, 20850, USA; michelle.l.yu13@gmail.com

ABSTRACT: A light emitting diode (LED) rectifying antenna, also known as a LEctenna, is an easily constructible device (consisting only of an LED and a Schottky diode) that converts electromagnetic energy into direct current electricity. The LEctenna falls into the larger scope of power beaming and space solar, which is the process of wirelessly transmitting energy derived from sunlight in space to locations on Earth. More specifically, a satellite in space collects energy that the sunlight carries and beams the energy to Earth in the form of waves. A rectifying antenna on Earth collects the energy, converts it into direct current, and it is transported for consumption. The LEctenna serves as a representation of the rectifying antennas that are stationed on Earth. By implementing a self-developed brightness scale and a homemade invention that enhances radio frequency detection quantitative data was recorded with different LEctenna units. With this quantitative data, the overarching goal of this research is to develop conclusions centered around the behavior of the LEctennas in different situations as well as to analyze LEctennas in order to better understand everyday microwave energy.

KEYWORDS: Physics; Energy; Solar; Engineering; Power Beaming; Rectifying Antenna.

Introduction

All around the world, millions of people lack electricity, making simple chores in daily life more difficult. Villages in Africa and the Middle East lack the proper resources to provide their residents with electricity. One possible solution is the use of space solar and power beaming. Space solar is the process of gathering energy from sunlight in space and wirelessly transmitting that energy to Earth.[1] Energy from sunlight is abundant in space, as the sunlight is not obstructed or reflected by various objects. Satellites in space can collect the energy in sunlight and beam the energy to antennas stationed on Earth. Power beaming can bring electricity to even the most remote locations in the world, thus helping residents living in the country.

Another potential advantage of space solar power is that it opens a new realm of effectively unlimited energy. As fossil fuels continue to decline, the power via space solar can be a solution that offers safe and clean power to both the most populated cities and the most remote locations of the world.[2] The LEctenna is a smaller representation of the rectenna that is stationed on Earth. The LEctenna uses the "invisible" microwaves to power a light that human eyes can detect. The research that was conducted explores this subcategory of the LEctenna. A brightness scale was developed and a device that allowed me to quantify the voltage and lux the LEctenna emitted, which had not previously been done before. This quantitative data helps to understand the properties of microwaves that are used in homes every single day and can be related to some aspects of power beaming.

Methods

Making the LEctenna:

When constructing the LEctenna, the black stripe on the 1N5711 Schottky diode was placed opposite the flat part of the LED, as seen in Figure 1 in a future section. It was recently found by a colleaque at the NRL that the NTE112 diode also works for the LEctenna.The black stripe represents the cathode side of the Schottky diode and the flat part of the LED represents its cathode side. The LEctenna performs best when the leads of the diode and LED are only wrapped around each other 2 to 4 times. The number of times the two leads are wrapped is relevant to the length of a microwave length. If the LEctenna's receivable wavelength is too long or too short compared to the microwave, the LEctenna will not light up to its full potential. Furthermore, the LEctenna is brighter if only one diode is paired with the LED, rather than pairing 2 or 3 diodes with an LED. Multiple diodes paired with one LED were tested, the results and more analysis can be found in Appendix B.

Additionally, a soldering iron was not used to join the two leads together. To clarify, the WiFi frequency was 2.4G Hz or a dual band. A plastic straw was used to hold and stabilize the LEctenna as it was held up to objects. Other objects, such as a plastic test tube or glass straw, could also be used. One end of the LEctenna was taped to the end of the straw and it was held up to the Wi-Fi router. As long as one doesn't come in direct contact with the leads of the LEctenna, the straw can be held at any distance away from the LEctenna. When one touches the lead of the LEctenna, the resistance in the circuit increases and the light of the LED fades.

Constructing the PARME Phone Attachable RF Meter Enhancer):

An important aspect when using the PARME is that the top of the LEctenna should be aimed towards the phone camera,

DOI: 10.36838/v3i1.7

seen in Figure 1, as viewed by the phone's camera. Additionally, when actually measuring the lux from the LEctenna, the device works best when the room is relatively dark, to avoid capturing extraneous light.

Figure 2 is a screenshot of the Lux Light Meter app opened on a phone. The application is free to use with a few helpful features, such as average and maximum lux. It should be mentioned that the numbers that are displayed in Figure 2 are

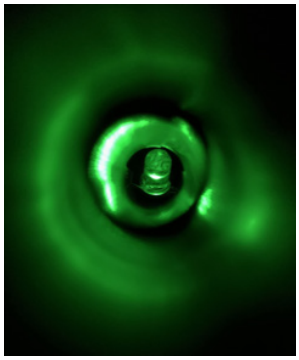

Figure 1: LEctenna inside of the shaft of the PARME.

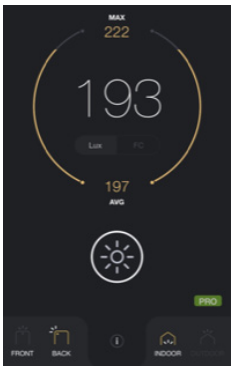

Figure 2: The application on a phone when pointed at a desk lamp.

measurements with the phone being pointed at a lamp rather than the LEctenna.

The PARME only requires easily attainable household items to construct. The main items consist of thick bubble tea straws, cardboard, and glue. The first part to build is the shaft and the area that supports the back of the phone. First a hole was cut through the center of a piece of cardboard, just large enough for the bubble tea straw to slide into, the dimensions being 3.20 x 3.20 cm. The diameter of the straw was about 1 cm long. The straw that served as the shaft was 3 cm in length. Then, two straws were measured to a length of 3.20 cm and placed them on either side of the shaft for support. Additionally, a smaller piece of straw, with a length long enough to reach the shaft and the outer edge of the cardboard, was attached. Finally, glue was to secure all the pieces on the cardboard. The finished piece is shown in Figure 4.

Next is the piece that allows the device to be attached to the phone. A piece of cardboard was cut to a width of 1 cm and a length between 3-5 cm (depending on thickness of phone) and glued flat on top of the center straw piece in Figure 4. Then, at the end not connected to the straws, the cardboard was bent downwards at a 90-degree angle and it was glued in place with the help of other small cardboard pieces. The bend location finished piece is shown in Figure 4. Multiple layers of cardboard can be added for stability. Once the glue dries, this next part is determined by phone size and may be slightly different for different phones. The phone was held so that the camera was aimed inside the shaft of the device. Then, small pieces of cardboard were added above and besides the phone so that the device attaches to the phone without any outside support.

Figure 3: The shaft and the arrangement of the bubble tea straws used for support.

Figure 4: The piece that allows a phone to be attached to the PARME.

The final piece held the LEctenna in place. A piece of straw that was cut to 3.5 cm in length was then cut horizontally in half on one end, so that the inside of the straw is exposed. At the exposed side, two slits, on either side, were cut so the LEctenna could be placed. Next, the other half was cut parallel down the middle of the straw so that the radius of the straw can be adjusted to a size that will be able to fit in the shaft. Again, a tighter fit was preferred over a looser fit. Some tape was used to secure the appropriate size. The finished piece is shown in Figure 5.The completed PARME device is shown in

Figure 5: The piece that holds the LEctenna in place.

DOI: 10.36838/v3i1.7

Figure 6: The PARME attached to the phone.

Figure 6. The piece in Figure 5 is slid inside the shaft of the piece shown in Figure 3. Figure 6 shows how the PARME should be attached to the phone. It is important to ensure before collecting data that the PARME is correctly placed over the phone camera. If the PARME ends up shifting around when in use, small pieces of cardboard can be added to increase stability.

Results and Discussion

The LEctenna:

The rectifying antenna is called the rectenna. A rectenna is a type of receiving antenna that converts electromagnetic energy, such as radio or microwaves, into direct current that can be used to power everyday objects.[3] The LEctenna is composed of two components: an LED and a Schottky diode, whose leads form the antenna. An image of the LEctenna can be seen in Figure 7. A Schottky diode is generally used because it has the lowest voltage drop and the fastest switching speed.[4] The diode only allows current flow in one direction, which occurs when it is forward-biased. The voltage across a forward-biased light emitting diode results in a current that will illuminate the LED.[5] When held up to different objects, such as Wi-Fi router antennas and microwave ovens, the LEctenna will have varying levels of brightness and lux values because the different objects transmit waves differently. Both red and green LEDs were used to make LEctennas to compare patterns and make assumptions.

Phone Attachable RF Meter Enhancer (PARME):

In an attempt to collect more concrete measurements, a downloadable application on a smart phone was used to measure the amount of lux that the LEctenna emitted. The name of the application being Lux Light Meter Pro.[6] Although the application works well and is fairly accurate, the flashing of the LEctenna causes the emitted light to only be partially captured, which results in some error margins. After some poor attempts to measure lux, it became clear that a better way for the light to be focused directly at the smart phone camera was needed. Then, a device, which can be attached over a phone camera was created, allowing the light from the LEctenna to be directed at the phone camera for more conclusive measurements. This device was only tested with an iPhone XS but can be altered to be compatible with other phone designs. Figure 8 shows the completed PARME, fitted to the dimensions of an iPhone XS.

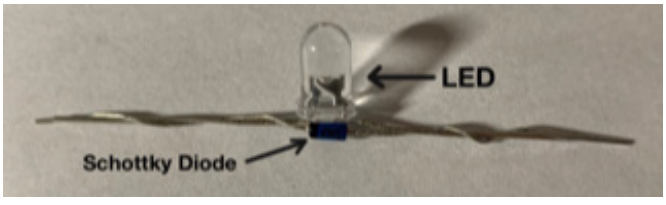

Figure 5: The piece that holds the LEctenna in place.

Brightness Scale:

Defining a brightness scale in more concrete terms is important, as describing the brightness of an LED has the potential for ambiguity. This brightness scale measures the voltage of the LEctenna in different situations and categorizes the brightness into 4 levels. As the data for the distinct brightness levels was collected, as shown in Table 1, a digital multimeter with alligator clips was connected to the LEctenna, which increased resistance in the circuit. In order for the voltage of the LEctenna to reach a specific amount, cardboard that is covered in aluminum foil was used to increase the brightness. These cardboard pieces are shown in Appendix A.

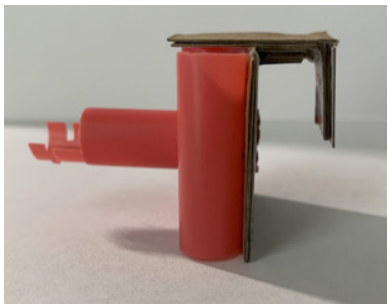

Figure 8: The finished PARME device.

The first brightness level is determined as just a speck of light. The LEctenna was held 5 to 7 cm away from the Wi-Fi antenna and slowly slid the LEctenna closer until a speck of light appeared. Then the Lectenna was slid towards the antenna until distinct changes in brightness was observed, which led to the development of more brightness levels. In Figures 9 and 10, images of level one brightness are shown for both different color LEctennas. Any voltage that was less than the minimum voltage for level 1 for either AC or DC was too dim to be observed or no light was emitted from the LED.

From level 2 to level 4, the distinction between levels is visually more subtle. The second brightness level is noticeably brighter than level 1, but still not incredibly bright. Figures 11 and 12 show generally what a level 2 brightness looks like compared to level 1.

Table 1: The 4 levels of brightness with the corresponding voltage values.

	Green LED		Red LED	
Voltage (volts)	DC Voltage	AC Voltage	DC Voltage	AC Voltage
Levels				
Level 1	0.15 - 0.30	0.20 - 0.30	0.10 - 0.20	0.10 - 0.20
Level 2	0.35 - 0.50	0.30 - 0.60	0.25 - 0.36	0.36 - 0.55
Level 3	0.60 - 0.75	0.70 - 1.00	0.40 - 0.55	0.65 - 0.90
Level 4	0.75 - 1.10	1.00 - 1.50	0.60 - 0.75	1.00 - 1.30

Figures 9 and 10: The appearance of level 1 brightness for the two different colored LEctennas.

The third brightness level is brighter than the second level and appears fuller than earlier levels. Figures 13 and 14 can be compared with prior figures to compare the brightness.

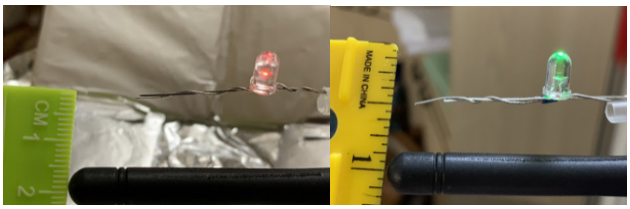

Figures 11 and 12: The appearance of level 2 brightness.

Although the voltages were greater for level 3, the pulsing of the LEctenna increased and, as a result, the brightness varied between extremes more rapidly.

The fourth and the highest tier in this brightness scale can be described as noticeably the brightest and fullest in light.

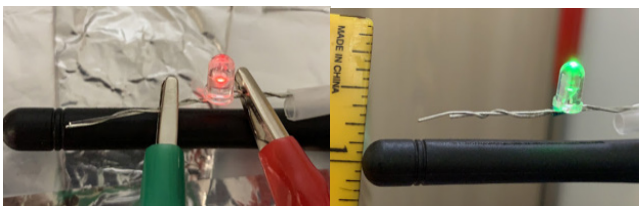

Figures 13 and 14: The appearance of level 3 brightness.

Overall, the voltage for the red LED LEctenna is generally lower than the green LED LEctenna, but as seen in Figures 15 and 16, their brightness' seem similar.

Figures 15 and 16: The appearance of level 4 brightness.

Brightness and Waves:

From prior sections and Appendix B, we can understand the effects the diode has on the LED and how the two components work as a whole. Each added Schottky diode corresponds with a voltage drop of 0.2 to 0.3 volts. Next, the behavior of the LEctenna, as it is held next to the WiFi antenna, was examined.

Initially, as the LEctenna was held up to the WiFi router antenna at distance zero with no alligator clips attached, the brightness varied around levels 2 to 4, depending on which color LED was used. The flashing of the LEctenna makes it more difficult to record completely accurate information, hence the error margins in the Figure 18 that appears qualitatively to be approximately 10 percent. The intermittent delivery of network packets is presumed to be the cause of the LEctenna's sporadic flashing. Network packets are individual units that carry information from an origin to a destination in a network.[7] When a message is sent, it is broken up into packets and sent to its destination, where it is then rearranged and reassembled. When more packets are sent over a specific unit of time, the LED's brightness increases, due to the larger amount of energy delivered. The amplitude of the wavelength correlates to the amount of energy that the packet carries. Larger amplitude means greater energy per packet. Additionally, many things, such as physical objects, other wireless appliances, and kitchen appliances, interfere with the Wi-Fi signal and can cause slow network speeds, pauses in connection, and poor signal strength.[8]

Another possible explanation for the pulsing of the LEctenna is the peaks and troughs of the waves. The different peaks and troughs correspond to how electrical charge is distributed through the wave. Since the diode only allows current flow in one direction, the positive amplitude portion of the wave will light up the LEctenna, but the negative amplitude portion will not. In Figure 17, a visual representation of a wave can be seen. The portions with a dotted line below the yellow line will cause the LEctenna to shut off. The solid lines represent the portion of the wave that turns on the LEctenna.

In Figure 18, a graph was created of how the voltages of

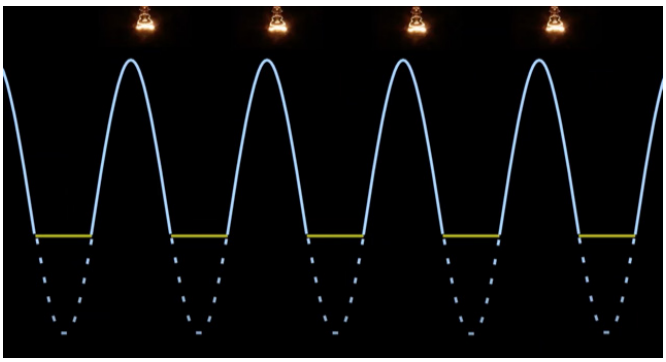

Figure 17: This is a representation of the different sections of the wave as it is rectified by the LEctenna.[9]

the different LEctennas and diodes vary as they are held at different distances from the center axis of the WiFi antenna. The forward voltage of the green LED is greater at around 3.2 to 3.8 volts compared with the red LED's forward voltage of 1.8 to 2.2 volts. When comparing the brightness of the two LEctennas, the green LED LEctenna appeared to be brighter than the red LED LEctenna. Additionally, humans perceive green light as being brighter than red light.[10] When collecting the data, the Schottky diode behaved very interestingly. Out of the three devices, the diode had the lowest average voltage. Occasionally, the Schottky diode's voltage would become very low at around 0.01 for a few seconds, but this data was mostly disregarded.

As suspected, the voltage of the LEctenna varies when it is held up to different objects. For example, when the LEctenna

DOI: 10.36838/v3i1.7

is held next to a microwave oven door crack, the voltage of the LEctenna is higher as a result of the microwaves being steadily delivered, rather than in small packets. When held directly on the crack of the door, the voltage of the green LED LEctenna was around 2.0 volts, which is about twice the voltage of the same LEctenna as it is held against the WiFi router antenna. The microwave oven generates more power than a WiFi router, which causes the LEctenna to be brighter.

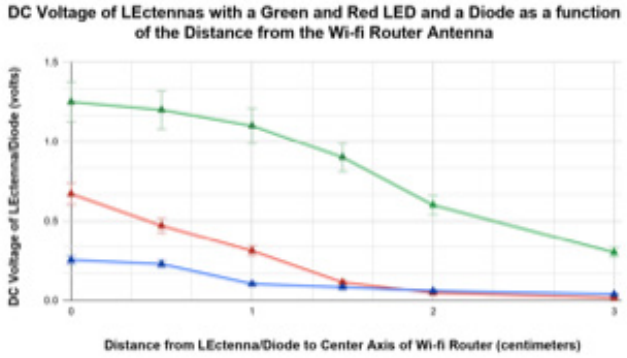

Figure 18: The measured DC voltage of LEctennas with green and red LEDs and a Schottky diode alone when measured at various distances from the center axis of the Wi-Fi router antenna.

Figure 19 shows the data that was recorded using the Lux Light Meter Pro application and the PARME. The LEctenna was held at different distances from the center axis of the Wi-Fi router antenna and the average and maximum lux for multiple trials were recorded. The values for average and maximum lux were taken directly from the application over a 10 to 20 second period. The periods were dependent on the behavior of the LEctenna. If the brightness was dimmer, the period would be extended in order to get more accurate results. For the values of average lux, the red LED LEctenna had overall higher values than the green LED LEctenna. Interestingly, for the maximum lux, the green LED LEctenna had greater values than the red LED LEctenna. This data could possibly be skewed by the inaccuracy of the Lux Light Meter app. Although the lux values varied between the different color LEctennas, at a distance of zero centimeters, both LEctennas emitted a level 4 brightness. However, the average values for a distance of 2 and 3 centimeters were very close to the value of zero, and as a result, the values were rounded to zero for simplification. Additionally, the maximum values for distances 2 and 3 centimeters were also around a value of 10, so similarly, they were rounded to 10 lux for simplification. The larger margins of error account for the inaccuracy of the lux meter caused by the pulsing of the LEctenna.

In both Figures 18 and 19, a general pattern is shown. As the LEctenna is moved away from the Wi-Fi router antenna, the lux and voltage decrease. Because of the way that antenna signals work, the power density of the signal decreases as the LEctenna is moved farther from the antenna.[8]

A separate experiment was conducted to determine how the range of the LEctenna could be increased. Simple household objects like tin foil and cardboard can be used to construct reflectors that can be aimed at the LEctenna and Wi-Fi router to increase range. More on this experiment is shown in Appendix A.

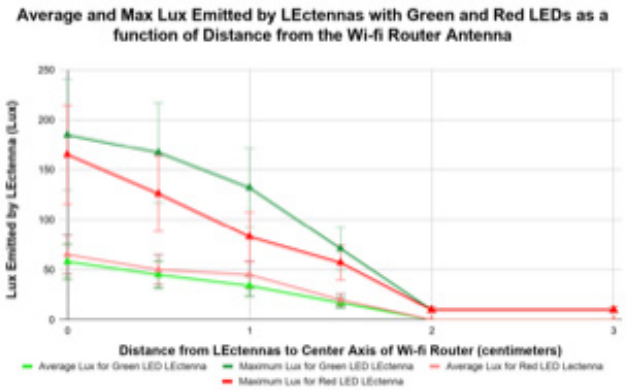

Figure 19: This line chart shows the average and maximum lux values of the LEctennas with a green and red LED when measured from the center axis of the WiFi router.

Conclusion

In conclusion, with the LEctenna as a visual representation, the voltage and lux recorded by the PARME allow us to understand the presence and relative strength of microwaves found in the home. The flashing of the LEctenna shows that there are individual packets being rapidly sent through the Wi-Fi network. Furthermore, the different voltage and lux values for the different color LEctennas reveal that color of the LED is a determining factor for perceived brightness. These conclusions can be drawn from the results that conform to the expected antenna characteristics. From the behavior of the LEctenna, general trends about increased distance and weakened power can be related and used in power beaming. In addition, the LEctenna can also be used as an example to show the public that the process of power beaming could be a safe and efficient way to transmit power to specific locations on Earth.

Acknowledgement

I would like to express my deepest gratitude to Dr. Paul Jaffe of the Naval Research Laboratory for assisting me and sharing his deep knowledge and experience in every stage of this research project.

References

1. Space Solar Power. https://space.nss.org/space-solar-power/ (accessed Jul 24, 2020).
2. Wood, D. Space-Based Solar Power https://www.energy.gov/articles/space-based-solar-power (accessed Jul 20, 2020).
3. Aboualalaa, M., & Elsadek, H. (2019, October 29). Rectenna Systems for RF Energy Harvesting and Wireless Power Transfer. Retrieved August 17, 2020, from https://www.intechopen.com/books/recent-wireless-power-transfer-technologies/rectenna-systems-for-rf-energy-harvesting-and-wireless-power-transfer
4. Schottky Diode Working and Its Applications. https://www.elprocus.com/schottky-diode-working-and-applications/ (accessed Aug 3, 2020).
5. Introduction to Diodes And Rectifiers.

https://www.allaboutcircuits.com/technical-articles/ (accessed Aug 2, 2020).
6. Polyanskaya, M. Lux Light Meter Pro; Measure Luminosity in Lux & FC, 2017.
7. What is a packet? https://beambox.com/townsquare/what-s-the-difference-between-2-4ghz-and-5ghz-wifi (accessed Aug 1, 2020).
8. How to troubleshoot Wi-Fi Interference with NetSpot https://www.netspotapp.com/wifi-interference.html (accessed Jul 30, 2020).
9. USNRL. LEctenna on ISS; Youtube: USA, 2020. https://www.youtube.com/watch?v=zo7w0D6vz5g
10. Visible Light and the Eye's Response https://www.physicsclassroom.com/class/light/Lesson-2/Visible-Light-and-the-Eye-s-Response (accessed Aug 1, 2020).

Appendix A: Maximizing Range

For maximizing the range of the LEctenna, three different cardboard pieces covered with aluminum foil were used. The first piece (piece A) is one that was placed on an object about 5-6 centimeters below the LEctenna and the router antenna. In Figure 20, piece A is shown. To start, the 3 larger cardboard aluminum foil pieces, identical to each other with dimensions of 7 x 10 cm, were connected at the longer side. One piece is laid flat on the table while the other two pieces are angled above the horizon. Figure 21 shows how the pieces were angled. This allows waves to be reflected off the aluminum foil and towards the LEctenna. Next, 2 smaller pieces of cardboard aluminum foil, with dimensions of 3 x 3.5 cm, were taped to the middle piece of the three pieces, directly above the shorter side, also at similar angles as the larger pieces were placed. Finally, aluminum foil was used to connect the edges of the smaller pieces to the edges of the larger pieces. In the pictures, the creases were covered with more aluminum foil, but it is unclear if it changed the effectiveness.

The second piece (piece B) is the smallest piece of cardboard covered with aluminum foil. Figure 22 shows the dimensions and the shape of the piece B.

Figure 20: This is the completed piece A.

Figure 21: The angle of the pieces.

The third piece (piece C) consisted of three smaller pieces taped together. The largest piece had dimensions of 15.25 x 7.60 cm and the smaller pieces were identical to each other

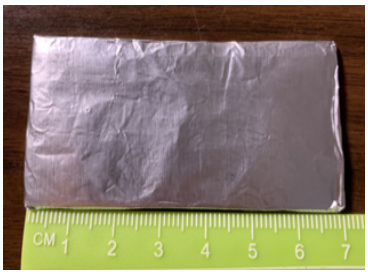

Figure 22: The dimensions (7 x 3.8 cm) of the second piece of cardboard covered foil.

with dimensions of 6.35 x 5.0 cm. As the largest piece was horizontally laid flat on the table, the two smaller pieces were taped at the top of the longer side, not beside the piece. Each piece was taped at the farthest ends of the larger piece, with a space between the two smaller pieces. Then as the larger piece was bent in the middle, the space between the two smaller pieces was connected with aluminum foil. These creases were covered with aluminum foil. For clarification, see Figures 23 and 24.

When experimenting, the method that was found to be effective was to hold pieces B and C up to the LEctenna and antenna, while piece A is placed beneath all the objects. Figure

Figure 23: The completed third piece for maximizing range.

Figure 24: The dimensions of the third piece.

25 shows how the pieces were set up. To better maximize the brightness results, piece B is held closer to the Wi-Fi router and piece C is held closer to the LEctenna. It is important to note that the aluminum foil part of piece C is held adjacent to the LEctenna. Piece B should be aimed at the LEctenna or

DOI: 10.36838/v3i1.7

the aluminum foil behind the LEctenna. Varying the direction that the pieces are facing and the positions that the LEctenna is held at besides the antenna will help to maximize brightness. To continue the experiment, the LEctenna was moved away from the router antenna while the cardboard aluminum foil pieces were moved accordingly and used the same method to determine the farthest distance from the router that the LEctenna would light up at. The farthest that was able to be reach was around 12.7 cm with a voltage ranging between 0.5 to 1 volt.

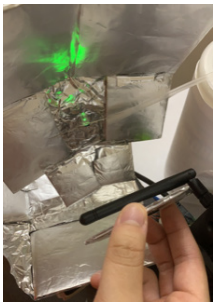

Figure 25: The set up the cardboard foil.

Appendix B: Multiple Diodes

When making the LEctenna with multiple Schottky diodes, two methods were used. The first method is similar to the one for making a simple LEctenna. First a simple LEctenna was used. Then the diode was wrapped around the LED 3-4 times while making sure that the ends of the leads were straight. Then, the other diode was wrapped it 3-4 times around the LEctenna that was just made. The second method that was used was, first, the diodes were wrapped around each other 3-4 times. Then, the double diode was wrapped around the LED. In both methods, the leads were twisted in a way that would maximize the amount of contact the two leads had with each other.

When using multiple diodes, it was clear that although both one diode LEctennas and two diode LEctennas lit up, the LEctennas with only one diode lit up brighter. When comparing the data that was collected from the two different types of LEctennas with green LEDs, the LEctenna with one diode had a DC voltage of around 1 volt while the LEctenna with two diodes had a DC voltage of around 0.8 to 0.85 volts. However, even though they have similar brightness levels, the behaviors of the two LEctennas were different. With only one diode, the pulsing of the LED fluctuated between brightness levels at a faster pace. With 2 or 3 diodes, even though the light was dimmer, it was emitted more steadily.

The method that was used to wrap the two diode LEctennas did not have much effect on the overall performance of the LEctenna. Whether method one or method two was used, the determining factor is the overall amount that the leads contacted each other.

One possible reason that the LEctenna with two diodes had a lower voltage is that the added diode caused the voltage to drop more. Through experimentation, one can conclude that an added diode resulted in a voltage drop from around 0.20 to 0.30 volts. This pattern was displayed with the LEctenna with the green LED as well as with the LEctenna with a red LED. The voltage drop of the green LED alone was around 3 volts and the red LED alone was around 2 volts. Although with one diode, the voltage dropped more than around 0.20 volts, but with every added diode this trend occurred. With one diode, the voltage of this LEctenna was around 0.80 to 0.90 volts. With two diodes, the voltage dropped to around 0.60 to 0.65, which is around a 0.20 to 0.30 drop.

Author

Michelle Yu, a junior at Thomas S. Wootton High School, is interested in many aspects of STEM, such as biology, biochemistry, and engineering. With high hopes to influence and help others around her, she wants to pursue either medicine or biomedical sciences.

Brain Cancer Cell-derived Exosomes Protect Scopolamine-Induced Death of SH-SY5Y Neuron Cells

Minseo Lee

Cranbrook Kingswood, 39221 Woodward Ave, Bloomfield Hills, MI 48304, USA; gosyber@suwon.ac.kr

ABSTRACT: Exosomes are the nano-sized extracellular vesicles secreted by most of the cell types. The role of exosomes in cells is to function as important intercellular messengers and contributors to both disease development and health. Many studies have discovered the role of exosomes in Alzheimer's disease (AD). Exosomes have been shown to induce apoptosis and neuronal loss. On the other hand, exosomes possess the ability to reduce brain amyloid-beta and to transfer neuroprotective substances between cells. However, the effect of exosomes derived from cancer cells has never been investigated. In this study, it was hypothesized that exosomes derived from cancer cells protect neurons from cell death because these exosomes are known to contain many cancer-promoting substances that proliferate cancer cells. This study found that exosomes derived from the A172 brain cancer cell line increase cell viability of differentiated SH-SY5Y neuron cells from scopolamine hydrobromide (SH)-induced cell death. Since cancer-derived exosomes have potential as therapeutic tools for AD with their neuroprotective effects, further studies are required to determine what substances inside the exosome protect the neuron cells from SH-induced cell death.

KEYWORDS: Biochemistry; Physiology; Exosome; Cancer; Neuron; Scopolamine Hydrobromide; Cell Death.

Introduction

Alzheimer's disease (AD) is a type of dementia that interferes with memory, thinking, and behavior; it is a progressive disease that worsens over time.[1] Early-stage Alzheimer's symptom entails having difficulty learning since it typically originates in the part of the brain that controls learning.[1] Subsequently, Alzheimer's patients go through severe symptoms, such as behavioral changes, confusion surrounding dates and events, and difficulty speaking and swallowing.[2] Two abnormal brain structures, plaques and tangles, are suspected of damaging nerve cells, and therefore leading to Alzheimer's.[2] Plaques are deposits of protein fragment beta-amyloid that takes space between nerve cells, and tangles are twisted fibers of a protein called tau.[3] Despite the common belief that Alzheimer's is reserved for the elderly, approximately 200,000 Americans have younger-onset Alzheimer's disease.[4]

SH-SY5Y is a human-derived cell line isolated from the bone marrow of a four-year-old female with neuroblastoma.[5] SH-SY5Y cells can be differentiated from a neuroblast-like state into mature human neurons using retinoic acid (RA).[5] The molecular mechanism of retinoic acid's role in neuronal differentiation has yet to be determined. However, a previous study hypothesized that it might regulate receptor tyrosine kinase-like orphan receptor 1 (ROR1) for retinoic acid-induced differentiation.[6] In this experiment, retinoic acid is used to differentiate SH-SY5Y into neuron cells.

Scopolamine hydrobromide (SH) causes cytotoxicity and downregulation of neuronal and glial cell markers.[7] SH blocks the activity of muscarinic acetylcholine receptor, which is frequently observed in those with AD. Even though SH cannot induce the full range of deficit seen in patients with AD, SH is often used to mimic the damage of AD in cell culture models.[7] Therefore, SH is used to mimic the damage of Alzheimer's disease on differentiated SH-SY5Y in this study.

The exosome is an extracellular vesicle released from cells that carries proteins and nucleic acid materials, including all types of RNA.[8] Cancer cell-derived exosomes also carry the biological contents of cancer cells but have different effects.[9] The four effects of cancer cell-derived exosomes are the formation of metastatic lesions, the acquisition of the capacity to avoid attacks from immune cells, the acquisition of migratory and invasive capacity, and the enlargement of cancer tissue angiogenesis and cell proliferation.[10] Also, cancer cell-derived exosomes are messengers of signals that involve pathogenesis, development, progression, and metastasis of cancer cells.[10]

In this investigation, the goal was to discover the effects of cancer-derived exosomes on cell viability of differentiated SH-SY5Y cells. It was predicted that these exosomes would increase the cell viability of neuron cells by delivering cancer cell-derived proteins and RNAs, which are known to enhance the cell cycle and inhibit apoptosis. Therefore, considering the close relationship between cancer cell-derived exosomes and cell proliferation and survival, the protective effect of cancer cell-derived exosome on cell viability of SH-induced neuronal cell death was examined.

Methods

SH-SY5Y and A172 cell line culture:

SH-SY5Y and A172 cell lines were purchased from Korea Cell Line Bank (KCLB). The cells were maintained at 37 °C in a CO_2 incubator. Cells were trypsinized and fresh RPMI media (GIBCO) was provided every three or four days.

Exosome isolation from cell culture media:

From its cell culture media, the exosome of the A172 cancer cell was isolated. After harvesting 8 mL cell culture media of A172, it was mixed with 4 mL exosome isolation reagent (Sig

DOI: 10.36838/v3i1.8

ma). Then, the culture media/reagent mixture was incubated in 4 ºC overnight. 1 mL 1X PBS (WELGENE) was used for resuspension. The isolated exosome is then stored in -80 ºC for long-term storage. Negative control exosome was prepared from RPMI 1640 cell culture media (i.e. treated the same but no cells added) to check if the media is completely depleted with any exosomes from cancer cells.

Retinoic Acid (RA) treatment:

The retinoic acid stock solution was made to have a concentration of 5 mM. 15.022 mg retinoic acid powder (SIGMA, R2625) was dissolved in 10 mL DMSO (JUNSEI, lab no. 201414005). After vortexing, the mixture of retinoic acid powder and DMSO, was filtrated of small floating matter by using a 0.22 filter on the tip of the injector. Final concentration of 5 mM of RA was used to differentiate SH-SY5Y cells into neurons.

Scopolamine hydrobromide (SH) treatment:

Scopolamine hydrobromide stock solution was made to have a concentration of 50 mM. 109.5 mg scopolamine hydrobromide powder (SIGMA-ALDRICH, PHR1470) was dissolved in 5 mL DDW (BIONEER, C-9011). The working condition for the scopolamine hydrobromide solution was decided as 2 mM, after examining and comparing the effect of five different concentrations of scopolamine hydrobromide.

Western blot analysis:

Whole-cell lysates were prepared using Passive Lysis Buffer purchased from Promega (Madison, WI). The cell extracts (50 µg) were loaded on a 15% sodium dodecyl sulfate-polyacrylamide gel for electrophoresis, and proteins were transferred to polyvinylidene fluoride membranes with a Mini Trans-Blot® tank (Bio-Rad, Hercules, CA). The membrane was probed with antibodies against Flotillin-1 (ab41927, Abcam), CD63 (EXOAB-KIT-1, System Bioscience), and GM130 (cell signaling). All secondary antibodies (Santa Cruz Biotechnology, Dallas, TX) were incubated for 1 hr. Detection was performed using an Amersham ECL GST Western Blotting Detection Kit (GE Healthcare Life Sciences, Piscataway, NJ).

Analyzing the total cell number and cell viability in SH-SY5Y:

The cells were trypsinized and afterwards isolated exosome and SH were incubated for 72 h. The percentage of viable cells was measured by counting cells, which were stained by acridine orange/propidium iodide, an apoptosis indicator, with the Luna-FL Dual Fluorescence Cell Counter (Logos Biosystems).

Statistical analysis:

Data were expressed as the mean values ± standard error and analyzed by Student's t-test using Prism 7 and Microsoft Excel. All statistical results were considered significant if p-values were 0.05 or less.

Results and Discussion

Differentiation of SH-SY5Y cells to neuron cells by retinoic acid:

Several studies indicated important differences between undifferentiated and differentiated SH-SY5Y cells.[11,12] When SH-SY5Y cells are undifferentiated, they appeared to be non-polarized and proliferate rapidly.[12] When they are differentiated, the cells appeared to be branched and extend long with a decrease in cell proliferation.[12]

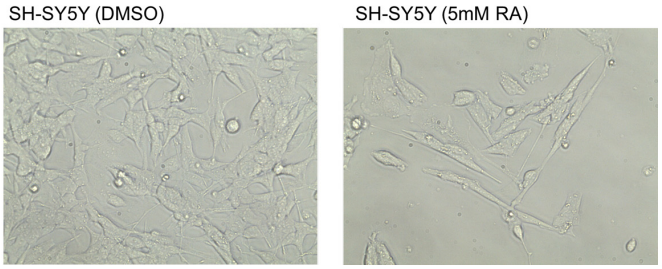

Figure 1: Images of SH-SY5Y cells treated with DMSO and 5mM Retinoic Acid (RA).

To confirm the differentiation of SH-SY5Y to neuronal cells by RA, we checked the changes in cell morphology and cell confluence. Figure 1 shows the change in cell morphology of SH-SY5Y cells after 5 mM RA treatment. Compared to the SH-SY5Y that was treated only with DMSO, SH-SY5Y with 5 mM RA displayed longer and narrower cell shape with fewer numbers of cells (Figure 1). This result indicates that RA successfully differentiated SH-SY5Y cells into neurons. However, the neuronal characteristics were not fully validated by the classical neuronal markers in this experiment.

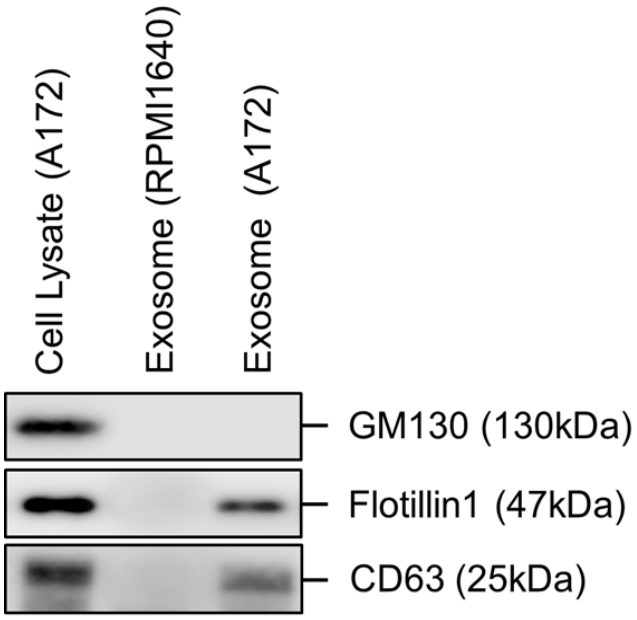

Figure 2: The protein expression level of GM130, Flotillin1, and CD63 analyzed by western blot. The protein size of the target proteins is indicated in kDa.

Exosome isolation from A172 cell culture media:

Human A172 cell line was used to collect brain cancer cell-derived exosomes from cell culture media. The western blot was used in this experiment in order to make sure that the exosome was completely isolated in our experiment without any contamination of cell lysate. Three samples were analyzed in this experiment: cell lysate for positive control, exosome isolated from RPMI1640 cell culture media for the negative control to make sure the media is truly depleted of cancer-de-

media (Figure 2). Figure 2 shows that the cell lysate contained all proteins, but the exosome isolated from RPMI 1640 media does not contain any proteins. It also demonstrates the presence of canonical exosome proteins (Flotillin1 and CD63) and the absence of Golgi protein GM130 from isolated A172 derived exosome (Figure 2). Taken together, the western blot demonstrated that A172 derived exosome produces high quality purified exosomes free from other cellular contaminants.

Protective effect of cancer cell exosomes on SH-mediated neuronal cell death :

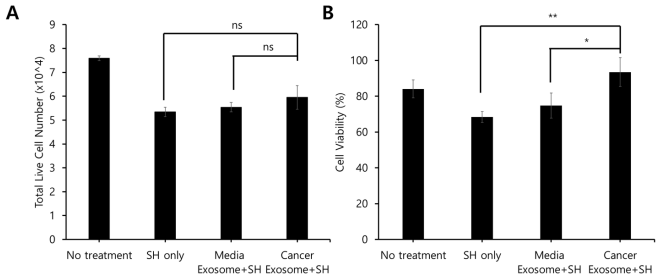

Figure 3: Effect of exosome pre-treatment on total cell number and cell viability of SH-SY5H. Three biological replicates were measured (n=3).

To confirm the protective role of cancer cell-derived exosomes on SH-SY5Y cell death driven by SH, we pretreated exosomes on SH-SY5Y for 1 hr. Then, the cells were further incubated with SH for 24 hr to induce cell death. To compare the effect of cancer cell-derived exosome on cell viability, we prepared four different groups of samples: no treatment, SH only, media exosome with SH, and cancer cell-derived exosome with SH. No treatment sample was used as a negative control that was not treated with SH and exosomes. The SH only sample was treated only with SH but not pretreated with any exosomes. Media exosome with SH sample was pretreated with RPMI1640-derived exosome and SH was post-treated. Cancer cell-derived exosome with SH sample was pretreated with cancer cell-derived exosome and SH was post-treated.

Figure 3 demonstrates the effect of cancer cell-derived exosome on SH-SY5Y cell number and cell viability. The cancer cell-derived exosome has no significant effect on total number of live cells (Figure 3A). However, cancer cell derived exosome significantly increased the cell viability compared to SH only sample and media exosome with SH sample (Figure 3B). Since this experiment only analyzes the early effect of cancer cell-derived exosomes on cell viability that the incubation time of both exosome and SH is limited to 25 hr., further experiments are needed to examine the change in cell viability for longer incubation times.

Exosomes are involved in the spread of 'toxic' proteins in neurodegenerative disorders such as AD, Huntington's disease (HD), and Parkinson's disease (PD).[13,14] The mutated or misfolded proteins induce neuronal cell death.[13] On the other hand, the role of exosomes on neuronal protection, nerve regeneration, and neuronal development have been studied, indicating the release of exosomes by neurons, microglia, and astrocytes.[15] However, the role of exosomes derived from cancer cells on neuronal protection has never been investigated. In this study we found that brain cancer derived exosomes have neuroprotective effects against SH-mediated cell death on differentiated neuronal SH-SY5Y cells. A previous study indicated that cancer derived exosomes from lung cancer cells inhibit cell apoptosis of normal lung fibroblast.[10] Colon cancer cells secrete exosomes to promote self-proliferation by shortening mitosis duration.[16] These studies suggested that exosomes from cancer cells delivered functional, transportable mRNA, miRNA, and oncogenic proteins and activated proliferation-related cellular pathways. Therefore, delivering these substances by cancer derived-exosome likely contributed to inhibiting neuronal cell death induced by SH. However, future studies are needed to confirm which molecules from the cancer-derived exosome protect the neurons.

SH is known to cause cell death through intrinsic apoptosis in neuronal cells.[17] In addition, scopolamine decreased cell viability and MMP, and increased caspase-3 activation and PARP cleavage in SH-SY5Y cells.[17] Therefore, it is possible that cancer derived exosomes may block the intrinsic pathway of apoptosis to protect SH-SY5Y cells. However, screening of apoptosis markers is needed to elucidate the molecular mechanism of neuroprotective effect induced by cancer-derived exosomes.

Conclusion

It was discovered that the cancer cell-derived exosomes have a protective role on neuronal cell death caused by SH. However, since our experiment was solely on the SH-SY5Y cell line, further experiments with different neuron cells are needed to confirm the role of cancer cell-derived exosomes. Since the research indicates that cancer-derived exosomes have potential as therapeutic tools for AD with its neuroprotective effect, further study is required to determine the substances inside the exosome that are responsible for the protection from SH-induced neuronal cell death. It will also be necessary to identify the effect of cancer-derived exosomes from many different types of brain cancer cell lines for performing validation experiments.

Acknowledgement

I would like to thank Dr. Woo Rin Lee, my mentor from University of Suwon for his assistance and guidance in this project.

References

1. Schachter, A. S.; Davis, K. L., Alzheimer's disease. Dialogues in clinical neuroscience 2000, 2 (2), 91-100.
2. Bature, F.; Guinn, B. A.; Pang, D.; Pappas, Y., Signs and symptoms preceding the diagnosis of Alzheimer's disease: a systematic scoping review of literature from 1937 to 2016. BMJ open 2017, 7 (8), e015746.
3. Chong, F. P.; Ng, K. Y.; Koh, R. Y.; Chye, S. M., Tau Proteins and Tauopathies in Alzheimer's Disease. Cellular and molecular neurobiology 2018, 38 (5), 965-980.
4. Mendez, M. F., Early-Onset Alzheimer Disease. Neurologic clinics 2017, 35 (2), 263-281.
5. Kovalevich, J.; Langford, D., Considerations for the use of SH-SY5Y neuroblastoma cells in neurobiology. Methods in molecular biology 2013, 1078, 9-21.
6. llendula, A.; Fultang, N.; Peethambaran, B., Retinoic acid induces differentiation in neuroblastoma via ROR1

DOI: 10.36838/v3i1.8

by modulating retinoic acid response elements. Oncol Rep 2020, 44 (3), 1013-1024.
7. Bajo, R.; Pusil, S.; Lopez, M. E.; Canuet, L.; Pereda, E.; Osipova, D.; Maestu, F.; Pekkonen, E., Scopolamine effects on functional brain connectivity: a pharmacologi cal model of Alzheimer's disease. Scientific reports 2015, 5, 9748.
8. Zhang, Y.; Liu, Y.; Liu, H.; Tang, W. H., Exosomes: biogenesis, biologic function and clinical potential. Cell & bioscience 2019, 9, 19.
9. Blackwell, R. H.; Foreman, K. E.; Gupta, G. N., The Role of Cancer-Derived Exosomes in Tumorigenicity & Epithelial-to-Mesenchymal Transition. Cancers 2017, 9 (8).
10. Huang, J.; Ding, Z.; Luo, Q.; Xu, W., Cancer cell-derived exosomes promote cell proliferation and inhibit cell apoptosis of both normal lung fibroblasts and non-small cell lung cancer cell through delivering alpha-smooth muscle actin. Am J Transl Res 2019, 11 (3), 1711-1723.
11. Forster, J. I.; Koglsberger, S.; Trefois, C.; Boyd, O.; Baumuratov, A. S.; Buck, L.; Balling, R.; Antony, P. M., Characterization of Differentiated SH-SY5Y as Neuronal Screening Model Reveals Increased Oxidative Vulnerability. Journal of biomolecular screening 2016, 21 (5), 496-509.
12. Shipley, M. M.; Mangold, C. A.; Szpara, M. L., Differentiation of the SH-SY5Y Human Neuroblastoma Cell Line. J Vis Exp 2016, (108), 53193.
13. Bellingham, S. A.; Guo, B. B.; Coleman, B. M.; Hill, A. F., Exosomes: vehicles for the transfer of toxic proteins associated with neurodegenerative diseases? Frontiers in physiology 2012, 3, 124.
14. Soria, F. N.; Pampliega, O.; Bourdenx, M.; Meissner, W. G.; Bezard, E.; Dehay, B., Exosomes, an Unmasked Culprit in Neurodegenerative Diseases. Frontiers in neuroscience 2017, 11, 26.
15. Kalani, A.; Tyagi, A.; Tyagi, N., Exosomes: mediators of neurodegeneration, neuroprotection and therapeutics. Molecular neurobiology 2014, 49 (1), 590-600.
16. Ren, R.; Sun, H.; Ma, C.; Liu, J.; Wang, H., Colon cancer cells secrete exosomes to promote self-proliferation by shortening mitosis duration and activation of STAT3 in a hypoxic environment. Cell & bioscience 2019, 9, 62.
17. Puangmalai, N.; Thangnipon, W.; Soi-Ampornkul, R.; Suwanna, N.; Tuchinda, P.; Nobsathian, S., Neuroprotection of N-benzylcinnamide on scopolamine-induced cholinergic dysfunction in human SH-SY5Y neuroblastoma cells. Neural regeneration research 2017, 12 (9), 1492-1498.

Author

Minseo Lee is a 12th-grade student in Cranbrook Kingswood Upper School. Since she is still a high school student, she hasn't decided on her college major yet. In college, she hopes to major in neuroscience with a biological approach.

Will a New Motorway Bridge Affect Avifauna of the Danube in Bratislava?

Miloslav Mišík

Tilgnerova 14, Bratislava, 84105, Slovakia; misik.milo@gmail.com

ABSTRACT: The aim of my study was to monitor avifauna on the seepage canal of the Danube River reservoir and the nearby Danubian arm prior to the motorway bridge construction near Bratislava in Slovakia. The monitored locations were the Protected Landscape Area and Important Bird Area (IBA) River Danube floodplains and the Site of Community Importance (SCI) Biskupice floodplains. Identification and counting of all visually and acoustically recorded species were performed using line transect method at monthly intervals and the species dominance and frequency were calculated. Altogether, 83 species of birds were recorded with 71 on the seepage canal and 57 on the Danube arm. During our visits, 9 of the 16 criteria water bird species for Danube floodplains IBA were recorded. The number of water bird species prevailed over other species from January until the nesting period when migratory species, including numerous song-birds, arrived. Wintering and migrating gradually stoppped starting in April. The rarest species within my surveys was the Caspian tern *(Hydroprogne caspia)*. The observation of the rare *Anas acuta x Netta rufina hybrid* was most surprising.

KEYWORDS: Ecology; Avifauna; Danube River; Slovakia; Monitoring; Motorway Construction; Bird Migration.

Introduction

The subject of this work was a survey of both the left-side seepage canal of the Danube River reservoir and the nearby parallel western arm of the Danube to obtain phenological data on bird occurrences during the migration, wintering, and breeding seasons of 2017-2018. This subject was chosen as the new D4 motorway construction was planned for 2018-2020 and obtaining avifauna data for the situation before, during, and after motorway construction is important for understanding the motorway's environmental impact. This location is not regularly monitored, so there is no recent data. The Hrušov water reservoir on the Danube River is the largest wintering and migratory stopover for water birds in Slovakia. Additionally, the Protected Landscape Area and IBA – River Danube floodplains and the SCI with educational path – Biskupice floodplains are located next to a large refinery as well as within protected areas of the NATURA 2000 network.[1] The Gajc and Kopáč Island Nature reserves are situated here as well.[2] Bird occurrence data with nesting categories can be found in the Slovak avifauna database.[3] The avifauna data from the IBA River Dunabe, focusing on criteria species, were summarized within the Special Protection Areas in Slovakia.[4] Researchers have also previously studied the wintering of Netta rufina on the Danube River.[5]

The main goals of the work were

- to research avifauna on the pre-defined areas before the motorway bridge construction (2017), focusing on ecology of water bird species;
- to monitor breeding, migrating and wintering species, especially criteria species for this area indicating their ecosozological status;
- to compare actual data from the seepage canal, with the older data and to find out differences within the water bird assemblages;
- to obtain data for the on-going projects "New Atlas of Birds of Slovakia" and also for "Winter Water Bird Counting" and record them to the ornithology web-database AVES Symfony;
- to perform a survey during the construction (2018) with to evaluate changes in taxa composition.

Two impacted water ecosystems of the artificial canal and the natural Danube river arm have not been regularly monitored. The related literature concerns large-scale areas and the main Danube River channel.

Results

In 2017, 83 bird species were recorded with 71 species on the seepage canal and 57 species on the Danube arm (Annex 1). Sixteen criteria species including water birds as a group represent the criteria birds for Danube floodplains IBA.[4] During our visits, nine citerita species were observed (Annex 1, Annex 2).

Seasonal dynamics of recorded species :

Since both sites have been monitored at monthly intervals during 2017, both the individual numbers and species numbers changed over time. There were more water bird species compared to other species from January until the nesting period when migratory species, including songbirds, arrived. Wintering and migrating species of ducks, geese, and swans gradually began leaving in April.

On the first visit in January there were 29 bird species in the seepage canal with 18 being water species. The ratio of water birds to other species remained constant during the second visit. In March, during the third visit, there were only five recorded species, an 80% decrease as well as the lowest recorded

DOI: 10.36838/v3i1.9

species total for the entire year (Figure 1). A similar trend was observed in the case of aquatic species numbers. They occurred in the hundreds in January and February but in March the numbers decreased an order of magnitude lower. In the Danube arm, however, the highest number of aquatic species, thirteen, was recorded in March (Figure 1). These changes in species numbers was most likely caused by the Danube arm freezing over in January and February forcing the water birds to move to the non-freezing seepage canal. In March, after the Danube arm surface had melted, the water birds returned. During spring and summer the numbers of individuals in both localities fluctuated only in the tens; in the seepage canal the numbers rose to 110 during October. At the end of the summer, the decrease in the Hrušov reservoir water level was also reflected on the Danube arm by formation of shallows as suitable feeding and resting places for water birds. Consequently, the number of individuals rose to 131 in September and remained in the hundreds for the rest of the year. By December, water bird species did not dominate anymore (total of nine species) while song birds became the dominant bird type beginning in May, with 25 of 35 species on the seepage canal and 20 species of 26 on the Danube arm. The ratio of song bird individuals was much higher around the canal (480 out of 566) than in the arm area (189 out of 232) compared to other groups. I especially appreciate the rare migrant or wintering ***Turdus iliacus*** which impressed with high numbers (8 in November alongside the canal and 14 in December on the oxbow arem).

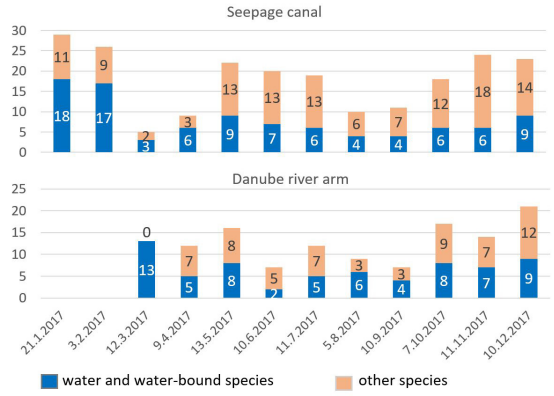

Figure 1: Seasonal dynamics of recorded species in monitored sites in 2017.

Comparison of water avifauna in monitored sites:

The greatest difference in occurrence of water birds between the arm and the canal was found in the group of waders (Figure 2). They prevailed over other water bird species on the Danube arm (7 species totalling 45 individuals versus 3 species totalling 19 individuals on the canal) that had more appropriate conditions like food and habitat. I found *Larus ridibundus*, *L. michahellis*, *Actitis hypoleucos*, and *Sterna hirundo* from the water bird group. *Hydroprogne caspia*, commonly known as the Caspian tern, was the rarest species in my surveys and recorded on April 9. Observing the rare crossbreed of *Anas acuta x Netta rufina* was the most surprising experience in the March visit to the Danube arm.

Anas platyrhynchos was the only constant (≥ 75%), regular aquatic species for both monitored sites as well as the most dominant species (> 5%). *Cygnus olor* and *Aythya fuligula* were also dominant species for both locations. *Aythya fuligula* is the criteria species for the Special Protection Area (SPA) because of its high numbers of wintering individuals.

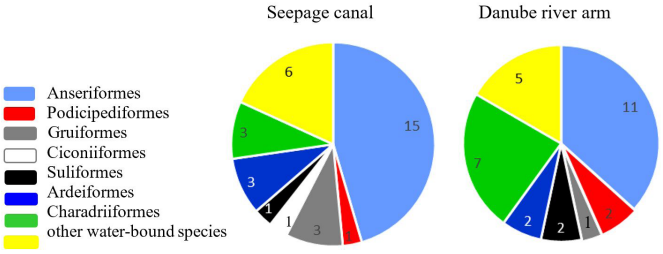

Figure 2: Ratio of numbers of species in monitored locations.

Occurrence and nesting of dominant species and other interesting species on the seepage canal:

In addition to the above-mentioned species, *Fulica atra* and *Tachybaptus ruficollis* were dominant species on the seepage canal where there was high amounts of vegetation. *Anas platyrhynchos* was present year-round and was observed to nest with chicks. *Cygnus olor* was also omnipresent except from July – September, but nesting has not yet been documented. *Aythya fuligula* was observed in high numbers in January-February-December. Two summer occurrences were recorded. Although it was not proved during this project, the possibility of nesting arose after observing one pair in June and four individuals in July. *Fulica atra* and *Tachybaptus ruficollis* appeared irregularly and formed groups in the migration and winter months. *Gallinula chloropus* was another species with all-year-round occurrence. Its nesting was demonstrated by an observation of several 1-2 day-old chicks in May. *Netta rufina* was a rare species with 4 individuals recorded in February. In May, a couple with the prossibiltiy of nesting was observed. In June, the suspicion increased when only a male was found on the site, nervously flying over the entire length of the canal. Despite our expectations, chicks were not found and thus nesting was not proven. The endangered *Aythya nyroca* was the rarest migratory species found on the seepage canal. Seven individuals were observed in October, a relatively high number. Based on our records of migratory and wintering species,[6] the location was shown to be suitable for wintering and migratory routes of aquatic birds. Several ducks, namely *Anas clypeata, A. penelope, A. crecca, A. querquedula, A. Strepera, Aythya ferina, A. nyroca, Bucephala clangula* and *Fulica atra*, were recorded on the canal in 2017 but were not found in 2018. This is most likely because the Danube arm did not freeze in 2018.

Criteria species recorded at localities:

In addition to aquatic birds, nesting species such as *Sterna hirundo* belong to the nine criteria species for the River Danube floodplains IBA. Three flying specimens of *Haliaeetus albicilla* were registered in December. It is a significant breeder[4] and a subject of protection as their numbers are expected to be negatively impacted by the D4 motorway construction.[7] The other criteria species were ducks – nesting species *Anas strepera*, *A. querquedula, Aythia fuligula, A. ferina, Netta rufina*, and migrating and wintering species *Bucephala clangula*, *Mer*

gellus albellus and *Mergus merganser*. The last species mentioned is also classified as a rare nesting bird in Slovakia.

Comparison of the results with older data:

When studying 2006 records from the seepage canal,[3] a similarity between the species composition of water birds with our data was found but others were not confirmed during our survey. For example, the occurrence of *Actitis hypoleucos*, *Mergus merganser, Mergellus albellus, Microcarbo pygmeus* were not found. I think these differences were mainly caused by the length of the monitored stretch. Most of the older data refer to the section from the beginning of the canal to Hamuliakovo village (i.e. almost to the Šamorín part of the Hrušov Reservoir) with large areas for wintering of these species. Our monitored section of the canal is much shorter and covered with trees. Hence it is often neglected by migrating birds. When comparing data on *Netta rufina*, it was determined that the species was more common in the Šamorín part of the canal than this study's area. The most important finding is the confirmation of the data about appropriate wintering places in the adjacent sections of the Danube River within the reservoir area.[5]

Conclusion

As expected, rare bird species appeared during migration and in the winter months when the number of individuals was the highest (in January it was up to 951 birds on the seepage canal). Of the predominant water species, the conditions were optimal for only five of them (constant or dominant) and for one proven nesting species. On the Danube river arm, the reason for an earlier increase in the number of water birds (both species and individuals) in autumn is that migrating species prefer a larger water surface. They move to the canal only when the arm is frozen. This was particularly obvious when several duck species were recorded on the canal in 2017 but not found here in 2018. The arm did not freeze in 2018 so ducks did not move there. The larger water area of the Danube arm is also more suitable for gull species. Wooden debris and shallows make them an appropriate shelter for resting or catching fish. The rare observation of the Caspian tern that flew over the spring migration is of high faunistical value, as well as the presence of 7 individuals of *Aythya nyroca*. I also recorded the rare *Anas acuta* and *Netta rufina* hybrid.

While during the coldest months (January to March) water and water-bound birds dominated, the rest of the year species-diverse song birds predominanted. They were particularly numerous near the seepage canal in a typical biotope of the old floodplain of the natural reserves of Kopáč Island and Gajc, the area being strongly affected by the planned motorway construction. In the coming years it will be important to monitor the changes in the surrounding natural environments. In nearby locations I have found a number of baseline data on the species composition and abundance of avifauna present which I can use toward future comparison with the conditions during and after the motorway construction. Upon refinement from bird song recordings I also plan to focus on acoustic calls by song birds. They could still be overlooked because of my ignorance. At the same time, I will concentrate on key months during the wintering, autumn migration and nesting periods to ensure species abundance. I would like to monitor the nesting time as long as possible according to the proposed method of nesting birds counting, in the second half of May and June.[13]

Methods

For the purpose of the avifauna monitoring on pre-defined locations the following methods were applied:

- mapping of avifauna once a month during the 2017 calendar year;
- identification and counting of all visually and acoustically recorded species in the specified transect (line transect method), calculation of the species dominance and frequency; a photo-documentation of the species and their habitats;
- comparison of the results obtained with available literature, websites, and data from ornithological databases; evaluation of monitoring results and graphical interpretation of the processed results; recording all observations into the ornithological database AVES Symfony, recording rare observations into the Birding Slovakia database;
- from 2018 additional surveys of wintering, nesting, and autumn migration.

Description of the monitored area:

The monitored area (N48°5'46.27", E17°9'21.94") lies in Central Europe in the cadastre area of Bratislava about 4 km south of the Slovnaft oil refinery (Figure 3). Both monitored sections are included in protected areas of different extent and levels. Both areas are affected by the planned construction of the motorway bridge as shown in Figure 4. The area of interest hides the preserved floodplain forests and oxbows. On the Kopáč Island there is a forest grove with special vegetation such as common reed and birch. The investigated seepage canal is 10 m wide. It is an artificially created canal situated alongside the reservoir dike and the floodplain forests with the purpose to capture the leaked water from the water reservoir (Figure 5). The canal was monitored in the section designated from its beginning to the first gate (2.85 km long). Bank vegetation of the canal is represented mostly by reed, young birch, poplar, and various scrubs. It is a relatively shallow and clean seepage canal with a gravel and muddy bottom which also affects the occurrence of individual bird species.

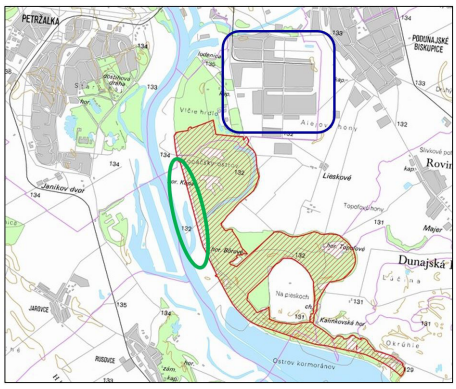

Figure 3: Designation of the Site of Community Importance SKUEV0295 Biskupické luhy (red-shaded); monitored area depicted in a green elipse; Slovnaft refinery depicted in a blue square.

DOI: 10.36838/v3i1.9

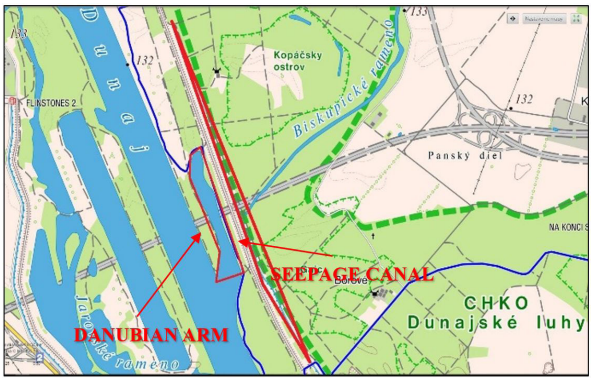

Figure 4: The monitored area of the Danube river arm and a seepage canal (red borders) with Protected Landscape Area River Danube floodplains (CHKO Dunajské luhy) and two Nature reserves Gajc and Kopáč Island. The sketch of the bridge construction across the monitored area is depicted in gray.

Figure 5: Seepage canal in spring (a), summer (b), autumn (c) and winter (d). Photos by M· Mišík, 2017.

The investigated parallel Danube arm, 50–150 m in width and 1.3 km in length, is surrounded mainly by the poplar vegetation of the floodplain forest. The arm has a muddy bottom and the banks are overgrown with reeds (Figure 6). In the mouth of the arm the driftwood and stones provide suitable rest places for some birds.

Mapping method:

The seepage canal was visited every month during 2017 where all the observed or heard species of birds were recorded and counted inside the 100 m wide and 2.85 km long stripe (from the beginning / 48°5'53.28"N, 17°9'2.13"E to the first lock at the Mini Vyza Buffet / 48°4'27.10"N, 17°9'58.06"E) with the monitored surface area of 0.285 km^2. The parallel Danube arm at a distance of about 150 m was investigated as well (Figure 6). Due to the frozen water surface of this Danube arm at the beginning of the year, it was monitored from March to December at monthly intervals. The mapped area of 0.17 km^2 corresponded to its length passing along the adjacent forest and fishing path and to the width between this path and the opposite bank of the arm. The same method was used in 2018 during the period of wintering (January – February), nesting (April – June) and autumn migration (September – November).

Figure 6: Danube river arm during low water (left) and standard water level (right).Photos by M· Mišík, 2017.

Method of evaluation:

Species were identified according to a 2016 paper.[9] The recorded species were divided into wintering species (occurring from December to February), nesting species (including species with year-round occurrence) and migratory species (both spring and autumnal migrators).[6]

The ecosozological status assessment of each species was based on the Red List of Birds of Slovakia.[8] The text classifies bird species into the categories of extinction risk, endangered, vulnerable and nearly threatened and on the IUCN Red Lists (for Europe and World).[10] Important Bird Area was declared in the given territory[11] for the protection of criteria species listed according to 2015 paper.[4] The frequency and dominance of species was calculated;[12] those with a frequency above 75% are considered to be constant year-round in an area. The dominance of water and water-bound species was determined where the dominant species had a dominance above 5%. Preliminary changes in a species composition were evaluated on the basis of the number of recorded species in 2018 compared to 2017 data.

Acknowledgement

I acknowledge my parents for their ongoing support during my field observations and in my research at home as well as Ms. Iveta Piršelová at Tilgnerova High School for her encouragement in each my endeavors. Special thanks to Jozef Ridzoň for the inspiration by the selection of theme and to Soňa Nuhlíčková and Ján Svetlík for their expert advice. I wish to also thank my English teacher Danka Mestická for her help with translating and Blanka Lehotská for her guidance in the preparation of the paper.

References

1. http://datazone.birdlife.org/home
2. http://uzemia.enviroportal.sk/
3. http://aves.vtaky.sk/index/
4. Karaska, D.; Trnka, A.; Krištín, A.; Ridzoň, J. Chránené vtáčie územia Slovenska [Special Protection Areas in Slovakia]. Štátna ochrana prírody SR, Banská Bystrica, 2015; 380 pp.
5. Rác, P.; Ridzoň, J.; Slabeyová, K. Zimovanie hrdzavky potápavej (Netta rufina) na Dunaji [Wintering of Red-crested Pochard (Netta rufina) on the Danube River]. Tichodroma 2009, 21, 106-107.
6. Danko, Š.; Darolová, A.; Krištín, A. Rozšírenie vtákov na Slovensku [Birds Distribution in Slovakia]. VEDA, Bratislava, 2002; 683 pp.
7. Proposal of Compensation Measures, National Motorway Company/NDS, 2014
8. Demko, M.; Krištín, A.; Pačenovský, S. Červený zoznam vtákov Slovenska [Red List of Birds of Slovakia]. SOS/BirdLife Slovensko, 2014; 52 pp.

9. Svensson, L.; Mullarney, K.; Zetterstrom, D. Ptáci Evropy, Severní Afriky a Blízkeho Východu [Birds of Europe, North Africa and Middle East]. Ševčík, 2016; 447 pp.
10. https://www.iucnredlist.org/
11. Nuhlíčková, S. (ed.) Chránime vtáctvo v územiach NATURA 2000 [We protect birds in teritories of NATURA 2000]. SOS/BirdLife Slovensko, 2014; 40 pp.
12. Janda, J; Řepa, P. Metody kvantitatívního výzkumu v ornitologii [Methods of quantitative research in ornithology]. Státné zemědělské nakladatelství, Praha, 1986; 158 pp.
13. Slovenská ornitologická spoločnosť /BirdLife Slovensko. Metodika systematického dlhodobého monitoringu výberových druhov vtákov v chránených vtáčích územiach. [Methods of systematic lonterm monitoring of criteria bird species in Important Bird Areas]. Štátna ochrana prírody SR, Banská Bystrica, 2013

Author

Miloslav Mišík is a student at Tilgnerova High School. His way of life has always been focused on ornithology and zoology. He spends all his free time observing and studying birds and plans to devote his future to this field of research.

ANNEX 1: Table of recorded species of birds in monitored area.

*– criteria species for Important Bird Area River Danube floodplains; Status of species: M – migrating species, W – wintering species, N – nesting species; Red list status: EN – endangered, VU – vulnerable, NT – nearly threatened, LC – least concern; Population trend: increasing, stable, decreasing, unknown; Frequency and dominance calculated according to Janda & Řepa[11]

WATER and WATER-BOUND species		Status of species in Slovakia	Red list status			Seepage canal		Danube River arm	
			SLOVAKIA	EUROPE	WORLD	Frequency of occurrence	Dominance within water species	Frequency of occurrence	Dominance within water species
ANSERIFORMES	*Cygnus olor*	N		LC	LC	75.0	12.0	50	24.4
	Anser sp.					25.0	27.5	–	–
	Anas platyrhynchos	N		LC	LC	91.7	16.0	90	30.1
	Anas clypeata	(N),M	VU	LC	LC	16.7	0.2	20	0.9
	Anas penelope	M,W		LC	LC	8.3	0.1	–	–
	Anas crecca	(N),M,W	EN	LC	LC	16.7	0.4	10	0.5
	*Anas querquedula**	(N),M	NT	LC	LC	8.3	0.2	–	–
	*Anas strepera**	N		LC	LC	16.7	0.9	10	0.1
	*Aythya ferina**	N		VU	VU	25.0	4.2	–	–
	*Aythya fuligula**	N		LC	LC	50.0	17.1	30	22.3
	Aythya nyroca	(N),M,(W)	EN	LC	NT	8.3	0.4	–	–
	*Netta rufina**	N,M,(W)		LC	LC	25.0	0.4	10	2.1
	Netta rufina x Anas acuta					–	–	10	0.1
	*Bucephala clangula**	M,W		LC	LC	8.3	0.1	10	0.1
	*Mergellus albellus**	M,W		LC	LC	–	–	10	2.1
	Mergus merganser	(N),M,W		LC	LC	–	–	10	0.1
PODICIOEDIFORMES	*Tachybaptus ruficollis*	N		LC	LC	58.3	5.1	10	0.6
	Podiceps cristatus	N		LC	LC	–	–	10	0.2
GRUIFORMES	*Rallus aquaticus*	N		LC	LC	50.0	1.2	–	–
	Gallinula chloropus	N		LC	LC	66.7	1.4	–	–
	Fulica atra	N		NT	LC	25.0	7.7	20	4.0
CICONIIFORMES	*Ciconia ciconia*	N		LC	LC	8.3	0.1	–	–
SULIFORMES	*Phalacrocorax carbo*	N	VU	LC	LC	25.0	1.7	80	4.0
	Microcarbo pygmeus	(N),M,W				–	–	20	0.3
ARDEIFORMES	*Ardea cinerea*	N		LC	LC	8.3	0.3	40	1.0
	Ardea alba	N	VU	LC	LC	8.3	0.1	20	0.6
	Botaurus stellaris	N	VU	LC	LC	8.3	0.1	–	–
CHARADRIIFORMES	*Chroicocephalus* sp.	N				8.3	0.1	40	1.7
	Larus michahellis	N		LC	LC	–	–	10	0.3
	Larus sp.					16.7	1.0	10	0.3
	Larus cachinnans/michahellis			LC	LC	8.3	0.1	50	1.4
	*Sterna hirundo**	N		LC	LC	–	–	20	0.5
	Hydroprogne caspia	M		LC	LC	–	–	10	0.1
	Actitis hypoleucos	N		LC	LC	–	–	10	0.3
ACCIPITRIFORMES	*Haliaeetus albicilla**	N	VU	LC	LC	8.3	0.2	–	–
CORACIIFORMES	*Alcedo atthis*	N		VU	LC	8.3	0.1	10	0.1
PASSERIFORMES	*Remiz pendulinus*	N		LC	LC	8.3	0.1	10	0.1
	Acrocephalus arundinaceus	N		LC	LC	41.7	1.1	20	0.7
	Motacilla alba	N		LC	LC	8.3	0.1	10	0.3
	Emberiza schoeniclus	N		LC	LC	16.7	0.2	10	0.5
Total number of WATER AND WATER-BOUND species						**33**		**30**	
Total number of WATER AND WATER-BOUND individuals						**1683**		**969**	

		species in Slovakia	SLOVAKIA	EUROPE	WORLD	Frequency of occurrence	Frequency of occurrence
ACIPITRIFORMES and FALCONIFORMES	*Buteo buteo*	N		LC	LC	41.7	30
	Accipiter nisus	N		LC	LC	16.7	20
	Falco tinnunculus	N		LC	LC	8.3	–
BUCEROTIFORMES	*Upupa epops*	N,M	NT	LC	LC	8.3	–
GALLIFORMES	*Phasianus colchicus*	N		LC	LC	25.0	–
COLUMBIFORMES	*Columba palumbus*	N		LC	LC	50.0	10
	Streptopelia turtur	N,M		VU	VU	16.7	10
APODIFORMES	*Apus apus*	N,M	NT	LC	LC	16.7	–
CUCULIFORMSS	*Cuculus canorus*	N,M		LC	LC	16.7	20
PICIFORMES	*Dendrocopos major*	N		LC	LC	50.0	40
	Picus viridis	N		LC	LC	8.3	–
	Dryocopus martius	N		LC	LC	25.0	20
PASSERIFORMES	*Oriolus oriolus*	N,M		LC	LC	–	10
	Lanius collurio	N,M		LC	LC	16.7	–
	Garrulus glandarius	N		LC	LC	50.0	20
	Corvus frugilegus	N		LC	LC	16.7	–
	Corvus cornix	N				50.0	40
	Cyanistes caeruleus	N		LC	LC	66.7	50
	Parus major	N		LC	LC	83.3	80
	Hirundo rustica	N,M	VU	LC	LC	25.0	–
	Aegithalos caudatus	N		LC	LC	25.0	20
	Sitta europaea	N		LC	LC	8.3	10
	Phylloscopus collybita	N,M			LC	33.3	30
	Phylloscopus trochilus	N,M		LC	LC	–	10
	Troglodytes troglodytes	N		LC	LC	25.0	10
	Regulus regulus	N		LC	LC	–	10
	Sturnus vulgaris	N,M,W		LC	LC	8.3	10
	Turdus merula	N		LC	LC	75.0	60
	Turdus iliacus	(N),M,W		NT	NT	8.3	10
	Turdus pilaris	N		LC	LC	16.7	–
	Turdus philomelos	N,M,(W)		LC	LC	8.3	–
	Phoenicurus ochruros	N,M,(W)		LC	LC	8.3	–
	Erithacus rubecula	N		LC	LC	8.3	10
	Passer montanus	N		LC	LC	8.3	–
	Fringilla coelebs	N		LC	LC	33.3	40
	Fringilla montifringilla	M, W		LC	LC	8.3	–
	Pyrrhula pyrrhula	N	NT	LC	LC	16.7	10
	Coccothraustes coccothraustes	N		LC	LC	16.7	10
	Chloris chloris	N		LC	LC	8.3	10
	Carduelis carduelis	N		LC	LC	50.0	10
	Emberiza citrinella	N		LC	LC	50.0	–
Total number of OTHER species						**38**	**27**
Total number of OTHER individuals						**566**	**210**
TOTAL NUMBER of SPECIES						**71**	**57**
TOTAL NUMBER of INDIVIDUALS						**2249**	**1179**

ANNEX 2: Photo gallery (Photos by M. Mišík, 2017).

DOI: 10.36838/v3i1.9

Targeted Cancer Therapy: From Scratch to Clinical Trials

Ojas Gupta

Lynbrook High School, 1280 Johnson Ave, San Jose, CA, 95129, Santa Clara Count, USA; ojasgupta1000@gmail.com

ABSTRACT: This paper attempts to flatten the learning curve for finding subtype-specific cancer drugs by outlining the different pathways to arrive at clinical trials starting from scratch. Targeted, or subtype-specific, cancer drugs work by targeting "cancer dependencies," or the products of certain genes that are necessary for cancerous cell growth. Unfortunately, process are very prevalent in the industry. This paper will outline and compare current methods of identifying a cancer dependency and the subsequent drug molecule. Only a careful consideration of current limitations will improve our ability to correctly uncover cancer genetic dependencies and will facilitate the development of improved therapeutic agents.

KEYWORDS: Molecular Biology; Computational Biology; Genetics; Genomics; Computational Chemistry.

Introduction

Despite recent critical technological advancements in medicine, cancer remains the number one cause of death worldwide, with one new diagnosis every 30 seconds in the US alone.[1,2] Over 200 different types of cancer have been identified, and 1 in 3 people will develop one of them in their lifetime.[1] Despite various cancer-related guidelines for diagnosis, treatment, and follow-up, improving the long-term prognosis of certain cancer patients remains difficult. One reason for this bottleneck is because of the sluggish process involved in drug discovery. Drugs take 10-15 years to bring to market, and 97% of cancer drugs that enter clinical trials fail, one of the highest across all pharmaceutical fields.[3] Additionally, the drug discovery process is long, confusing, and filled with barriers. Thus, to maximize efficiency and improve outlooks, establishing and comparing current methods to find cancer drugs is imperative.

Cancer is the name given to a collection of related diseases that can start in nearly any organ or tissue when abnormal cells grow beyond their usual boundaries, invade adjoining parts of the body and/or spread to other organs. The latter process is called metastasis and is the major cause of death from cancer.[1] Tumors are often confused with cancer, however tumor is the word given to any uncontrolled cell growth, whereas cancer is a type of tumor that is malignant.[1] Cancer is caused by alterations, or mutations, in the genome. These changes in the DNA are induced by chemicals or radiation,[4] biological factors (virus and bacteria),[4] or spontaneously during DNA replication.[5] Mutations can result in genome instability, which can lead to aneuploidy, silencing of tumor suppressors, and/or alterations in protein functions, resulting in dysregulation of crucial biological pathways that lead to cancer.

Finding cancer dependencies is the norm for developing targeted cancer cell drugs. Like a person who is dependent on coffee to be productive, cancer cells are dependent on the products of certain genes in order to dominate their environment and grow.[6] Cancer cells will stop growing and die when the activity of these gene products is blocked. Thus, a cancer dependency is a specific gene or protein that is required for cancer survival. Deleting that gene or inhibiting the encoded protein's activity, would result in repressed growth and/or death of the cancer cells.[6] As a result, researchers are constantly looking for cancer dependencies and developing drugs to block their activity.

However, finding cancer dependencies is unfortunately much easier said than done. Most cancer dependencies result from alterations in numerous genes, making their identification nearly impossible due to the sheer number of possible genes and proteins in any given cell.[7] Additionally, techniques used to find dependencies are not perfect, and there have been many instances of revolutionary studies claiming to have found a cancer dependency only to be debunked later on (Table 1).[6] That is why cancer drugs have one of the highest failure rates of 97% and take over a decade to bring to market.[3] Thus, the goal of this paper is to review the available methods of finding a cancer dependency, and the methods of finding the subsequent cancer drug, as well as how to reduce the chances for failure or misidentification of a target.

Table 1: Examples of widely publicated yet misidentified cancer dependencies, adapted from Lin *et al.*[6]

Misidentified gene	Role/Cancers reported to be dependent
CD95 (or Fas)	Apoptosis & growth/various cancers
HDAC6	Protein Maintainence/various cancers
MELK	Cell Cycle/Triple-Negative Breast Cancer
MEN1	Tumor & growth suppressor/Glioma
MTH1 (or NUDT1)	Oxidization of DNA/various cancers
PAK4	Signaling and cytoskeleton/various cancers
PIM1	Glycolysis and growth/various cancers
SMYD2	Signaling/various cancers
STK33	Invasion and upregulation of transcription/various cancers

DOI: 10.36838/v3i1.10

Discussion

Cancer dependencies are almost always identified by using loss-of-function assays (LOF), where the effects of blocking the function of a gene is studied.[7] If the result is repressed growth and/or death of the cancer cells, then a promising cancer target has been identified. Following the central dogma of biology-transcription and translation-LOF assays can target 3 distinct molecules: DNA, RNA, or protein (Figure 1). By its definition, the inhibition of a cancer dependency will lead to repressed growth and/or cancer cell death. Thus, a successful cancer drug is one that can target a cancer dependency. For many of these methods, the DNA or RNA sequence needs to be known, which won't be detailed in this paper but has extensively been detailed in others.[8]

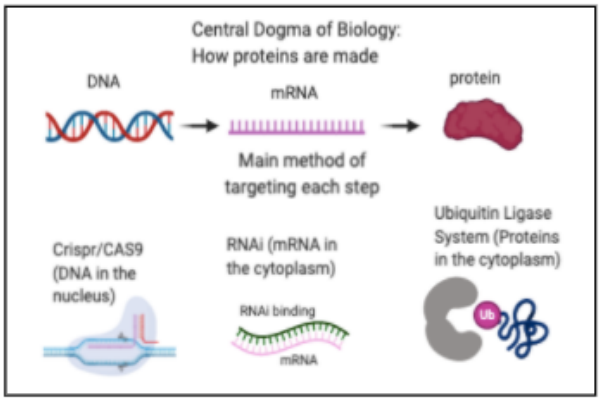

Figure 1: Summary of the main Loss-of-function techniques deatiled in this paper, sorted by which molecule the method targets. By the central dogma of biology, these could target DNA, mRna, or the protein, and are achieved using CRISPR/Cas9, RNAi, and PROTAC/ULS respectively.

DNA level targeting:

Direct DNA alterations, or genome therapy, is primarily achieved through recently discovered CRISPR/Cas.[9] This system naturally evolved as the "immune system" of bacteria to remove foreign DNA injected by bacteriophages.[9] CRISPR stands for Clustered Regularly Interspaced Short Palindromic repeated DNA sequences. This term was coined because when sequencing bacterial genomes, scientists observed clustered repeat sections in DNA separated by non- repeating DNA sequences named spacers unlike typical tandem repeats in the genome.

At first, no conclusions or investigations were made into this strange coincidence. Eventually, the non-repeating spacer DNA sequences were identified as belonging to viruses and other mobile genetic elements. After extensive research, it was determined that small-hairpin RNAs known as CRISPR RNAs (crRNAs, also called guideRNA/gRNA or single guideRNA/sgRNA) are synthesized from bacteriophage DNA sequences stored in these spacers in bacterial DNA. This crRNA binds to a protein in the Cas enzyme family and stays in the cytoplasm just as antibodies would stay in human blood. When the same phage injects its DNA again, the crRNA will bind to it via complementarity. Then, the Cas9 enzyme will initiate a double strand break in the foreign DNA, preventing an infection. However, why the crRNA and Cas enzyme complex did not destroy the virus DNA stored in the discovered that in order for Cas enzymes to be activated, it needs to bind to a protospacer-adjacent motifs (PAMs), which is a specific short sequence of nucleotides uniquely found on foreign DNA, but removed once integrated into the bacterial genome.[9] Individual Cas proteins have their own "activation" PAM sequences. The most common enzyme, Cas9, has a PAM site of NGG, or any base followed by two guanines.[9] Because of the simple PAM requirements and versatility, Cas9 has become a commonly used enzyme in genome manipulation.[10] There are two ways CRISPR can be introduced into the cell nucleus for gene knockout: transfection and transduction.[10] Transfection is when molecules enter the cell directly through their cellular membrane. In CRISPR transfection, there are three types of molecules that can be used: DNA, RNA, or in its final protein form (Ribonucleoprotein complex).[10] Electricity, liposomes, and microinjection are commonly used to introduce the molecule of choice into the cell.[10] Either way, the final protein complex of the crRNA and the Cas enzyme will be assembled in the cells. Transduction, on the other hand, utilizes a Lenti or Adeno Associated virus to carry the complex and insert it directly into the cell. From this point, the two methods work the same. The complex binds to the target sequence as directed by the crRNA and causes the double stranded break. From here, the cells will attempt to repair the double stranded break through one of two pathways: non-homologous end joining (NHEJ) or homology-directed repair (HDR). In NHEJ, error-prone DNA-Ligase attempts to fix the break, often adding random bases resulting in frameshift mutations. This generates a null, or total LOF.[9] HDR, on the other hand, can insert the missing gene from homologous or sister chromatids, or insert a completely new gene.[11] Additionally, scientists sometimes insert a gene like GFP or antibiotic resistance so they can label and observe cells that underwent the change. Usually, these selection markers are inserted along with the CRISPR complex. If transfection is used, then short single-stranded DNA (ssDNA) also called donor oligonucleotides or synthetic DNA, carry the genes.[11]

CRISPR is one of the most commonly used tools in LOF assays, and by far the most popular method of direct gene knockout.[12] There are many older and less-commonly used DNA editing tools that can also be used in knockout assays. One of them is the Artificial Restriction DNA Cutter (ARCUT) method. This method does not use enzymes and can knockout or insert genes of interest by using pseudo-complementary peptide nucleic acid (pcPNA). The pcPNA specifies the cleavage site and binds to each side of the DNA, unraveling it. Chemicals cerium (CE) and EDTA (mixture) carry out the actual splicing. Then, DNA ligase in the cell attaches genes of interest as provided. This technique is particularly useful in extreme conditions where enzymes cannot function properly; however, ARCUT is not popular due to longer turnaround time and need for site-specific pcPNA.[12] Another less common method of DNA knockout is Protein-Based Nuclease systems. Humans naturally contain Meganucleases, also called endonucleases, which are molecular DNA scissors. This technique has three steps: first is the recognition of a cleavage site, then Meganucleases splice out

DOI: 10.36838/v3i1.10

the region, and finally the desired DNA sequence is inserted by DNA ligase. The first recognition step is done by either Zinc-Finger-binding protein domains, or TALEN's. Zinc Fingers can be programmed to recognize combinations of codons, which makes TALEN's a little easier to work with as they can recognize combinations of individual base-pairs.[12] This technique is not preferred due to high cost and time involved in generating a Zinc-Finger or TALEN recognition sequence, even though it has shown to be less toxic than CRISPR since meganucleases naturally occur in the body whereas foreign Cas enzymes can trigger an immune response.[12]

Although CRISPR is much faster, cheaper, and more specific than all other DNA inhibition techniques, it is not perfect. The biggest issue is that crRNA tends to have relatively high mismatch tolerance. In other words, Cas9 commonly cleaves off-target sites, a problem shared by all LOF techniques to some degree.[12] Different Cas proteins and more specific gRNA's have combated this issue, but these efforts are far from perfect. However, it is worth mentioning that CRISPR is widely considered to be the most accurate and specific form of LOF assays.[6,12] Another issue is that the use of knockout techniques to remove one gene's expression might result in compensatory upregulation in a paralogous gene that achieves the same phenotype or role, thus falsely portraying the role of the targeted gene as null.[13] Additionally, the immunogenicity of Cas9 is of concern. Around 50% of humans contain antibodies to the two most common CRISPR nucleases. This leads to low knockout efficiency and possibly a serious immune storm in vivo.[13] Recent research has also shed light on CRISPR's

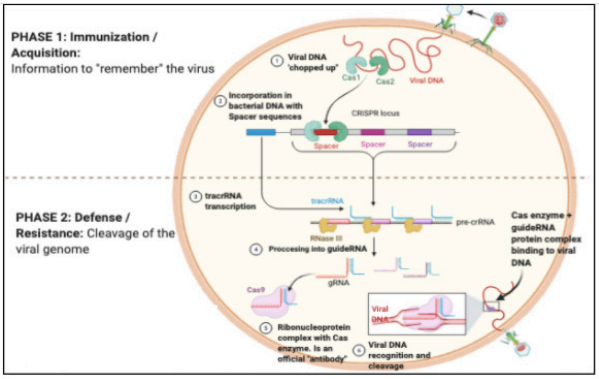

Figure 2: Summarizes the 6 steps involved in natural CRISPR/Cas9 in bacteria as an "immune response for viral DNA infections. First, the intruding viral DNA is chopped up into many small sections. Then, it is incorporated into the bacterial cromosome with repeating "spacer" or dummy sequences between different viral segments. Next, in the Defense/ Resistance half, tracrRNAs are sequenced directly from the viral sequences stored in the chromosome. These RNA's are modified and mature into guide RNAs by RNaseIII. Next, the mature gRNA binds to the Cas enzyme (Cas9 in this case) and forms the active and ready protein complex. In an analogy to the human body, this would be considered an active antibody in the blood. Finally, when the complex recognizes the foreign DNA, it will bind to it and prevent any damage from occurring.

role in disrupting the cell cycle and activating p53, which is a protein that senses DNA damage inside the cell. Since CRISPR/Cas9 induces double stranded breaks in the DNA, it can cause the p53 DNA-correction pathway to activate if the cell has the wild type, or natural (not mutated) version of p53, leading to apoptosis.[13] Finally, the CRISPR-induced mutation will not always completely ablate gene expression. Sometimes functional truncated proteins, or "zombie" proteins, can still be expressed in small amounts.[14] CRISPR/Cas9 has allowed us to manipulate gene expression and study gene function on a whole new scale, but it is still far from ideal (Figure 2).

RNA level inhibition:

Unlike direct genome inhibition, perturbations at the RNA level do not completely knockout a gene: instead it induces significant knockdown, or downregulation, of a gene to the point where the importance of the gene can be determined.[15] It is important to note that RNAi is a natural mechanism used by cells to limit mRNA expression, and for use in LOF assays, a synthetic version that mimics the natural mechanisms is used (Figure 3). Natural RNAi works by introducing a double stranded microRNA (miRNA), that binds to the mRNA of the target gene in the cytoplasm.[15] Once bound, the natural miRNA can recruit cell machinery such as the DICER enzyme, forming a RISC complex, and cut the mRNA into small, useless chunks.[15] Alternatively, the RISC complex can bind to the target mRNA, simply preventing translation.[15]

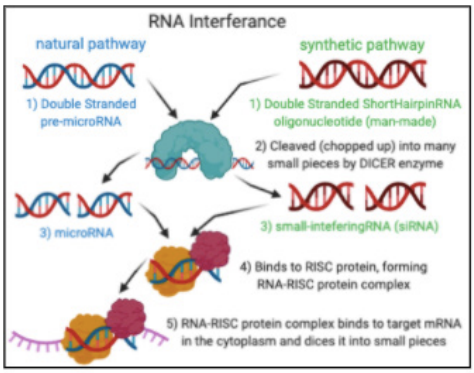

Figure 3: RNAi is an natural mechanism used to limit gene expression. The clinical RNAi is a synthetic version which can mimic the natural mechanism and produce the same results. The natural pathway is shown blue, synthetic in green, and overlapping steps in black.

Short hairpin RNA (shRNA) and small interfering RNA (siRNA) are the two types of oligonucleotides, or man-made DNA, which can mimic the same role as natural occurring miRNA.[16] The method for application in humans is straight-forward. Transduction via adeno or lenti viruses is most commonly used *in vitro*, as with CRISPR, but if assay is occurring in suspension, transfection is also used. Both methods get the amplified synthetic shRNA or siRNA, which needs to be complementary to the target mRNA sequence, into the cells of interest where the mechanism of binding to the RISC protein and subsequent steps occurs naturally.[16]

As mentioned before, because RNAi downregulates a gene's expression but does not remove it, RNAi harbors several advantages relative to other systems in the drug discovery process than any other LOF technique. This is due to the fact that it closely mimics the role of a drug, which also will downregulate the protein but not completely inhibit it.[15] Another advantage of RNAi over CRISPR is that it is more efficient as it is able to remove the function of homologs, as

RNAi targets mRNA instead of the actual genome, accounting for the issue of upregulation of homologs in CRISPR. If there are more mRNA then you would need more microRNA to knockdown the gene, hence its knockdown efficiency is reliant on gene prevalence.[15] However, RNAi's largest disadvantage is its prevalent off-target effects.[16] MELK, PIM1, PAK4, HDAC6, STK33 and other oncogenes were initially deemed essential to cancer cells by using RNAi (as listed in Table 1), but peer reviews revealed that the outcomes observed by most initial studies were actually due to RNAi degrading other mRNA strands that were not the initial target.[6]

Protein level inhibition :

Finally, LOF assays can also inhibit function on the proteome level. Targeted proteolysis is desirable both in drug applications and in basic research. There are two main options for disrupting protein function: the inhibition of protein activity and the induction of protein degradation.[16] Small-molecule inhibitors (SMIs) are the most widely used tools for the first method of protein activity and are amenable to high-throughput screening, making their use and detection easier.[16] These are specially designed molecules that inhibit protein function by binding to a protein, thereby preventing it from doing its normal function. While these are fast acting, controllable, and efficient, SMI's have two main drawbacks preventing their widespread use. Each protein has a different structure, and the majority of proteins lack a SMI that can cause effective inhibition.[16] Additionally, SMI's have several off-target instances since many proteins in the body have similar receptors.[16]

Recently, the protein inhibition field has shifted towards the ubiquitin ligase system (ULS), a protein degradation system. Like RNAi, this mechanism was observed in organisms and then a synthetic version was created that can mimic the natural process and induce the same outcome (Figure 4). ULS is a tagging system that attaches ubiquitin to the protein of choice, which then signals degradation by a protease.[17] The process in the human body uses three steps, each with a different ubiquitin-activating enzyme.[17] The first step of the reaction is mediated by the E1 ubiquitin- activating enzyme that activates the ubiquitin monomer. Next, the activated ubiquitin is passed on to the E2 ubiquitin- conjugating enzyme, before ultimately being attached to the target protein through the action of an E3 ubiquitin ligase. The ubiquitin monomers can be further ubiquitinated to form chains, with distinct chain types linked to specific biological processes. If, for example, ubiquitin molecules added to the target protein form a lysine 48-linked chain, the ubiquitinated protein is marked for proteasomal degradation.[18]

The synthetic "copycat" version of ULS is PROTAC, or PROteolysis-TArgeting Chimeras. PROTACs are a more efficient way to cause protein degradation using the natural Ubiquitin recycling system. It consists of a ligand to the target protein bound to a ligand to the E3 Ubiquitin Ligase.[19] This binds the target protein directly to the E3 ligase, speeding up the ubiquitination process, triggering degradation in the same method.[20] In application, a ligand for the target protein needs to be established and reproduced in order for PROTAC to work.[20] In summary, PROTAC mimics the natural ULS system mentioned before, by holding the protein close to the E3 enzyme by using ligands and more efficient binding

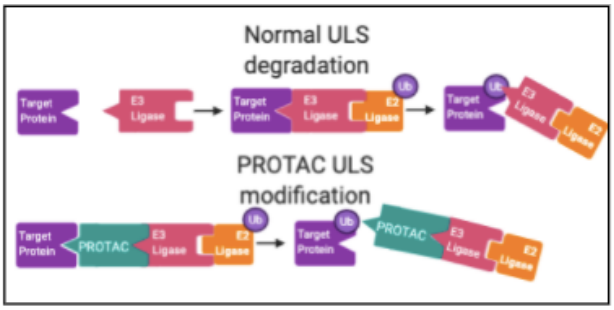

Figure 4: Smilarly to RNAi, ULS is a natural pathway of limiting expression, but unlike RNAi, scientist have given a name to the synthetic version; PROTAC. The main difference is that PROTAC and natural ULS is that PROTAC can force controlled degradation, whereas the natural ULS pathway is only triggered by certain receptors. It is important to note that the function of the E1 ligase has not been included in this figure, which normally brings the Ubiquitin protein from the rhibosome and delivers it to the E2 ligase.

techniques, which forces ubiquitination and subsequent degradation by protease.

Currently, the PROTAC approach in LOF assays has four main limitations. The first three are: the lack of E3 ligases that can bind to the protein of interest, the lack of nanobodies or SSM to bind to the protein of interest, and the large size of PROTACs which occasionally prevent passage through the cellular membrane.[18] Luckily, the recent popularity has led to a huge increase in the enzyme and molecule libraries, as well as various adaptations with increased permeability.[18] in other words, due to the high efficiency and popularity, as well as the low toxicity, the first three problems are being rapidly solved. The fourth limitation, however, is more difficult to overcome. The Synthetic Small Molecules work by binding to the active site of a protein. However, 75% of the human proteome lacks active sites, as they don't actively perform any enzymatic function (ex: scaffolding or structural proteins & transcription factors).[20] However, there are still many proteins with active sites yet to be discovered and detailed, and humans have miles to go before we run out of "targetable" proteins.[20]

Comparison and Emerging Tools:

Currently, CRISPR and RNAi are the two most common methods for testing and identifying cancer dependencies and the only possible methods used for genome-wide screens.[6] As a head to head comparison, CRISPR generally outperforms RNAi in terms of single gene experiments regarding specificity and off target effects.[21] CRISPR also presents the unique opportunity to study cells with genetic changes, since the changes that are induced by CRISPR are inherited by the offspring.[22] RNAi, on the other hand, also possesses other benefits. It imitates the role of a natural drug better compared to CRISPR: decreasing but not eliminating the protein of interest. Additionally, unlike CRISPR, RNAi effects can be reversed and controlled, allowing researchers to test for the consequences of restoring gene expression.[23] Additionally, determining the DNA sequence that codes for a specific protein can be mis-

DOI: 10.36838/v3i1.10

that are trimmed out before RNA translation. Thus, finding the DNA sequence for a set of amino acids isn't always straightforward, giving RNAi a slight advantage in convenience due to the relative simplicity in the direct mRNA-protein translation.[23] Finally, CRISPR sometimes initiates anti-tumorous cell machinery by activating the p53 DNA correction pathway, a problem that RNA does not have.[13]

Although these techniques are far from perfect, recent alterations to the transcriptome editing toolbox have shown promise. The ubiquitin ligase system is one of these systems. By utilizing the body's natural recycling system, it has shown fewer off target effects and significant knockdown ability.[18] Additionally, three modifications to the CRISPR/Cas9 technology hold immense potential. CRISPR interference (CRISPRi) is one such modification. As its name suggests, it also relies on the CRISPR protein complex, which is a Cas enzyme bound to a guideRNA that is complementary to the target DNA sequence. Unlike CRISPR, CRISPRi implements an inactive or dead Cas enzyme (dCas) that lacks endonuclease activity. It acts as a repressor protein, binding to the target sequence and blocking transcription from RNA polymerease.[24] Thus, although CRISPRi does not directly edit DNA like CRISPR, it can efficiently block expression of targeted genes. CRISPRi also appears to produce a more consistent and robust knockdown with fewer off target effects and has advantage over CRISPR as it does not activate the p53 DNA correction pathway.[21] The application or method of delivery for CRISPRi is identical to that of CRISPR. Cas12a has also received significant attention recently as an alternative Cas enzyme utilized in normal CRISPR gene knockout. It has a significant advantage over traditional Cas9 because Cas12a contains DNAase and RNAase activity within the protein complex, which allows for "scanning" and processing of multiple guideRNA's simultaneously.[25] Although it operates at a slower pace, Cas12a offers higher efficiency if multiple genes need to be screened, which happens many times as multiple genes often code for proteins with redundant functions.[25] Other than multiple guideRNA's and a different Cas enzyme, the Cas12a gene-knockout mechanisms and application is identical to CRISPR. Finally, Cas13 is another recently discovered Cas enzyme that has attracted a lot of attention in LOF assays. Unlike other Cas enzymes, Cas 13 has the ability to recognize and bind to mRNA instead of DNA, inducing gene knockdown the same way as RNAi does.[26] Although there are many additional techniques used to find cancer dependencies, the most popular ones were discussed (Figure 5).

Drug Discovery:

Unfortunately, conventional drugs face the same problem as protein-level inhibition: many proteins are simply not able to be targeted. Traditional drugs work by binding to the active site of a protein, thus preventing its normal function. However, out of the millions of proteins in the body, a vast majority (75%) of the human proteome lacks these active sites and thus are undruggable by conventional medicine.[20] Of the 25% that we can exploit, a vast majority has still been untouched.

There are already a variety of methods and drugs that are commonly used to combat cancer. These include anti-growth drugs and techniques such as chemotherapy and radiotherapy, which are generally used despite the type of cancer and can help limit the growth of most cancers.[27] However, the goal of LOF assays, as well as the goal of this paper, is to establish the steps for targeted-drug therapy for cancers that display a certain biomarker. Due to its specificity, these drugs tend to have twice as high success rates in approval and higher relative efficiency in treatment than drugs without specificity to certain cancer subtypes.[28] The goal of targeted drug development is to find and deliver a molecule that will bind to the target protein and prevent its function, without disrupting other proteins' activities. This paper only focuses on the first task of finding the right molecule. The path to finding a drug is long and complicated, with no "right way" or industry- accepted path. Once a cancer dependency has been found using LOF assays for the desired cancer subtype, then there are two general pathways for drug development: Structure Based Drug Design & Ligand

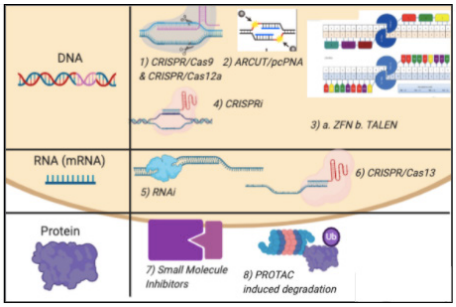

Figure 5: Summary of the eigtht main LOF methods detailed in this paper. These are sorted by which molecule they target. On the DNA level, we have the CRISPR complex first that serches for the target gene and induces a DSB. Both enzymes Cas9 and Cas12a can be used, except Cas12a can hold/scan for multiple genes at once. Second, there is the ARCUT method which works by introducing pcPNA that unwinds and holds DNA where it is exposed to certain chemicals inducing DSBs. Third, there are the ZFN and TALEN methods, who both scan for the target gene and recruit naturally occurring meganuclease "DNA sciccors" to induce DSB's. ZFN recognizes codons whereas TALEN recognizes individual bases. Fourth, the CRISPRi method which is a dCas potein an simply bind to the promoter, blocking transcription. On the mRNA level, there is the fifth method of RNAi which mimics the natural process to dice target mRNA into useless pieces. Sixth, the CRISPR/Cas13 complex taht binds to and dices mRNA, preventing translation. Finally on the protein level, there is the seventh method of SMI's which bind to the active site of a protein, preventing any useful accion from ocurring. The eighth and final system is PROTACs which imitate the body's natural protein recyling system and induce protein degradation.

Based Drug Design (Figure 6).

Structure Based Drug Design:

This pathway is undertaken when the structure of receptors (active sites) of the target protein is known.[29] As detailed in the protein inhibition section, the structure of the receptor is determined by X-ray crystallography, NMR, or through an online database. Protein structure can also be predicted by computational methods like threading and homology modeling. Threading predicts the shape based on established shapes of sequences of amino acids and domains.[29] Homology modeling predicts the shape based on a homologous protein whose shape has been identified.[30] Finally, the pseudo-receptor technique can also generate an accurate model of what the target protein's structure is. Once the target protein's receptors have been detailed and mapped, then the formation of a new drug can

DOI: 10.36838/v3i1.10

occur. In the diagram, this is represented by the *de novo* drugs pathway as de novo means "from the beginning". Some of the methods to create viable drugs are listed below.[29]

Figure 6: Although any possible method of identification is accepted, these are some of the most popular routes of finding a potential drug candidate. The methods are mainly grouped on whether they need to know the structure of the receptor of the target protein (cancer dependency) or not. The one exception to this is the Pseudoreceptor method. Although it is listed as a LBDD method in the text, this technique essentially utilizes the properties of a receptor protein, which means that it could be used to find the target structure as well as a drug.

1) Fragment location methods: To determine desirable locations of atoms or small fragments within the active site (the detailed receptor structure).

2) Site point connection methods: To split up the big hole into small gaps, or "site points", and then place fragments in those small gaps until all such locations are occupied by suitable molecules.

3) Fragment connection methods:

Fragments are positioned and "linkers" or "scaffolds" are used to connect those fragments and hold them in a desirable orientation. This is usually used in conjunction with method 2.

4) Sequential buildup methods: Construct a ligand atom by atom, or fragment by fragment.

5) Whole molecule methods: Random established compounds are placed into the active site in various conformations in silico (computer model), assessing shape and/or electrostatic complementarity until the optimal molecule has been chosen.

In addition to *de novo* drug synthesis, Structure Based Virtual Screening (SBVS) has become a popular way to test for viable drugs.[30] First, a 3D scan of the target receptor is required. Then, using virtual compound libraries, computer-generated representations of known small molecules are "placed" in the 3D model of the receptor in a variety of positions, conformations and orientations.[30] Each such docking mode is called a 'pose', and are given a score based on its complementarity to the target in terms of shape and properties such as electrostatics. A good score for a given molecule indicates that it is potentially a good binder. This process is repeated for all molecules in the collection, which are subsequently rank-ordered by their scores, revealing the most viable drug options.[30] AutoDock is one of the many websites containing both the compound library and the random placement+scoring technology, which have played a crucial role in making SBVS accessible.[31] The one limiting factor of SBVS is that it only evaluates known molecular compounds instead of creating truly new compounds, which might not always produce beneficial results or result in copyright battles.

Ligand Based Drug Design:

Ligand Based Drug Design is an approach used in the absence of the target receptor structure, and instead it relies on knowledge of molecules that bind to the biological target of interest, or ligands. This approach can be broken down into four main strategies: Pseudoreceptors, QSAR, Scaffold Hopping, and Pharmacophore modeling.

The pseudoreceptor method not only functions as a valuable tool in the drug design process, but also provides an accurate idea of the structure of a target protein, which in some cases is enough to warrant Structure Based Drug Design approaches.[29] This method functions by studying known bioactive ligands, or proteins in the body that naturally bind to the target protein.[29] The drug is then modeled off of this natural substrate, and in some cases, the natural protein with slight editing actually becomes the drug.[29] Additionally, by studying the natural substrates of the target protein, much is learned about the target proteins requirements and structure, which aids in the drug design process.

Quantitative Structure Activity Relationship (QSAR) is one of the most widely used Ligand Based Drug Design approaches. At its core, QSAR is very simple. It is based on the assumption that structural or physiochemical properties yield similar activity.[32] Thus, by comparing the function of a molecule in other reactions, as well as known ligands or reactions involving the target protein, the reaction between a molecule and the target protein can be predicted. The end result is the same as the SBVS method. By performing this prediction on a large molecule library, and by assigning scores, the most promising "regions" and molecules are identified.[33] For 3D QSAR application, two main types of approaches are used: CoMFA and CoMSIA. Comparative Molecular Field Analysis (CoMFA) evaluates basic non-binding interactions between a ligand, or molecule, and the protein.[34] Comparative Molecular Similarity Indices Analysis (CoMSIA) measures more in-depth physico-chemical properties of the target protein, not molecule interactions.[34] Basic computation and cluster-mapping are used for prediction and scoring features.

The next method of LB Drug Design is scaffold hopping. This method is used when a ligand that binds to the protein of interest is already known. Scaffold hopping preserves the structure of the molecule but swaps out certain molecules and elements in favor of others.[19] Thus, it maximizes the efficiency of a molecule while making sure it still "fits". Scaffold Hopping might be necessary for many reasons: improved pharmacokinetic properties, lower toxicity, better efficiency, and/or intellectual property rights.[19] It is important to note that this is more of a "finishing step" approach rather than starting from scratch. Research of a molecule (natural or synthesized) that already binds to the target is a prerequisite to this step.

The fourth main method of LB Drug Design is pharmacophore modeling. This is the oldest method of drug design, however recent online variations have revived popularity.[29] Pharmacophore modeling is a strategy focused on identifying

DOI: 10.36838/v3i1.10

structural and biological features and putting together molecules that will meet the requirements. A popular used analogy is identifying and combining basic building blocks of molecules to make a compound that can perform all needed functions. For direct application, this happens in three simple steps:

1) finding the features required for a particular biological activity
2) determining the molecular shape or confirmation required
3) developing a superposition or order for the series of molecules.

This is usually now performed using online screening, with online 3D screening of databases to find the right molecules and order to make a compound, or drug. There are various commercially available websites, such as CATALYST, each with different filters promising better results.[29] Because a lot of the approaches are similar, some distinguishing is needed. This approach of pharmacophore modeling is similar to methods 2 and 4 in the de novo drug design process (Site point connection methods & Fragment connection methods), except those methods build up drugs mainly on structure whereas pharmacophore modeling builds up molecules mainly by function. Pharmacophore modeling is also similar to QSAR LBDD as they both build up drugs molecule by molecule, but pharmacophore modeling is focused more on starting from scratch and meeting the "final drug" attributes or features, whereas QSAR is focused more on scientific feasibility, chemical properties, and maximizing efficiency. However, there is a lot of gray area, and often the two are used in conjunction.

Validation:

Many of these approaches are often used together in the drug design process. Besides legal and financial problems, the top two reasons why 97% of drugs fail the development process

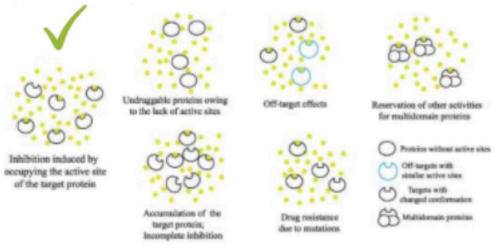

Figure 7: A summary of some problem drugs can run into. The one correct or positive outcome is shown with a green checkmark.

is due to lack of efficacy and off-target or toxic effects.[35] There are many causes for this, mainly due to other proteins with similar active sites that the molecule will unnecessarily effect (Figure 7). Thus, it is incredibly important to validate results using as many orthogonal techniques as possible to ensure that A) the drug target is actually a cancer dependency and B) the synthesized drug is able to effectively act only on the proposed target. This can be achieved in many ways, but the "golden-standard" for drug validation is a mutation assay.[6] This is done by inducing a mutation in the target protein that prevents the synthesized drug from binding. Thus, the drug should have no effect on growth of these mutant cells as it shouldn't be able to bind to anything. If there is repressed growth or lack of growth even from the mutant cells, an off-target effect has been identified and the drug design process needs to restart. However, inducing a mutation in the target protein isn't always plausible, as not all proteins are easily mutated.[6] Additionally, the molecule might have other off-target or toxic effects when introduced in the body, which can't be tested for in preclinical trials or in "golden-standard" mutation assays.[6] Currently, these other possibilities accounted for using mice or animal trials, although these don't always represent the same factors in a human body. At this point, the drug is ready to go into clinical trials to test effects on a larger scale.[36]

Conclusion

This paper attempted to describe current methods for finding a cancer drug from scratch and flatten the learning curve for the overall drug discovery process. First, a definition and background of cancer was given. The three main causes of cancer, the body's natural defense mechanisms for mutations, and the six hallmarks of cancer were given. Next, cancer dependencies were defined, which are needed for targeted-drugs therapy. Loss-of-function (LOF) assays were described as the primary experimental technique for establishing cancer dependencies, targeting either the DNA, RNA, or protein levels. Popular LOF techniques used to identify drug targets were discussed, with CRISPR/Cas9, RNAi, and PROTAC emerging as the most popular methods for every respective molecule. Additionally, a head-to-head comparison of CRISPR/Cas9 and RNAi was also listed, as well as an introduction to recent modifications that show enormous potential to the gene expression toolbox. Finally, the process of creating a drug targeting the protein arising from the cancer dependency was covered, split on whether the structure of the target protein was known or not. The validation process and the golden standard were also given.

The pathway to developing cancer drugs, however, still has a couple of major hurdles. One big hurdle is the fact that when creating a cancer drug molecule, there are possible off-target effects in the body which cannot be predicted in advance. This is only sufficiently observed in clinical trials, after a lot of time and money has already been invested. There are databases that are being created that try to contain all the active sites of proteins in the human body, and the compatibility or effects of a certain molecule can be simulated. Unfortunately, these databases are nowhere close to containing all the proteins or matching the complexity of reactions in the human body.

The future for fighting cancer is bright. Since the year 1991, there has been a 29% decrease in cancer deaths, with last year providing the single biggest yearly drop in deaths ever recorded. This has been fueled by many things. There has been a public awakening about carcinogens, smoking, and other environmental factors that increase cancer prevalence. There has been extensive research on obesity, diet, and some on the role of the gut microbiome in preventing or causing cancer. Increased public awareness and inevitable discoveries yielding more about cancer will further help decrease the number of cancer deaths and continue this trend in the future. The cancer research field will also undergo massive growth. Most of the

processes discussed in this paper were discovered at the end of the 20th century, apart from some of the DNA gene knockout techniques. Over the next decade, future technologies will no doubt render today's leading techniques obsolete as well. Out of those discussed in this paper, the field is shifting towards CRISPR/Cas12a, Cas13, and PROTAC systems in particular, although a variety of techniques both new and old are used in different labs. The biggest factor that needs improvement, as well as the benchmark for measuring the efficiency of new methods, is the prevalence of off-target effects: that is, when a target or molecule binds to something that wasn't intended, causing unintended consequences. Although cancer has been wreaking havoc on humanity for centuries, recent technologies have led to exponential amounts of research and development, and the end of cancer as we know it might be sooner than we expected.

Acknowledgements

Huge thanks to Ann Lin, Ph.D. candidate at Stanford for genetics and microbiology, who gave me this idea and introduced me to the scientific paper comprehension and writing process. She is both the "why" and the "how" of this paper. I truly could not have done it without her.

References

1. WHO. Cancer https://www.who.int/westernpacific/health-topicscancer (accessed Jul 8, 2020).
2. Cancer Facts & the War on Cancer | SEER Training https://training.seer.cancer.gov/disease/war/ (accessed Oct 2, 2020).
3. Lin, A.; Giuliano, C. J.; Palladino, A.; John, K. M.; Abramowicz, C.; Yuan, M. L.; Sausville, E. L.; Lukow, D. A.; Liu, L.; Chait, A. R.; Galluzzo, Z. C.; Tucker, C.; Sheltzer, J. M. Off-Target Toxicity Is a Common Mechanism of Action of Cancer Drugs Undergoing Clinical Trials. Sci. Transl. Med. 2019, 11 (509). https://doi.org/10.1126/scitranslmed.aaw8412.
4. Van Elsland, D.; Neefjes, J. Bacterial Infections and Cancer. EMBO Rep. 2018, 19 (11). https://doi.org/10.15252/embr.201846632.
5. Cooper, G. M. Oncogenes. Cell Mol. Approach 2nd Ed. 2000..
6. Lin, A.; Sheltzer, J. M. Discovering and Validating Cancer Genetic Dependencies: Approaches and Pitfalls. Nat. Rev. Genet. 2020, 1–12. https://doi.org/10.1038/s41576-020-0247-7..
7. Tsherniak, A.; Vazquez, F.; Montgomery, P. G.; Weir, B. A.; Kryukov, G.; Cowley, G. S.; Gill, S.; Harrington, W. F.; Pantel, S.; Krill-Burger, J. M.; Meyers, R. M.; Ali, L.; Goodale, A.; Lee, Y.; Jiang, G.; Hsiao, J.; Gerath, W. F. J.; Howell, S.; Merkel, E.; Ghandi, M.; Garraway, L. A.; Root, D. E.; Golub, T. R.; Boehm, J. S.; Hahn, W. C. Defining a Cancer Dependency Map. Cell 2017, 170 (3), 564-576.e16. https://doi.org/10.1016/j.cell.2017.06.010.
8. DNA Sequencing: History, Steps, Methods, Applications And Limitations. Genetic Education, 2019.
9. Adli, M. The CRISPR Tool Kit for Genome Editing and Beyond. Nat. Commun. 2018, 9. https://doi.org/10.1038/s41467-018-04252-2.
10. CRISPR Transfection Protocols Guide: How To Select The Best Method https://www.synthego.com/guide/how-to-use-crispr/transfection-protocols (accessed Aug 11, 2020).
11. Cortez, C. CRISPR 101: Homology Directed Repair https://blog.addgene.org/crispr-101-homology-directed-repair (accessed Jul 28, 2020).
12. Khan, S. H. Genome-Editing Technologies: Concept, Pros, and Cons of Various Genome-Editing Techniques and Bioethical Concerns for Clinical Application. Mol. Ther. Nucleic Acids 2019, 16, 326–334. https://doi.org/10.1016/j.omtn.2019.02.027.
13. You, L.; Tong, R.; Li, M.; Liu, Y.; Xue, J.; Lu, Y. Advancements and Obstacles of CRISPR-Cas9 Technology in Translational Research. Mol. Ther. Methods Clin. Dev. 2019, 13, 359–370. https://doi.org/10.1016/j.omtm.2019.02.008.
14. Meraldi, P. Bub1—the Zombie Protein That CRISPR Cannot Kill. EMBO J. 2019, 38 (7). https://doi.org/10.15252/embj.2019101912.
15. Fire, A.; Xu, S.; Montgomery, M. K.; Kostas, S. A.; Driver, S. E.; Mello, C. C. Potent and Specific Genetic Interference by Double-Stranded RNA in Caenorhabditis Elegans. Nature 1998, 391 (6669), 806–811. https://doi.org/10.1038/35888.
16. Housden, B. E.; Muhar, M.; Gemberling, M.; Gersbach, C. A.; Stainier, D. Y. R.; Seydoux, G.; Mohr, S. E.; Zuber, J.; Perrimon, N. Loss-of-Function Genetic Tools for Animal Models: Cross-Species and Cross-Platform Differences. Nat. Rev. Genet. 2017, 18 (1), 24–40. https://doi.org/10.1038/nrg.2016.118.
17. Chamberlain, P. P.; Hamann, L. G. Development of Targeted Protein Degradation Therapeutics. Nat. Chem. Biol. 2019, 15 (10), 937–944. https://doi.org/10.1038/s41589-019-0362-y.
18. Advances in targeted degradation of endogenous proteins | SpringerLink https://link.springer.com/article/10.1007/s00018-019-03112-6#Tab1 (accessed Aug 15, 2020).
19. Bergmann, R.; Linusson, A.; Zamora, I. SHOP: Scaffold HOPping by GRID-Based Similarity Searches. J. Med. Chem. 2007, 50 (11), 2708–2717. https://doi.org/10.1021/jm061259g.
20. An, S.; Fu, L. Small-Molecule PROTACs: An Emerging and Promising Approach for the Development of Targeted Therapy Drugs. EBioMedicine 2018, 36, 553–562. https://doi.org/10.1016/j.ebiom.2018.09.005.
21. Boettcher, M.; McManus, M. T. Choosing the Right Tool for the Job: RNAi, TALEN or CRISPR. Mol. Cell 2015, 58 (4), 575–585. https://doi.org/10.1016/j.molcel.2015.04.028.
22. Giuliano, C. J.; Lin, A.; Girish, V.; Sheltzer, J. M. Generating Single Cell–Derived Knockout Clones in Mammalian Cells with CRISPR/Cas9. Curr. Protoc. Mol. Biol. 2019, 128 (1), e100. https://doi.org/10.1002/cpmb.100.
23. Gupta, S.; Schoer, R.; Egan, J.; Hannon, G.; Mittal, V. Inducible, Reversible, and Stable RNA Interference in Mammalian Cells. Proc. Natl. Acad. Sci. U. S. A. 2004, 101, 1927–1932. https://doi.org/10.1073/pnas.0306111101.
24. Qi, L. S.; Larson, M. H.; Gilbert, L. A.; Doudna, J. A.; Weissman, J. S.; Arkin, A. P.; Lim, W. A. Repurposing CRISPR as an RNA-Guided Platform for Sequence-Specific Control of Gene Expression. Cell 2013, 152 (5), 1173–1183. https://doi.org/10.1016/j.cell.2013.02.022.
25. Gier, R. A.; Budinich, K. A.; Evitt, N. H.; Cao, Z.; Freilich, E. S.; Chen, Q.; Qi, J.; Lan, Y.; Kohli, R. M.; Shi, J. High-Performance CRISPR-Cas12a Genome Editing for Combinatorial Genetic Screening. Nat. Commun. 2020, 11 (1),

DOI: 10.36838/v3i1.10

3455. https://doi.org/10.1038/s41467-020-17209-1.
26. Wessels, H.-H.; Méndez-Mancilla, A.; Guo, X.; Legut, M.; Daniloski, Z.; Sanjana, N. E. Massively Parallel Cas13 Screens Reveal Principles for Guide RNA Design. Nat. Biotechnol. 2020, 38 (6), 722–727. https://doi.org/10.1038/s41587-020-0456-9.
27. Cancer treatment – Mayo Clinic https://www.mayoclinic.org/tests-procedures/cancer-treatment/about/pac-20393344 (accessed Aug 17, 2020).
28. Ch, W.; Kw, S.; Aw, L. Estimation of clinical trial success rates and related parameters https://pubmed.ncbi.nlm.nih.gov/29394327/ (accessed Sep 15, 2020). https://doi.org/10.1093/biostatistics/kxx069.
29. Aparoy, P.; Kumar Reddy, K.; Reddanna, P. Structure and Ligand Based Drug Design Strategies in the Development of Novel 5-LOX Inhibitors. Curr. Med. Chem. 2012, 19 (22), 3763–3778. https://doi.org/10.2174/092986712801661112.
30. Kroemer, R. T. Structure-Based Drug Design: Docking and Scoring. Curr. Protein Pept. Sci. 2007, 8 (4), 312–328. https://doi.org/10.2174/138920307781369382.
31. AutoDock — AutoDock http://autodock.scripps.edu/ (accessed Aug 23, 2020).
32. Acharya, C.; Coop, A.; Polli, J. E.; MacKerell, A. D. Recent Advances in Ligand-Based Drug Design: Relevance and Utility of the Conformationally Sampled Pharmacophore Approach. Curr. Comput. Aided Drug Des. 2011, 7 (1), 10–22. https://doi.org/10.1093/biostatistics/kxx069.
33. Grover, M.; Singh, B.; Bakshi, M.; Singh, S. Quantitative Structure–Property Relationships in Pharmaceutical Research – Part 1. Pharm. Sci. Technol. Today 2000, 3 (1), 28–35. https://doi.org/10.1016/S1461-5347(99)00214-X.
34. Zhao, X.; Chen, M.; Huang, B.; Ji, H.; Yuan, M. Comparative Molecular Field Analysis (CoMFA) and Comparative Molecular Similarity Indices Analysis (CoMSIA) Studies on A1A-Adrenergic Receptor Antagonists Based on Pharmacophore Molecular Alignment. Int. J. Mol. Sci. 2011, 12 (10), 7022–7037. https://doi.org/10.3390/ijms12107022.
35. Fogel, D. B. Factors Associated with Clinical Trials That Fail and Opportunities for Improving the Likelihood of Success: A Review. Contemp. Clin. Trials Commun. 2018, 11, 156–164. https://doi.org/10.1016/j.conctc.2018.08.001.
36. Cancer Drug Development: How Therapies Move Through the Pipeline https://www.cancertherapyadvisor.com/home/tools/fact-sheets/how-cancer-drug-development-pipel ine-treatment-patient-fact-sheet/ (accessed Aug 18, 2020).

Author

Ojas Gupta is a current sophomore at Lynbrook High School in Santa Clara, California. His interest in science and genetics mainly through school competitions such as Science Olympiad led him into the wonderful world of bioinformatics and cancer research, where he was lucky enough to meet Ann Lin, a pioneer in the field. He hopes this paper can help educate the general population on the methodology of cancer research.

Determinants of Coronary Vascular Events Responsible for Sudden Death- Vulnerable Plaque Trial (DISCOVER-VP)

Rachel Rivera

New Rochelle High School, 265 Clove Road, New Rochelle, New York, 10801, USA; rrivera10095@gmail.com

ABSTRACT: Annually, 500,000 deaths are attributed to cardiac arrests. Of these cases, 66% are caused by the accumulation of vulnerable plaque. This plaque increases the chance of a rupture exposing the necrotic core to blood flow and initiating a clot.[1] Although vulnerable plaque poses a significant public health risk, its existence is usually unknown until death. The purpose of this study was to devise a method for vulnerable plaque identification among living patients using computed tomography (CT) scans of postmortem hearts and comparing single energy computed tomography (SECT) to dual energy computed tomography (DECT). The hearts underwent histopathology to determine the locations of all components. The arterial segments were sliced based on cross sections in regions of interest. These locations corresponded to specific areas on the CT scan, whose Hounsfield (HU) units were subsequently compared. It was found that the mean HU of necrotic cores within vulnerable plaque of various regions of the ostium significantly differed from that of fibrous plaque on a DECT scan.[2] This data suggests that DECT scans can be used to accurately distinguish dangerous vulnerable plaque from stable plaque in living patients when compared to SECT scans.

KEYWORDS: Cardiovascular Diseases; Sudden Cardiac Death; Coronary Computed Tomography; Unstable Plaque; Vulnerable Plaque.

Introduction

The American Heart Association approximates that 17.9 million people die of cardiovascular diseases annually and 500,000 of which are attributed to sudden cardiac death (SCD).[3] SCD is characterized by the fatal sudden loss of heart function. Several underlying factors, such as coronary artery disease and ventricular fibrillation, contribute to SCD. However, the primary cause of SCD, responsible for more than 66% of cases, is thrombosis, or the clotting, of vulnerable plaque. Vulnerable plaque is a type of atherosclerotic plaque developed within arterial segments in high-risk cardiovascular patients.[4] The presence of vulnerable plaque is often detected only after death. As the cases of cardiac episodes, especially cardiac arrest,[1] continue to increase exponentially, the urgency to take preventative action is critical.

Vulnerable plaque (VP) is identified by enlarged lipid necrotic core tissue, spotty calcification, and remodeling of the arteries due to plaque burden.[5] VPs are also comprised of an enlarged lipid pool and thin fibrous cap (Figure 1). VP begins development as unstable VP. Unstable plaque is prone to rupturing and clotting.[6] After rupturing, these plaques slowly gain stability and fully become calcified.[6] In contrast, fibrous plaque, a common type of stable plaque, generally consists of a smaller necrotic core and thicker fibrous cap (Figure 1). The VP rupture exposes the necrotic core to blood flow, resulting in extensive clotting.[7] The thin fibrous cap occasionally erodes, exposing the necrotic core to the inner lining of the arterial segment called the lumen. Macrophages attempt to restrict this exposure by forming a clot. The presence of VP is asymptomatic before the initial acute cardiac episode making it difficult to identify living patients with VP before the onset of SCD.[8] Previous research has identified that the lipid pool is a precursor for an unstable necrotic core.[8] This region is highly unstable and exposed blood flow can result in fatal clotting. It is urgent for cardiologists to distinguish VP from stable plaque in living patients to ultimately prevent death.

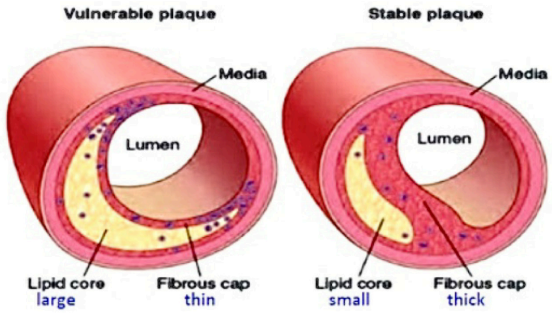

Figure 1: Vulnerable plaque with enlarged lipid core and thin fibrous cap (left) and stable plaque with thick fibrous cap and small lipid core (right).[4]

Coronary computed tomography angiography (CCTA) is commonly used for the characterization of atherosclerotic plaque, the determination of calcium scores, the precise identification of stenosis, and the diagnosis of plaques. Calcium scores refer to calcium accumulation within coronary segments. A high calcium score indicates the presence of extensive stable plaque and is a marker for coronary artery disease. Computed tomography (CT) scans can precisely identify stenosis and plaques. The two predominant CT scan types are single energy CT scans (SECT) and dual energy CT scans (DECT). Both scans are used to visualize coronary anatomy and eliminate calcium artifacts typical of other scans (Figure 2).

DOI: 10.36838/v3i1.11

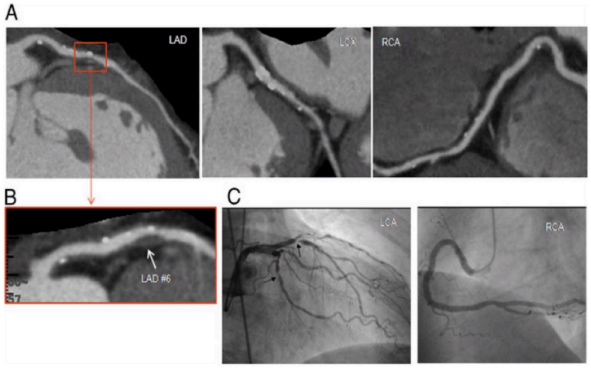

Figure 2: A) calcification of the left anterior descending artery (LAD), left circumflex, and right coronary artery; B) positive remodeling in the LAD; C) acute coronary syndrome 6 months after a CCTA.[8]

SECT scans are often used for diagnosis. Alternatively, DECT has the potential to more accurately identify various atherosclerotic plaques and other landmarks within the heart thanks to its higher resolution images.[9,11] The current study compared the two scans to determine which one can best distinguish between VPs and stable plaques through the identification of high-risk plaque features. Since SECT is limited by its inability to effectively evaluate the characteristics of high-risk plaque, the DECT scan is preferable for VP identification and tissue characterization.

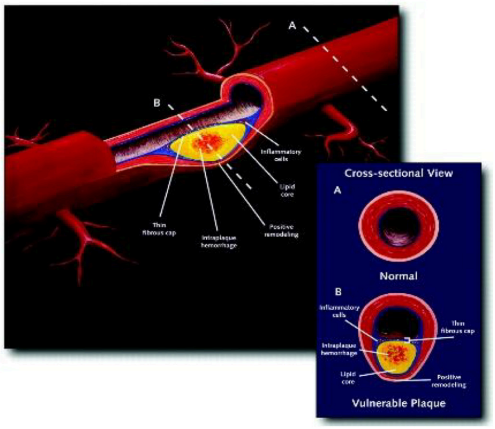

Figure 3: Composition of vulnerable plaque.[5]

Histopathology is another useful method for analyzing different plaque tissue characterization. This technique studies cross-sectionalized arterial segments under a microscope.[12] Such visualization results in precise identification of each component, shown in Figure 3.

Objective:

To improve current methods of high-risk plaque diagnosis in SCD-suspected patients by comparing the accuracy of DECT and SECT during tissue characterization of VP.

Hypothesis:

H1. DECT will be more precise in identifying and characterizing VP *ex-vivo* in comparison to a SECT scan.

H2. DECT will more accurately characterize tissue of VP.

H3. High-risk plaque features will be identifiable from stable plaque features as expected to be justified through histology.

Results and Discussion

DECT/SECT Identification of Necrotic Cores & Fibrous Plaques:

Ninety-four cross sections were identified. The sample was made up of 71% male subjects and 29% female subjects. The mean age of the cohort was 61.4±10.9 years. From this, a total of 8 necrotic cores (NC), 50 fibrous plaques (FP) or atherosclerotic plaques, and 36 lipid pools (LP) were identified using histopathology. Hounsfield units were computed by GE software to measure the substances' radiodensity.[2] The mean HU for both the NC and FP using SECT was 29.4 and 78.95, respectively. The highest resolution to differentiate these two features was at 40 keV of energy using a DECT scan. At 40 keV, cardiologists are best able to differentiate between the stable and unstable VPs. On the other hand, the mean HU for the NC and FP for a DECT scan was 85.34 and 210.57, respectively, also at 40 keV. These values indicate that DECT scans are superior at NC and FP identification. A higher HU value coincides with a more precise identification of the examined substance on any CT scan. There was no notable difference for the mean values for LP.

Histopathology confirmed cardiologists' prediction that DECT scans are better at the prediction of vulnerable plaques within a heart. This correlates to observations on both the SECT and DECT scans since the position of the NCs, LP, and FPs aligned almost perfectly with the images produced following histopathology, illustrated in Figure 4.

With supporting results, it can be concluded that DECT scans more accurately identify VPs from stable plaques with the aid of high-risk plaque markers.

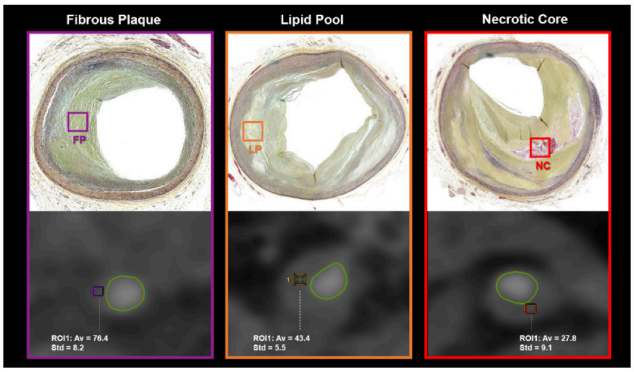

Figure 4: Accuracy of the predicated location of NC, LP, and FP on CT scans and histopathology images.[2]

Conclusion

Based on the experiment's results, the hypothesis is supported. DECT scans are most effective at identifying VPs in the post-mortem hearts used in the study. Using histopathology, the presence of VPs was identified and mirrored the predictions of the plaque's lipid core and NC locations presented in the CT scans. Additionally, DECT scans were preferred because the resolution was better compared to SECT. Histopathology was useful to further examine the plaques and their

compositions. It allowed for the measurements of NC, LP, and the thin fibrous cap. Furthermore, DECT using 40 keV produced the most desirable results compared to a typical SECT scan.

DECT is the most efficient in distinguishing fibrous plaques from VPs through the identification of NC and LP location. This is groundbreaking for the cardiovascular medical field. Now that DECT has been shown to be most accurate, decreasing the high rates of mortality due to sudden cardiac death is almost at reach. DECT scans can be used to identify dangerous VPs within living patients who are susceptible to cardiovascular diseases. This allows doctors to take the necessary precautions to reduce a patient's risk of a potential cardiovascular disease thereby extending their life expectancy. Hundreds of thousands of lives can be saved through the simple identification of potentially hazardous plaques in high-risk cardiovascular patients.

Methods

Data Analysis

CT Scan Optimization:

The goal of this step was to determine the reliability of CT scans using Youden's method. Youden's method allowed accuracy testing using the equation:

J = sensitivity + specificity – 1

where J is the Youden test statistic. J=0 indicates many false positive and false negative results and J=1 indicates a perfect test with no errors.[13] CT scans measure in Hounsfield units which measure a substance's radiodensity. DECT and SECT scans were each run at differing energy levels until J differed compared with paired t-tests. This test was performed with the assistance of the supervisor and J-values were unavailable to the student due to data privacy concerns. The statistical significance of the J-values indicated the reliability of both DECT and SECT scans for this experiment.

Comparison of CT scan HU and Histopathology Values:

Vessel and plaque parameters from histopathology were compared on SECT and DECT scans to a quantitative computed tomography. Histopathology analysis was computed using the Pearson correlation coefficient. The area of plaque components was measured directly with histopathology. This area was compared to the area of plaque components detected by optimally calibrated dual and single energy CT-scans with the Pearson correlation coefficient. A coefficient of 1 indicates a strong, positive relationship between the actual plaque component size and that measured while a coefficient of 0 indicates a weak relationship. The higher r-value indicated that the CT-scan accurately measured plaque components between the estimations and actual locations.

A two-sided p-value was derived from each calculated correlation coefficient. This test was performed with the assistance of the supervisor and r-values were unavailable to the student due to data privacy concerns. This test indicated DECT scans accurately measure the size of vulnerable plaque components ($p<0.05$). The correlation was calculated using the 95% confidence interval.

All Other Variables:

Continuous variables were represented with means or standard deviations, while categorical variables were expressed as percentages. Additionally, a separate equation was generated to account for the plaque features in all the individuals included within the study.

Student and Mentor Roles :

This study was a multi-site collaboration where each institute had separate responsibilities within the project. The earliest steps of the project were to go through the inclusion and exclusion criteria for each participant. Inclusion criteria consisted of newly deceased patients suspected of having SCD and meeting the minimum age requirement of 18 years. If eligible, the next of kin (NOK) provided recorded oral consent and requested an autopsy of the post-mortem heart.

My mentors oversaw each step within the study. After the heart was extracted, it underwent coronary cannulation where it was rinsed with normal saline to clean the heart. Contrast (Diatrizoate) was injected into the left and right main coronary artery at the Office of Chief Medical Examiner (OMCE) in Maryland. Following the coronary cannulation, the heart was taken to CVPath in Baltimore where SECT and DECT scans were performed. These images were taken seconds apart as the contrast flowed throughout the arteries within the heart. The images were sent to the Dailo Institute for Cardiovascular Imaging (DICI) where cardiologists used both the DECT and the SECT to determine total vessel area, NC area, calcified plaque area, luminal area, degree of positive remodeling, presence of spotty calcification with any mixed plaque, the presence of any napkin rings, intraluminal stenosis severity and proximal location by distance in millimeters to the coronary ostium. These values were obtained in HU. The cardiologists made annotations on these scans, directing incision points where a histopathologist performed histopathology during which the plaque was analyzed at a microscopic level. This allowed for better distinction between the stable and the vulnerable plaques identified within the arteries.

The student's role was to analyze the DECT and SECT scans of each *ex-vivo* heart and generate centerlines of each vessel (left anterior descending (LAD), left circumflex (LCX), right coronary artery (RCA), and the diagonals) using a reference CT scan for guidance. The student also observed any high-risk plaque features such as spotty calcification (Figure 3A) or positive remodeling (an extended diameter difference greater than 1 mm) (Figure 3B). Additionally, the student assisted in the management of the data & measurements of the segments in HU. The mentor performed all other procedures.

Acknowledgement

Thank you to Dr. Fay Lin (principal investigator, Weill Cornell New York-Presbyterian, Dalio Institute of Cardiac Imaging) for allowing me to assist in your ongoing research. Thank you to Dr. Umberto Gianni (research fellow, Weill Cornell New York-Presbyterian, Dalio Institute of Cardiac Imaging) for deciding to have me on your team and having the patience to explain this study's complexity to me. I would also like to give a special thanks to June Thumpituk, Emma

DOI: 10.36838/v3i1.11

Hollenberg, Alexander Van Rosendael, Inge Van den Hoogen, Dr. Leslee Shaw, Dr. Benjamin Lee, Zahra Fatima, and Niree Hindoyan for your guidance and willingness to include me in additional projects. I would like to give a special thanks to my science research teacher, Mr. Wuebber. Thank you for your endless support and guidance through this journey!

References

1. Gillum, R.F. Sudden coronary death in the United States: 1980-1985. Circ. 1989, 79, 756-65. DOI: 10.1161/01.cir.79.4.756.
2. Amoa, F.; Dwivedi, A.: Al Hussein Alawaml, O.; Sato, Y.; Bax, A.; Elshafeey, A.; Gianni, U.; Wijeratne, R.; Hollenberg, E.; Lu, Y; et al. Lab Record. Weill Cornell NewYork-Presbyterian Dalio Institute of Cardiac Imaging, April 2018.
3. Chugh, S.S.; Reinier, K.; Teodorescu, C.; Evanado, A.; Kehr, E.; Al Samara, M.; Mariani, R., Gunson, K.; Jui, J. Epidemiology of Sudden Cardiac Death: Clinical and Research Implications. Prog. Cardiovasc. Dis. 2008, 51(3), 213-228. DOI: 10.1016/j.pcad.2008.06.003
4. Virmani, R.; Kolodgie, F.D.; Burke, A.P.; Farb, A; Schwartz, S.M. Lessons from sudden coronary death: a comprehensive morphological classification scheme for atherosclerotic lesions. Arterioscler. Thromb. Vasc. Biol. 2000, 20(5), 1262-1275. DOI: 10.1161/01.atv.20.5.1262
5. Bentzon, J.F; Otsuka, F.; Virmani, R.; Falk, E. Mechanisms of Plaque Formation and Rupture. Circ. Res. 2014, 114(12), 1852-1866. DOI: 10.1161/CIRCRESAHA.114.302721.
6. Finn, A. V.; Nakano, M.; Narula, J., Kolodgie,; F. D.; Virmani, R, Concept of Vulnerable/Unstable Plaque. Arteriosclerosis, Thrombosis, and Vascular Biology 2010, 30(7), 1282-1292. DOI: 10.1161/atvbaha.108.179739.
7. Al'Aref, S.J.; Su, A.; Gransar, H.; Rosendael, A.R.; Rizvi, A.; Berman, D.S.; Callister, T.Q.; DeLago, A.; Hadamitzky, M.; Hausleiter, J.; Al-Mallah, M.H.; Budoff, M.J.; Kaufmann, P.A.; et al. A cross-sectional survey of coronary plaque composition in individuals on non-statin lipid lowering drug therapies and undergoing coronary computed tomography angiography. J. Cardiovasc. Comput. Tomogr. 2019, 13(2), 99-104. DOI: 10.1016/j.cct.2019.01.015.
8. Otsuka, F.; Yasuda, S.; Noguchi, T.; Ishibashi-Ueda, H. Pathology of coronary atherosclerosis and thrombosis. Cardiovascular Diagnosis and Therapy. 2016, 6(4), 396-408. DOI:10.21037/cdt.2016.06.01.
9. Motoyama, S.; Sarai, M.; Harigaya, H.; Anno, H.; Inoue, K.; Hara, T.; Naruse, H.; Ishii, J.; Hishida, H.; Wong, N.D.; et al. Computed tomographic angiography characteristics of atherosclerotic plaques subsequently resulting in acute coronary syndrome. J. Am. Coll. Cardiol. 2009, 54(1), 49-57. DOI: 10.1016/j.acc.2009.02.068.
10. Nakanishi, R.; Baskaran, L.; Gransar, H.; Budoff, M.J.; Achenbach, S.; Al-, Mallah, M.; Cademartiri, F.; Callister, T.Q.; Chang H., Chinnaiyan, K.; et al. Relationship of Hypertension to Coronary. Atherosclerosis and Cardiac Events in Patients with Coronary Computed Tomographic Angiography. Hypertension 2017, 70(2), 293-299. DOI: 10.1161/HYPERTENSIONAHA.117.09402
11. Bortnick, A.E.; Bartz, T.M.; Ix, J.H.; Chonchol, M.; Reiner, A.; Cushman, M.; Owens, D.; Barasch, E.; Siscovick, D.S.; Gottdiener, J.; et al. Association of inflammatory, lipid and mineral markers with cardiac calcification in older adults. Heart 2016, 102(22), 1826-1834. DOI: 10.1136/heartjnl-2016-309404.
12. Narula, J.; Nakano, M.; Virmani, R; Kolodgie, F.D.; Petersen, R.; Newcomb, R.; Malik, S.; Fuster, V.; Finn, A.V. Histopathologic characteristics of atherosclerotic coronary disease and implications of the findings for the invasive and noninvasive detection of vulnerable plaques. J. Am. Coll. Cardiol. 2013, 61(10), 1041-1051. DOI: 10.1016/j.jacc.2012.10.054.
13. Ruopp, M.D.; Perkins, N.J.; Whitcomb, B.W.; Schisterman, E.F. Youden Index and optimal cut-point estimated from observations affected by a lower limit of detection. Biom. J. 2008, 50(3), 419-430. DOI: 10.1002/bimj.200710415.

Authors

Rachel Rivera is a junior from New Rochelle High School who anticipates following a pre-med track in college. Throughout her junior year, Rachel qualified for multiple regional competitions including selection as an international GENIUS Olympiad finalist.

Aeropalynologic Features of Plants and Fungi Pollination in Kazan and Their Influence on Hay Fever

Rakhim Khamitov, Rafcat Kireev

Lyceum boarding school No:2, Shamilya Usmanova 9, Kazan, 420095, Russia; RKhamitov2016@litsey2.ru

ABSTRACT: The greatest cause of respiratory allergens related to human exposure to biological and chemical components is atmospheric air, which has powerful sensitizing agents.[1] Among the large number of stimuli, it is the pollen and fungal spores that most frequently exacerbate hay fever. The objective of this study is the identification of impact on the human body by the pollen of various plants. This task involves aeropalynology monitoring, enabling assessment and prediction of the environment, and is aimed at the timely correction of treatment of allergic diseases in patients. In this study we observed the pollen of different plants with help of hand-made device. In the end of our review we found that the problem is very relevant, and we need to help people with allergies from pollen. In the future we are planning to make a convenient app which will help people with allergies in identifying the most dangerous zones and times.

KEYWORDS: Ecology; health; allergies; monitoring; pollen; pollinosis; aeropalynologic features.

Introduction

The importance of pollen monitoring is growing more and more due to the prevalence of diseases caused by allergies, environmental deterioration, and need for the development of effective drugs for fighting allergic reactions. However, in Russia, pollen monitoring is carried out partially and non-regularly in certain regions. This does not allow one to see the whole picture across the country, as the available data is clearly insufficient. The importance of local information for regional studies is high, since this data has a substantial informational value given the regional nature of hay fever.[2]

Pollen allergy (pollinosis) is a classic allergic disease, the clinical manifestations of which are allergic inflammation that arises in response to pollen allergens. Due to global climate change, changes in nutrition and the way of our life, and air pollution, the number of people suffering from allergic diseases is increasing.[3]

For pollen monitoring and interpretation, it is also important to take into account that the pollen of plants is of differing in size, and the presence or absence of grooves spines, and outgrowths. On such grounds, pollen identification is carried out. For instance, when a pollen grain with a diameter of 60 to 100 microns is inhaled, it settles on the mucosa of the upper respiratory tract, while one with a diameter of 20-30 microns - penetrates the bronchial mucosa.[4]

Pollen of angiosperms - birch, alder and hazel, ash, maple, linden, oak, willow, etc., has a much stronger allergen activity. Pollen of birch has the most pronounced activity, since its content in the air is quite high, often: 20,000 pollen grains in 1 m^3. It should be noted that most species of willows and limes are insect-polluted plants and they also produce a lot of pollen, which contributes to the emergence of allergies.[5]

The composition of the pollen of some tree species has the same protein complexes, which is the reason for the formation of common allergenic properties and cross allergies. For example, people suffering from birch hypersensitivity to pollen can simultaneously react to the pollen of hazel and alder.[6]

The allergy to pollen of woody plants affects more people in cities than in rural areas, where the concentration of pollen is several times higher. Numerous scientific findings indicate that pollen in cities is covered with a layer of pollution from the environment. These pollutants include carbon dioxide (CO_2), and various petroleum products which makes the pollen more allergenic. According to another scientific study, the reaction of the immune system in a polluted environment is stronger than in ecologically clean areas.[7]

Researchers also note that the prevalence of sensitization to birch pollen in Europe. According to allergic survey data, birch pollen concentrations also vary significantly: from 5% in the Netherlands to 54% in Switzerland. Even in Northern Italy, the share of positive allergic tests has increased, which is associated with the increased popularity of birch as an ornamental plant in this area. In addition, there is evidence of a significantly stronger allergenicity of pollen from trees grown at elevated temperatures.[8]

This study covers the regional aspect of the fungal and plant pollination features and presents the results of conducted pollen monitoring in the city of Kazan in the Republic of Tatarstan. The data obtained during the research, with the further development of pollen monitoring programs, will create a network of observation stations for the maximum coverage of Russia's regions and the development of an effective forecast system.

Results and Discussion

Pollen monitoring is a unique interdisciplinary project that is being conducted in some regions of Russia. Data on monitoring conducted in Samara, Saratov and other cities has been recorded. The pollen monitoring has been developed together with specialists from the Russian Association of Allergists and

DOI: 10.36838/v3i1.12

Clinical Immunologists (RAAKI), the Moscow State University, and the pharmaceutical company Takeda.

Thus, data collected in the framework of dust monitoring for five groups of plants allow us to conclude that the most intensive pollination in Kazan is observed in groups of mushrooms, weeds and coniferous trees. In all groups, the greatest intensity is from May to September, with coniferous and deciduous trees being the most active in May, cereals in June, and weeds and fungi in July and August (Tables 1-3).

The highest intensity transfer of pollen occurs in the daytime (from 5 to 11 a.m.), while at night the intensity of pollination is minimal. In this case, the exacerbation of pollinosis occurs at a time when the concentration of pollen in the air already has threshold values: 10-20 pollen grains per 1 m³ of air.

Consider the data of our pollen monitoring in Kazan by groups.

Group I - Deciduous trees:

This group includes the following plant names: birch, elm, oak, willow, maple, linden, alder, hazel, poplar.

Table 1: Data of pollen monitoring by deciduous trees, p.g. The greatest intensity is from May to September.

Plant specimen	2016		2017				
	May	June	April	May	June	July	August
Birch	327	4	18,43	153,26	95,18		
Elm					16,49		
Oak				555			
Willow					0,97		
Maple	7		0,97		0,97		
Linden	1	153			94,09	146,35	5,8
Alder			12,61				
Hazel					0,97		
Poplar	4,97		1,94	0,97	1,94		

(All numbers are shown in p.g./ m³)

According to the data, it is evident that the highest activity of pollen emissions was recorded in the birch, maple, and linden trees. Although many researchers agree that the most allergenic trees are considered to be maple, hazel, alder, birch and ash, and the majority of patients with pollinosis consider poplar to be their main enemy. In our study the highest pollination value was observed in birch. It is this deciduous plant that is the most dangerous causative agent of pollinosis. The distribution according to tree types is shown in (Figure 1)

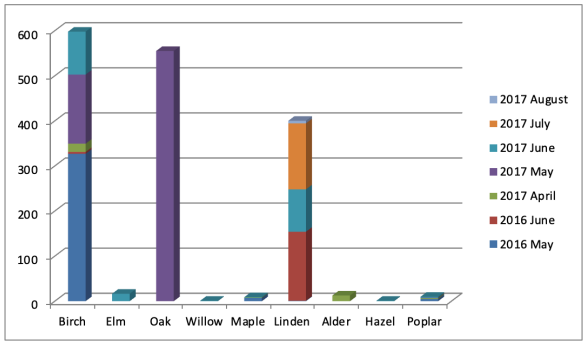

Figure 1: Pollen monitoring data by types of deciduous trees.

For an allergy sufferer, the place of residence is of paramount importance. It is better to live in a locality with a predominance of coniferous trees.

The distribution of the intensity of pollination of deciduous trees by months is shown in the graph (Figure 2).

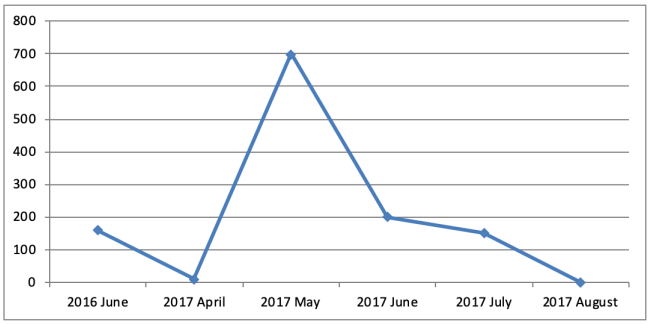

Figure 2: Data from pollen monitoring of deciduous plants, p.g. (monthly).

The largest release of pollen in combination with deciduous trees occurs at the end of spring and early summer. The maximum pollination occurs in mid-May.

Group II - Coniferous trees:

Group II is represented by coniferous trees: pine (Pínus) and spruce (Pícea).

The period of pollination the pine is 2 months - from April to May. Ate - only one month - May. The pollination of the pine is shown in Figure 3.

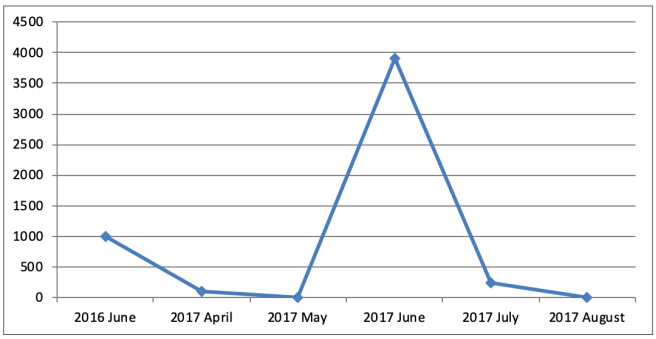

Figure 3: Data of pollen monitoring of pine, p.g. The greatest intensity is from May to September.

According to the data it can be seen that the greatest pollination occurs in May.

Let us consider in detail the dynamics of pollination in May for 2016 and 2017 (Figures 4 and 5).

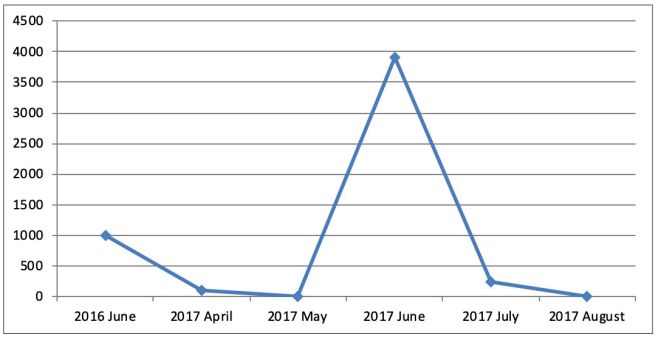

Figure 4: Dynamics of pine pollination in May 2016, p.g./ m³.

It can be seen from the graphs that the highest intensity of pollination occurs in the first ten days of the month. Then,

from the middle of May, the intensity of pollination gradually decreases.

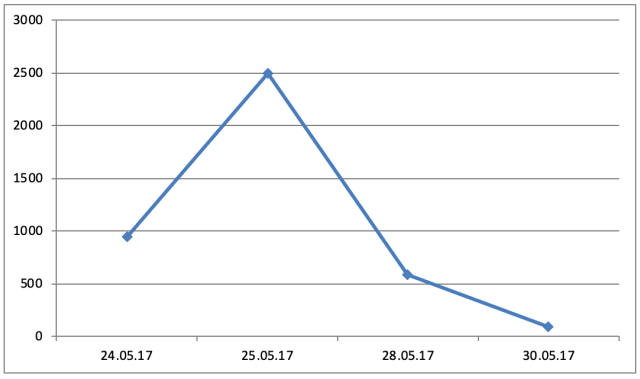

Figure 5: Pollen monitoring of the pine for May 2017, p.g./m³.

For spruce, the pollen indicators in May 2016 and 2017 are as follows by day (Figure 6).

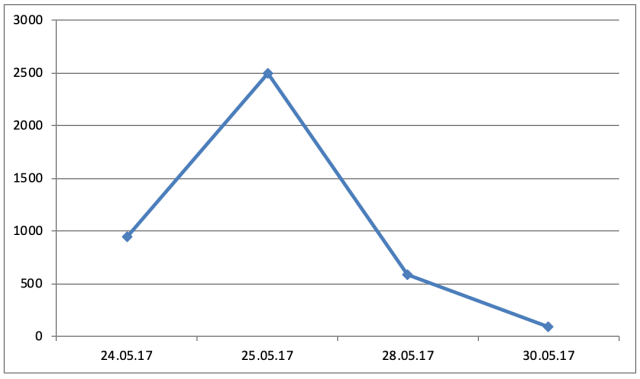

Figure 6: Pollen monitoring of spruce for May 2016, p.g. / m³.

Thus, in spruce and pine trees there is an increase in the intensity of pollination in mid-May and a decrease by the end of the month. For allergy sufferers, the pollen of coniferous trees is not as dangerous as that of deciduous trees, because its allergenicity is low due to their large diameter (30 microns). However, gymnosperms produce a lot of pollen, so sensitivity to it is still present. In the European part of Russia, coniferous trees that most often causes allergies are spruce and pine.[9]

Group III – Mushrooms.

The cause of an allergic reaction is the ingress of microorganisms into irritated nasal mucosa, which cause plant diseases, for example, mold fungi. Common species of mushrooms of the genera Cladosporium and Alternaria, represent a certain danger when spores are actively detected in the air – from March to November.

Manifestations of an allergy of this origin are expressed in the diseases – dermatitis, hives, eczema, allergic rhinitis, conjunctivitis, and bronchial asthma. Fungal spores can form eosinophilic infiltrates in the lungs and are visible on an X-ray image as small blackouts. When detecting the sensitivity of mucous to fungal spores, signs of allergy can be identified after contact with raw, musty grass and hay, after staying in rooms with increased dampness and affected by mold, and also when eating foods fermented during cooking – such as sauerkraut and kvass. From May to November, the danger of getting an allergy to fungal spores increases to one hundred percent.

Data on the intensity of dust mushrooms of the genus Cladosporium, Alternaria collected during the period from April to September 2017 is shown in Figure 7.

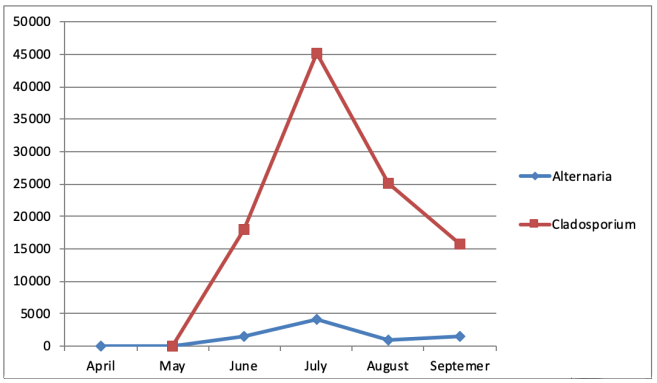

Figure 7: Data from the pollen monitoring of the alternative and Cladosporium for the period from April to September 2017, p.g.

According to the monitoring data, it can be concluded that the greatest activity is from Cladosporium, and the greatest peak of pollination intensity occurs in the summer months, most notably in July.

Furthermore, the increase in the intensity of dust begins in May and ends in July, and the decline occurs until September.

The intensity of pollination of the Cladosporium by months is shown in Figure 8.

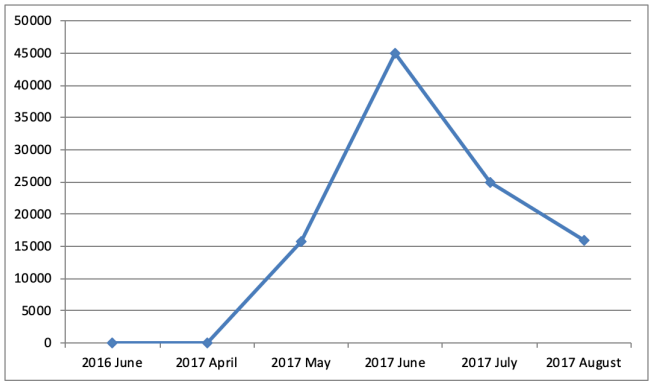

Figure 8: Data of pollen monitoring of the cadozporium for the period from April to September 2017, p.g.

Infection usually occurs on weakened or dying plants, primarily as a result of the diseases at the base of the stem, caused by the yellow dwarf virus, as well as partial felopopulosis due to fusariosis. If during the ripening there are prolonged rains, there is a strong infection.

Secondary fungi also inhabit areas of necrosis on leaves arising from mechanical damage (hail, spring harrowing of winter crops), or due to the erosion of leaves with solutions of nitrogen fertilizers, slurry, herbicides.

Group IV - Cereals.

Allergy to cereals is the most common of all the major types. According to statistics, one in 200 people has an allergy to cereals. This disease can lead to problems, because many foods

DOI: 10.36838/v3i1.12

contain flour or flour products such as pasta and confectionery. There are several reasons for the occurrence of such an allergy

- impact on the organism of pollen of cereals;
- proteins contained in the plant can cause food allergies;
- gluten, contained in cereals, can cause the appearance and development of gluten enteropathy, which is a complication of the disease.

The pollen monitoring data for cereals is shown in the graph

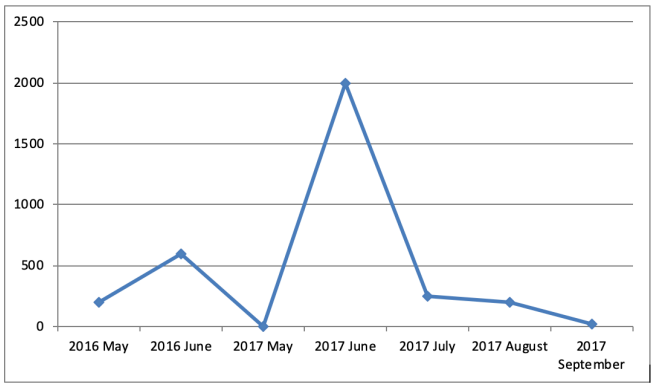

Figure 9: Data of pollen monitoring of the cadozporium for the period from April to September 2017, p.g.

(Figure 9).

The data shows that the greatest activity of the cereal allergen in Kazan falls on June. This is confirmed by the results of pollen monitoring for 2016 and 2017. The increase in the intensity of pollination occurs from May to June, while the intensity decreases from the end of June to September. From July to September, the intensity of pollination is low. The conservation or sometimes even the resumption of pollination of cereals in the second half of the summer is due to the growth of cereals after mowing.

Group V - Weeds.

This group is represented by weed plants, namely of the genera Ruhmex, Plantágo, Ambrosia, Chenopodioídeae, Artemisia and Urtíca. Pollen monitoring data for a group of weed plants were collected from May to June 2016 and from May to September 2017. The results are shown in Table 2.

Table 2 pollination of a group of weed plants in 2016-2017. Graphical change in the dynamics of pollination by weed plants is shown in Figure 10.

Table 2: Table 2 pollination of a group of weed plants in 2016-2017.

Plant Specimen	2016		2017				
	May	June	April	May	June	July	August
Ambrosia						6,88	52,44
Nettle		23	8,73	2054,5	2911,9	791,67	62,36
Mare		85		74,09	330,18	217,3	58,32
Plantain		4	74,69	1599,5	1234,2	666,05	22,44
Sagebrush		1			117,67	460,72	146,88
Sorrel	5	9		362,76	125,55	164,07	

(All numbers are shown in p.g./ m^3)

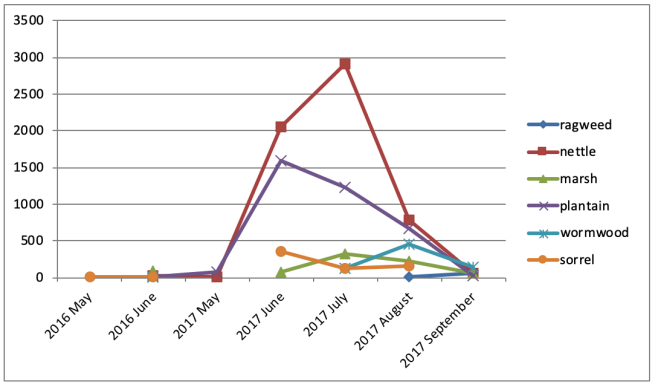

Figure 10: Data of pollen monitoring of weeds for the period from May to June 2016 and from May to September 2017, p.g..

According to the data, in most plants of the weed group, the greatest intensity of pollination occurs during the period from May to September, with a peak in June-July. In addition, for some plants (for example, wormwood), the peak intensity of pollination falls on August.

The greatest pollination among weed plants during the indicated period was observed in nettle and plantain. Consider the dynamics of pollination of these plants in more detail (Figures 11 and 12).

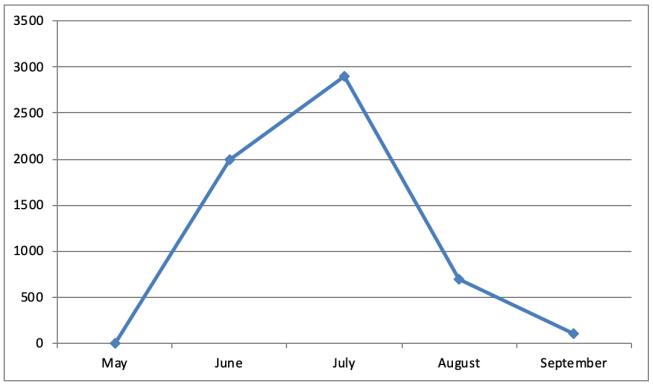

Figure 11: Dynamics of nettles pollination (2017), p.g.

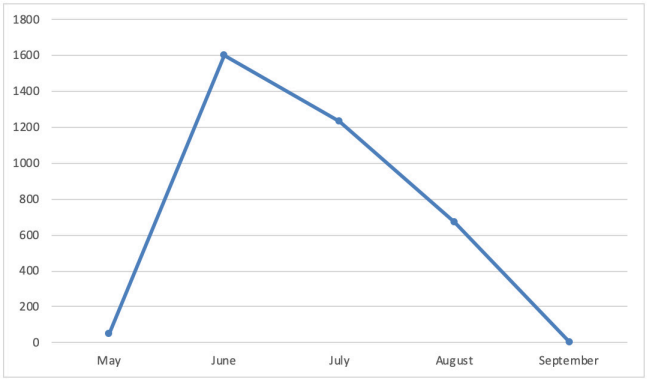

Figure 12: Dynamics of plantain pollination (2017), p.g.

The intensity of nettles pollination tends to increase in the period from May to July 2017 and to decrease from July to September. The occurrence of allergies occurs during a period when pollen, actively floating in the air, settles in the mucous

membrane of the nose, falls into the eyes and mouth, penetrates into the bronchi, and has contact with the skin.

The intensity of the plantain pollination is accompanied by a shorter period of growth, from May to June, and at the end of June growth decreases noticeably, and the fall in the degree of pollination stretches from the end of June to September.

Summary data for all plants included in pollen monitoring during the period under review are presented in Table 3.

Table 3: Consolidated results of pollen monitoring for all groups of plants and fungi.

	2016		2017					
Plant family	May	June	April	May	June	July	August	September
Deciduous trees	891	157	33,95	154,23	206,61	146,35	5,8	
Coniferous trees	1174	86	2,91	3901,34	229,89	0,97		
Mushrooms			0,97	142,59	19559,07	49409,81	26074,12	17333,28
Cereals	236	627		27,16	2010,77	242,56	177,76	32,76
Weeds	5	122		83,42	4088,86	4719,47	2306,69	342,44

(All numbers are shown in p.g./ m^3)

Graphical dynamics for the families of plants and fungi is presented in Figures 13 and 14.

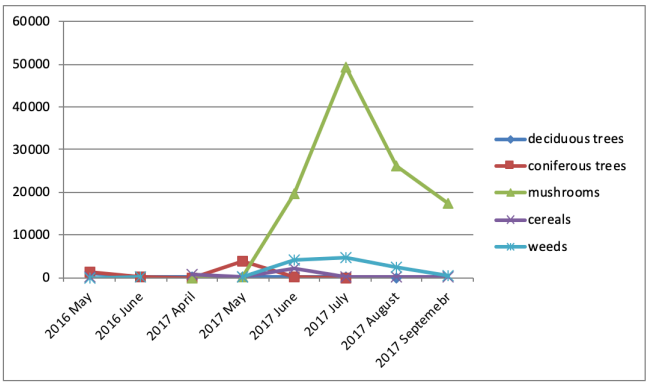

Figure 13: Summary dynamics of pollination in all plant groups for 2016 and 2017, p.g.

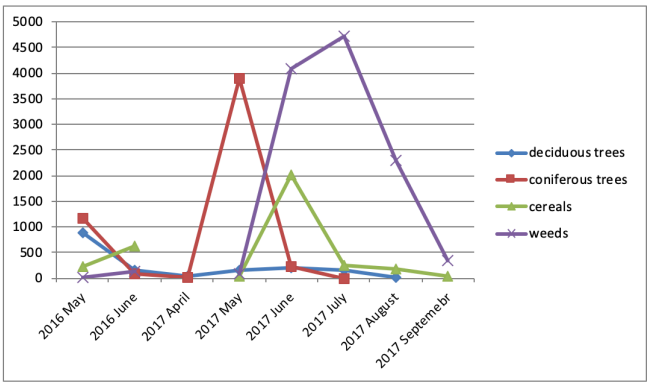

Figure 14: Summary dynamics of pollination in all plant groups for 2016 and 2017, p.g.

Thus, data collected in the framework of dust monitoring for five groups of plants allow us to conclude that the most intensive pollination in Kazan is observed in the groups of mushrooms, weeds and coniferous trees. In all groups, the greatest intensity is from May to September, with coniferous and deciduous trees being the most active in May, cereals in June, and weeds and fungi in July and August.

Conclusion

The pollen monitoring that was carried out in the city of Kazan makes it possible to accurately record the initial and peak flowering periods of the plants in the region and to interpret the data on pollen monitoring more accurately. We plan to use the results obtained to inform the public through the resources of our pollen monitoring website.

The monitoring results make it possible to compile plant and fungal pollination calendars for a region, as well as to reveal how pollination of various plant and fungi species increases pollinosis and other allergies in people. These calendars are an effective tool to create appropriate medications for the prevention and treatment of allergic diseases.

Our study increases the opportunities for Kazan scientists to regularly study the qualitative and quantitative composition of the spore-pollen spectrum of the surrounding air. It also allows for dynamic real-time corrections of the calendar and plant dust maps, leading to a higher degree of certainty in predicting the health status of sensitized patients.

According to the analysis of the results, in Kazan there is a high risk of having an allergic reaction to the pollen of mushrooms (of the genus Cladosporium), weeds (nettles and plantain), and conifers, and a low risk of allergic reaction from the pollen of deciduous trees: elm, willow, maple, alder, hazel and poplar.

Seasonal pollen allergy to flowering plants (pollinosis) is a very common disease that can present in both adults and young children. The best solution is to avoid contact with the allergen. During the time of flowering, some people may leave to regions where the allergy-inducing plant is not common, for example, in the foothills or to places with colder climates. However, circumstances don't always allow for those with allergies to just leave, so alternative solutions should be explored.

Pollen monitoring plays an equally important role in environmental studies. As a biological indicator, pollen can be used to assess the environmental situation. Under the influence of air and soil pollution, the properties and quality of pollen change (in particular, sterile or mutant pollen grains can appear).

Thus, the aeropalinological features of pollination may have seasonal differences in the clinical signs of pollen. The duration of the symptoms may depend on the duration of the main period of pollination, and the intensity (The concentration of pollen). The nature of the dependencies of different combinations of factors among themselves continues to be studied at the present time. Epidemiological studies require a more detailed and long-term study.

Methods

The purpose of the study is to identify the aeropalinological features of plants and fungi pollination in Kazan, namely certain species of deciduous and coniferous trees, fungi, grasses, and weeds - by interpreting the results of pollen monitoring conducted in Kazan during two seasons (2014 - 2015 and 2016 - 2017), as well as a comparison of plant species and their periods of maximum pollination in order to determinethe effect of these plants and fungi species on the increase of pollinosis.

DOI: 10.36838/v3i1.12

In Kazan, during the two seasons mentioned above, monitoring work was conducted with the use of a pollen trap. The hand-made pollen trap device was installed on the roof of the Institute of Fundamental Medicine and Biology at Karl Marx Str., 74, at 10 meters above ground.

Thus, within the given period, data from pollen of twenty plants and fungi specimen were collected. This data made it possible to reveal the regularities and peculiarities of their pollination process.

A tape was fixed with a special silicone solution that was attached to the drum of the device so that the pollen could stick better. The drum functioned due to a clockwork mechanism installed in it, that started periodically. After removal, the tape was cut into seven parts (depending on how many days passed) and stained with a special dye, to which only the shell of plant pollen and fungal spores reacted. Preparations were viewed by transects, and the amount was multiplied by a correction factor (0.97).

Palynological analysis is based on differences in the morphological structure of pollen grains and spores of different plant species. Important characteristics for analysis are the size and shape of pollen grains and spores, the types of apertures and their number, and the types of sculpture and texture.

Aeropalanological studies are conducted by collecting pollen from plants and spores of fungi contained in the air, identifying them, quantifying them by visual counting in the field of view of the microscope, and developing pollination calendars.

At present, there are no universal snares suitable for the study of all types of biological particles. Each area of research (palynology, mycology, virology, etc.) requires its own methods of sampling, subsequent processing and identification of the material. Two principles are used for trapping biological particles: gravity (gravitational particles suspended in the air are precipitated by gravity on a horizontal surface) and impact/collision (the particles suspended in air move together with the air flow and settle on the surfaces of various types materials and orientations). Biological particles, in turn, are natural (by means of wind) or artificially created (different pumps). Most of the impact traps belong to the volumetric type, in which the air flow is created forcibly, due to the operation of the air pump.

The latter method, along with the analysis of the total content of pollen in the air, makes it possible to estimate the daily rhythms of pollination of individual plants.

The importance of monitoring assumes that the type of pollen that causes allergies emanates from trees, grass, and weeds, where fruits or flowers are usually not visible. On such plants there are many small, light granules of dry pollen, which is very quickly spread through the air. The general characteristic of plant allergens is given in Table 4.

As an object for the analysis within this pollen monitoring, 20 plants were selected in the following groups:

1. Group: "Deciduous trees" - birch, elm, oak, willow, maple, linden, alder, hazel, poplar.

2. Group: "Coniferous trees" - spruce and pine.

3. Group: "Mushrooms" - alternarium, cladosporium.

4. Group: "Weeds" - ragweed, nettle, stink, plantain, wormwood, sorrel.

5. Group: "Cereals".

Table 4: General Species Characteristics of Allergen Plants..

Plant species	Subspecies
Weeds	Ambrosia wormwood, wormwood, shirits (plant of the family *amaranth*), white mar, marsh, tumbleweed (Russian solyanka - *Salsola ruthenica*), plantain lanceolate (*Plantago lanceolata*).
Cereals	Timothy-grass (*Phleum pratense*), Kentucky bluegrass (*Roa* family grass), sorghum (*Sorghum*), porcine palmate, white grass (*Agrostis alba*), hedgehog (*Dactylis glomerata*), ylang-ylang, perennial darnel, uniola ears, bukharnik woolly (*Holcus lanatus*) and fescue (*Festuca*).
Deciduous perennial trees	Oak, ash, elm, birch, maple, alder, hazelnut, as well as hickory (genus of the North American hazel), walnut pits, boxwood evergreen, Mexican juniper.

It is also necessary to note the features that allowed researchers to make a high-quality pollen monitoring. First, pollen concentration in the atmosphere is related to air temperature, atmospheric pressure, wind speed, and even the time of day. The concentration of pollen largely determines the intensity of the allergic reaction. In dry, warm weather, plants begin to dust more intensively than on cold, rainy days, but the period of flowering of plants during the cold period is prolonged. Windless weather also prevents the transfer of pollen.

Acknowledgement

The work was performed under the guidance of the biology teacher Malikova Farida and the biology teacher and supervisor Mirsaitov Nail.

References

1. Klymenko V.A., Karpushenko J.V., Servetnik A.V., Optimization of the laboratory diagnosis of allergies with regard to regional peculiarities; Clinical Pediatrics 2015 No6 (66).
2. Statistics in Russia, the main cause of pollinosis. URL:http://allergy-mask.ru/articles/allergiya-statistika-v-rossii.html ; (date of the application: 26.09.2020).
3. Pollen allergy symptoms and treatment. URL:https://allergen-net.ru/allergiya-na-pylcu-simptomy-i-lechenie.html ; (date of the application: 26.09.2020).
4. All about pollen allergy. URL: https://dompchel.ru/zdorove/allergiya/na-pyltsu/#i-9 ; (date of the application: 26.09.2020).
5. Plant pollen: when does it appear, where and in what quantity? URL: https://prosimptom.ru/a-z/pylca.html#literature ; (date of the application: 27.09.2020).
6. Khutueva S.K., Fedoseeva V. N. Aeroallergens, allergen nomenclature. URL: https://medbe.ru/materials allergeny/aeroallergeny-nomenklatura-allergenov/?PAGEN_2=2 ; (date of the application: 27.09.2020).
7. Allergenic activity of pollen of some plants. URL: https://studbooks.net/911345/estestvoznanie/allergennaya_aktivnost_pyltsy_nekotoryh_rasteniy ; (date of the application: 27.09.2020)
8. Sofiev M., Berger U. et al. MACC regional multi-model ensemble simulations of birch pollen dispersion in Europe. 23 Jul 2015. URL: https://acp.copernicus.org/

articles/15/8115/2015/ ; (date of the application: 27.09.2020).
9. Flowering calendar. URL: https://www.letograf.ru/drugs/kalendar-pyleniya-derevev-v-moskve-kalendar-cveteniya/ ; (date of the application: 27.09.2020).

Author

Rakhim Khamitov was born in Kazan, Tatarstan on the 7th of September 2003. Rakhim entered the 2nd lyceum in 2016, and he is still studying there. He is keen on football (soccer), and also interested in chemistry.

Rafcat Kireev was born in Kazan, Tatarstan on April 25th, 2002. Studied at the 2nd lyceum for 5 years, this year he has entered to the University –KFU Specialty-medical care. He is interested in fencing.

DOI: 10.36838/v3i1.12

Investigating Effectiveness of Different Salt Reagents ($NaCl$,$CaCl_2$, $MgSO_4$) On Solid Ice Cubes

Satya S. Juttada

Milliken Mills High School, 7522 Kennedy Rd, Markham, ON L3R 9S5, Canada; sathwik1215@gmail.com

ABSTRACT: The goal for this experiment was to investigate which form of salt, calcium chloride ($CaCl_2$), sodium chloride ($NaCl$), and magnesium sulphate ($MgSO_4$), is most efficient for adequately deicing an ice cube ($25.0cm^3$) by using freezing point depression and mass trials (with timings 5min, 15min, 30min, 45min, and 60min) when the mass of salts ($5.0cm^3$) and the environment temperature (22°C) is maintained constant. The results that were yielded from the experiment was that calcium chloride ($CaCl_2$) is the most efficient salt reagent out of the three other tested reagents, sodium chloride ($NaCl$) and magnesium sulphate ($MgSO_4$).

KEYWORDS: Chemistry; Salts; Ice-cube; Deicing; Timing.

Introduction

From a young child, when immigrating from India to Canada, I was greeted by tons of snow and ice every year. During my life in India, I had always thought of salt as an additional seasoning to food to add an extra bit of flavor, but soon after moving to Canada, I learned of the possibilities and usefulness that salt has. I was fascinated by the fact of how even a small amount of salt could melt ice that was up to 5 or 10 times larger than the salt itself. In grade 8, our science class attempted a similar experiment with different procedures and variables. When doing the experiment, I understood that some salts would increase the rate of melting of the ice cube, but never quite understood the internal process of the reaction between the salt and ice cube. This process sparked an inspiration for this chemistry exploration, and lead me to the research question: Which form of salt, calcium chloride ($CaCl_2$), sodium chloride ($NaCl$), and magnesium sulphate ($MgSO_4$), is most efficient in adequately deicing an ice cube (25.0 cm^3) by using freezing point depression and mass trials (with timings 5 min, 15 min, 30 min, 45 min, and 60 min) when the mass of salts (5.0 cm^3) and the environment temperature (22°C) is maintained constant?

***Background Information*:** This investigation was conducted as a percent-mass trial that will be analyzing the efficiency of each salt melting the ice cube when given a specific amount of time. To maximize the accuracy of the results yielded by the trials and ensure that truly efficient salt is found, we will use the freezing point depression equation. The freezing point depression equation has multiple components that will need to be reviewed and the experiment itself has some key information needed to be understood.

The experiment: This experiment consists of four solutions, and three of which will have a solvent and solute (the fourth solution will be the ice cube alone in the beaker that will melt at room temperature, also known as the control). The solvent will be H_2O and solute will be the salts ($CaCl_2$, $NaCl$, $MgSO_4$). When our solute is added to the solvent, molecules of the solute will dissolve in the solvent. This is because the force of attraction between the solute and solvent molecules is greater than the force of attraction between the molecules only in the solute. H_2O is partially polarized because of the distribution of electrons caused by the partial positive charge at hydrogen ends, and the partial negative charge at the oxygen end. This disturbance makes H_2O a specifically better solvent, as it becomes possible for water molecules to shift around solute ions. Our salt solute can then lower the freezing point of the water. This is the basis of this investigation.[1]

Freezing point depression: Freezing point depression is the decrease of the freezing point of a solvent which occurs when a non-volatile solute (a solute that has little tendency to escape the solution) is added. The solution thereby has its freezing point become lower than of the original solvent. Freezing point depression is a colligative property of matter. These properties do not depend on the specific type of compound or collective mass, but rather on the number of the particles present in the solvent. Other colligative properties include vapor pressure, boiling point elevation, and osmotic pressure. Applications of freezing point depression including removing ice from roads to prevent safety hazards. And this concept can be applied to create ice cream, as the salt helps keep the ice cream cold for long periods of time.[2]

Freezing point depression formula: The combination of two equations, the Clausius-Clapeyron equation, and Raoult's law, forms the freezing point depression formula:[3]

$\text{Freezing Point}_{total} = \text{Freezing Point}_{solvent} - \Delta T_f$,

where $\Delta T_f = i * K_f * m$

ΔT_f: ΔT_f is the change in temperature which will be measured in degrees Celsius (°C). This is essentially the value that is focused on because it will indicate which solute will have the highest change in freezing point for the solvent. This value will then be substituted in the total freezing point depression formula to calculate the final freezing point of the solution.[2]

DOI: 10.36838/v3i1.13

van't Hoff factor (i): The van't Hoff factor or "i" is used to determine the number of molecules or ions the solute splits into when it dissolves in a solvent. This factor varies for different solutes depending on the form of electrolyte they are. The forms include strong, weak, and non-electrolytes. To identify if which group the solute is in, the conditions are provided:

strong electrolyte: strong acids, strong bases, and soluble ionic compounds (solute will dissociate ions in solution, i > 1)

weak electrolyte: weak acids, weak bases, and insoluble ionic compounds (solute will dissociate but only to a limited extent, 1< i <2)

non-electrolyte: covalent compounds (solute will not dissociate in solution, i = 1)

When the van't Hoff factor is found it can then be substituted into the freezing point depression equation.[4]

K_f: The cryoscopic constant (K_f) can be defined as the molal depression constant and has units °C Kg mol^{-1}. This constant will vary for different solvents, but for this experiment, the solvent will be H_2O which has K_f = 1.86°C kg mol^{-1}.[3]

"m": The variable "m" in the freezing point depression formula, is defined as molality which is the concentration of moles of solute per kg of solvent, mol kg^{-1}. A value of 2 moles per kilogram can also be referred to as 2 molal.[5]

Table 1: A raw data table showing the relative performance (± 0.01%) of the salt reagents, $CaCl_2$, NaCl, and $MgSO_4$ (5 cm^3), to melt their specific distilled water ice cube (25cm^3) in different trials with timings 5 min, 15 min, 30 min, 45 min, and 60 min at room temperature (22°C).

Reagents / Trial Number	Calcium chloride ($CaCl_2$)	Sodium chloride (NaCl)	Magnesium sulfate ($MgSO_4$)	Control ice cube
Trial 1 (5 mins)	11.2% ± 0.01%	10.3% ± 0.01%	9.6% ± 0.01%	5.2% ± 0.01%
Trial 2 (15 mins)	33.6% ± 0.01%	31.9% ± 0.01%	28.8% ± 0.01%	16.8% ± 0.01%
Trial 3 (30 mins)	67.3% ± 0.01%	62.6% ± 0.01%	57.5% ± 0.01%	32.5% ± 0.01%
Trial 4 (45 mins)	99.0% ± 0.01%	92.9% ± 0.01%	86.3% ± 0.01%	46.7% ± 0.01%
Trial 5 (60 mins)	100.0% ± 0.01%	99.6% ± 0.01%	93.5% ± 0.01%	72.3% ± 0.01%

Results

Qualitative observations: As time continued, the ice cube melted but also created holes where the salt particles were placed, thereby making it look as if shards were made in the cube. The smell of the salt was slowly decreasing and fading away as time continued, likely because the salt particles slowly mixed with the water and the smell reduces. For example, the $MgSO_4$ salt particles at first had a minty fresh smell, but as the time of the trials increased the smell dulled. The distilled water (which was frozen and taken out as an ice cube) was clear and opaque, but when the salt particles were reacted with the ice cube the water that melted was thick and viscous, and more faded. This is because the salt mixed in with the water combining and diluting the color of the water.

The results suggested that calcium chloride ($CaCl_2$) is the most efficient salt reagent out of the three other tested reagents, sodium chloride (NaCl) and magnesium sulfate ($MgSO_4$). This is shown through the experiment's line graph in Figure 1, which indicates the relative performance of each salt solute at experiment time trials of 5, 15, 30, 45, and 60 minutes. The blue line, representing calcium chloride, on the graph, shows

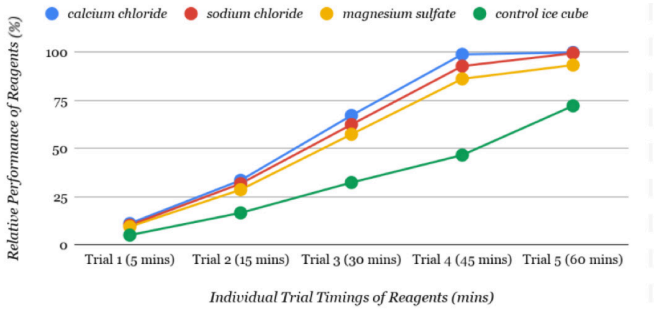

Figure 1: Line Graph Indicating the Relative Performance (± 0.01%) of the Salt Reagents, $CaCl_2$, NaCl, and $MgSO_4$ (5 cm^3), to Melt Ice cube (25cm^3 of distilled water) in Different Timing Trials (5 min, 15 min, 30 min, 45 min, 60 min) at Room Temp (22°C).

ride consistently melts the ice cube the most in comparison to the other reagents and the control. The specific data results are shown in the Table 1. The line graph, on the other hand, depicts the pattern of the $CaCl_2$ being the fastest reagent. A close competitor to calcium chloride is sodium chloride solute.

Conclusion

In the first four trials, there is a visible gap in the relative percent mass, but at the last trial, which was 60 minutes, NaCl and $CaCl_2$'s difference in performance was very minuscule (0.37%) and almost negligible. The reason that $CaCl_2$ has a higher performance in deicing the ice cube may be due to the fact that when sodium chloride (NaCl) melts ice, the salt dissolves into separate sodium ions and chloride ions however calcium chloride ($CaCl_2$) is more effective at melting ice as it can break down into three ions, one calcium ion, and two chloride ions and as a result, the increase ions means that more ions are placing themselves in the rigid bonds of the ice cube. In addition to this, the calculations in section 6 also prove this is accurate but in the form of showing that $CaCl_2$ lowers the freezing point of the ice cube the most.

Using the freezing point depression equation $CaCl_2$, the theoretical freezing point that the ice cube can possess when in contact with $CaCl_2$ is -11.16 °C, NaCl is -11.09 °C and $MgSO_4$ is -6.20 °C. With this theoretical and experimental values as sufficient evidence to support calcium chloride ($CaCl_2$), I can conclude this investigation with the statement: calcium chloride ($CaCl_2$) is the most efficient salt reagent to deice an ice cube of distilled water when compared to sodium chloride (NaCl) and magnesium sulfate ($MgSO_4$) under the conditions of all salts having the mass 5cm^3, ice cubes with masses 25cm^3, and trails taking place at room temperature, 22 °C.

This chemistry investigation has limitations. The over-sanitation and artificiality of the lab can result in unnatural reactions that do not reflect real-life and have low ecological validity (the degree to which an investigation represents real-life experiences). These variables limit the accuracy of the experiment.[7]

Some improvements can be applied to this exploration as there are several weaknesses. One is the variance in the number of salt particles that come in contact with the ice cube. When the petri dish with the salt reagent is poured in the

DOI: 10.36838/v3i1.13

beaker, not all the salt is in contact with the ice cube, and the results of the different trials may not be accurate.

Other experimental errors include impurities in the vessel that contained the reactants, inaccurate measurement readings from the scale, fluctuations in humidity, pressure, airflow, etc. Furthermore, another improvement for this experimentation is the number of trials, the experiment had 5 trials but with more time available the trials can go up to 7-8 trials so as to increase the number of data points on the graph so as to have more consistency. A final improvement is the website used to plot the data points in the Table 1. Google sheets was utilized for this experiment, but there is a limit to the detail of the value that the graph on sheets can examine. The more detail and separation in the reagent lines, the more detailed the analysis can be.[7]

Methods

This experiment requires multiple variables to identify the most efficient salt, while simultaneously keeping factors in the trials constant so as to keep them fair. The variables used in this experiment are listed and explained below.

Independent variables:

1. In each trial, the salt used includes calcium chloride ($CaCl_2$), sodium chloride (NaCl), and magnesium sulphate ($MgSO_4$). The different number of salts used shows the difference in the mass trial between the salts. The use of the different variables shows the increased reliability of the results as more data points on the graph creates visual patterns that can be analyzed.

2. In this experiment, we tried to minimize the number of pollutants, but there will always be the uncertainty of possible molecules on the solvent. They can possibly affect the rate at which the ice cube melts and as a result, will become an independent variable. But it is important to note that this is not a variable that was chosen on purpose, it is merely listed as a possibility for this experiment.

3. The amount of time allocated for each trial was varied where Trial 1 was given 5min, Trial 2 was 15min, Trial 3 was 30min, Trial 4 was 45min, and the last trial (5) was allocated 60minutes. These timings were varied with the purpose to show that one salt can consistently lower the freezing point of the ice cube the most and thereby melt the ice cube the most.

Dependent variables:

1. Amount of water melted from the ice cube: This is what will be calculated to see the percent mass of how much the ice cube has melted with the given amount of time. In the different trials, the reagent will result in different masses of the ice being melted at different times.

2. Reduction in the freezing point of the ice cube when in contact with the salts:

The different solutes reduce the freezing point of the ice cube by different values. This variable depends on the number of molecules dissolved in the solvent and as a result, becomes a dependent variable. Even though this variable is not a value this experiment itself will find, it still becomes a dependent variable part of the reaction.

Controlled variables:

1. Refrigerator temperature (-18°C) where the ice cubes were stored was kept constant: The storage where the ice cubes were stored is quite important as changing the location of ice cubes could alter the precision of the experiment, because some refrigerator-freezers may have their temperature changed.

2. Time ice cubes were left out before solutes were dissolved in them: Precisely 10 minutes after the ice cubes were taken out of the freezer, the salt solutes were placed in the beakers to keep the trials fair and constant. Keeping this a controlled variable was difficult, as I had to start a timer and quickly rush retrieving the ice cube tray, measure each ice cube and salt all within 10 minutes. I realized that I could have extended the time the ice cubes were left out, but also realized that the ice cubes could also start melting.

3. Masses of the solutes ($CaCl_2$, NaCl, $MgSO_4$) and solvents (ice cubes) were kept constant as well: Each solute was measured with an electronic mass balance to be 5.0 cm^3 (Figure 2), and the solvents were measured to be 25.0 cm^3. These masses were kept constant throughout the trials.

4. Location of the trials: The location of the trials is essential as different locations have different variables and factors that may affect the speed of the salt to lower the freezing point of the ice cube. This is why the location of the trials in this experiment was kept constant.

5. The purity of the solutes and solvents: In each trial, the salt and ice cube had to be used in such a way to minimize the exposure to possible contaminants. This included using the same bottle of distilled water in which the ice cubes were frozen in and using clean apparatus (scoopulas, beakers, Petri dishes, etc.) to retrieve the salts from their jars. Even the jars from which the reagents were used were kept constant throughout the trials.

6. Size of salt particles: This may seem minuscule but has the possibility to greatly affect the rate at which the salt lowers the freezing point of the ice cube. The surface area that which the reagent covers is important, leaving the reagent in a more solid form can slow down the process of freezing point depression, which is why for this experiment I ground all the salts so as to keep the differences between the salts minimal.

Photograph of set-up:

Figure 2: Photograph of my experimental set-up, weighting out 5.0 grams of Calcium chloride reagent using a mass balance.

Experimental procedure: The procedure outlined by ScienceBuddies.org with modifications to coincide with the different variables and factors in my experiment was utilized. The modified procedure is described in detail below.

100.0 cm^3 of distilled water was collected from Glacéau Smartwater Vapour water bottle using the pipette and pipette pump, I then slowly and carefully poured 25.0 cm^3 into 4 squares in the ice cube tray. Once again, 100.0 cm^3 of distilled water was collected and poured into another 4 squares on the ice cube tray. Finally, this process was repeated until 20 ice cube squares in the ice cube tray were filled with distilled water. The ice cube tray was carefully transferred into a freezer and let sit overnight. The following day, I used a scoopula to transfer an eyeballed amount of calcium chloride in the mortar. I grounded the calcium chloride ($CaCl_2$) with the pestle to small particles. I repeated step 3 for sodium chloride (NaCl) and magnesium sulphate ($MgSO_4$), used different Petri dishes for the other salts. I retrieved ice cube tray from freezer and set a 10-minute timer, then placed 1 ice cube into each of the four 200.0 cm3 labelled glass beakers. Next, I placed the three salts on three ice cubes, but the last ice cube was the control. At the end of the 10 minutes, I started another timer for 5 min. I used a clean scoopula to try to place and shift as much of the salt on or near the ice cube and used Sony Xperia X Performance to take photos of the experiment. After the timer ended, I quickly used tweezers to retrieve the ice cubes from the four beakers and placed on new clean Petri dishes which were weighed (cm3) on the Acculab V 600 electronic mass balance, but not before the Petri dishes were zeroed out. In the four following days, the same experiment was conducted but with the timing in which the ice cubes were left in the beakers were changed to 15 min, 30 min, 45 min, and 60 min for the rest of the trials.

Calculation

Calculating freezing points: As stated earlier, the freezing point depression equation was used in addition to the experimentation as a safeguard to ensure that the results that I collected are accurate in the terms that the most effective salt will have the greatest change in the freezing point of the ice cube. The calculations of the values of the freezing point depression are shown below:

Calcium chloride ($CaCl_2$): To calculate the Freezing Point Depression[3] for $CaCl_2$ the formula is Freezing $Point_{total}$ = Freezing $Point_{solvent}$ - ΔTf, where $\Delta Tf = i * K_f * m$. Here we are given the Kf of water which is 1.86°C kg/molal and the freezing point of water is 0 °C. We require ΔTf, van't Hoff factor (i), molality of solute (m), and Freezing $Point_{total}$.

Given the moles of $CaCl_2$ and volume of water in kg, we can calculate the molality of $CaCl_2$ which is 2.00 mol/kg. The next step is about the van 't Hoff factor "i". $CaCl_2$ is an ionic compound making it a strong electrolyte and therefore has "i" > 1. To determine the exact value of "i" we need to know the number of ions $CaCl_2$ that will dissociate in aqueous solution. The answer is 3 because there are 1 Ca+ ion and 2 Cl- ions, totaling s3. Finally, since we have calculated the molality of $CaCl_2$, "i", and Kf, it can be calculated that the ΔTf of $CaCl_2$ is 11.16 °C. By calculating the ΔTf of $CaCl_2$ to be 11.16 °C, the Freezing Pointtotal was -11.16 °C.

Using a method similar to $CaCl_2$, the Freezing Pointtotal for NaCl was -11.09 °C and $MgSO_4$ was -6.10 °C.

Sample Calculation:

(for showing how relative performance was calculated):

Trial 1 for calcium chloride:

Relative Performance = [(original mass of ice cube - the new mass of ice cube)/(original mass of ice cube)]*100%

= [(25cm^3 - 22.19cm^3)/(25cm^3)]*100%

= 11.24%

Acknowledgement

I would like to thank and acknowledge my mentor, teacher, and experiment supervisor, Mr. Leung for his expert advice throughout this extensive yet compelling paper. In addition, I would like to thank him for his help in guiding me with the equipment in the laboratory.

References

1. Science Buddies. (2020, January 12). What Makes Ice Melt Fastest?: Science Project. Retrieved from https://www.sciencebuddies.org/science-fair-projects/project-ideas/Chemp049/chemistry/wh
2. Helmenstine, Anne Marie, Ph.D. (2020, February 11). Freezing Point Depression. Retrieved from https://www.thoughtco.com/understanding-freezing-point-depression-609182
3. Helmenstine, Todd. (2020, February 11). Freezing Point Depression Example Problem. Retrieved from https://www.thoughtco.com/freezing-point-depression-example-problem-609493
4. Determining the van't Hoff factor of a substance from its formula?: Socratic. (2016, April 13). Retrieved from https://socratic.org/questions/how-can-i-determine-the-van-t-hoff-factor-of-a-substance-fro
5. Mott, V. (n.d.). Introduction to Chemistry. Retrieved 18:29, March 17, 2020, from https://courses.lumenlearning.com/introchem/chapter/molality/
6. Zamboni, Jon. (2020, June 9). How to Calculate Percent Change in Mass. sciencing.com. Retrieved from https://sciencing.com/calculate-percent-change-mass-5133030.html
7. McLeod, S. A. (2012, Jan 14). Experimental method. Simply psychology. Retrieved from https://www.simplypsychology.org/experimental-method.html

Author

Satya Sathwik Juttada is a grade 12 student attending Milliken Mills High School and is currently enrolled in the IB Diploma program. She enjoy chemistry, math and statistics and She plans on applying to Cornell University for Chemical Engineering in 2021.

DOI: 10.36838/v3i1.13

ACASU

American Commission for Accreditation of Schools and Universities

STANDARDS

* Governance

* Education

* Culture

* Operations

* Quality

Lifetime Qualities

MORAL
Caring, Modest, Ethical, Respectful

THINKER
Knowledgeable, Inquirer, Curious

PRODUCTIVE
Achiever, Excellence Seeker

INNOVATIVE
Problem Solver, Explorer

VISIONARY
Global Citizen, Inclusive

ACASU BENEFITS

Enhances your institution's reputation and garners the esteem of Americans.

Assures students and their families that your institution meets American standards for high quality education.

Shows students and parents your institution's commitment to success and your ability to perform at high quality educational standards.

Shows your colleagues and the general public that your institution has a genuine interest in institutional improvement.

Sets your institution apart as a leader among others.

Provides you with a network of skilled professionals and resources to assist meeting your accreditation, enrollment, and college attainment goals.

Ensures that your standard operating procedures are compliant with U.S. international student regulations.

ACASU.ORG

The International Journal of High School Research is published
by Terra Science and Education